

https://dspace.org/

An investigation into the crystallization of ammonium para-tungstate

Lutz, Waldo Friedrich

1973

http://hdl.handle.net/10539/22194

Lutz, Waldo Friedrich (1973) An investigation into the crystallization of ammonium para-tungstate, University of the Witwatersrand, Johannesburg, <http://wiredspace.wits.ac.za/handle/10539/22194>

Downloaded from a DSpace repository. https://dspace.org/

AN INVESTIGATION INTO THE CRYSTALLIZATION OF AMMONIUM PARA-TUNGSTATE

by

Waldo Friedrich Lutz

B.Sc.(Eng.)(Rand)

A thesis submitted in fulfilment of the requirements for the degree of Doctor of Philosophy in the Department of Chemical Engineering, University of the Witwatersrand.

January 1973

UNDERTAKING

I hereby certify that this is my own work and has not been submitted for a Doctorate at any other University.

W.F. LUTZ

ACKNOWLEDGEMENTS

The author wishes to express his gratitude to the following persons.

Dr. D. Glasser and Dr. A.W. Bryson for their advice and guidance in their capacities as supervisors for this thesis.

Hard Metals Ltd. for sponsoring the author.

Boart Research Laboratory for supplying the equipment and for research facilities provided during the initial stages of this project.

Miss R.J. Ireland for the painstaking task of typing this thesis.

LIST OF CONTENTS

Page No.

1 CHAPTER I - INTRODUCTION

4 CHAPTER II - LITERATURE SURVEY

4 2.1 Crystal Growth Rate Determinations

2.1.1. Experiments with Fixed Crystals

2.1.2. Experiments with Fluidised Bed Crystallizers

2.1.3 Experiments Performed in Stirred Tank Crystallizers

2.2 Nucleation Rate Determinations

2.2.1. Batch Experiments Performed in Stirred Vessels

2.2.2. Experiments Performed in Continuous Stirred Tank Crystallizers

13 CHAPTER III - APPARATUS AND ANALYTICAL TECHNIQUES

13 3.1. Apparatus

3.1.1. The Crystallizer

3.1.2. The Heating Circuit

3.1.3. The Flowrate Control of the Feed Solution

3.1.4. The Mixed Product Removal

17 3.2 Analytical Techniques

3.2.1. Crystal Size Analysis

(a) Comparison between the Microscope and the Sedimentation Balance

(b) Description of the Sedimentation Balance

3.2.2, Determination of the Solution Concentration

Page No.

24 CHAPTER IV - THE DEPENDENCE OF THE GROWTH RATE OF APT ON THE CRYSTAL SIZE

24 4.1 The Particle Balance Equations

4.1.1 Batch Crystallization

4.1.2 Continuous Crystallization

25 4.2 The Effect of Crystal Size on the Growth Rate of APT Crystals

4.2.1 Experimental Procedure

4.2.2 Results

31 CHAPTER V - THE GROWTH RATE MODEL

31 PART I: BATCH CRYSTALLIZATION

31 5.1 Experimental Procedure

32 5.2 Experiments performed

32 5.3 Batch Crystallization Results

5.3.1 The Critical Nuclei Size of APT Crystals

5.3.2 Solution of the Batch Particle Balance Equation.

5.3.3 The Dependence of the Crystal Growth Rate on the Supersaturation.

45 5.4 Crystal Break-up Investigation

47 5.5 The Effect of Impurities on the Crystal Growth Rate.

50 5.6 The Growth Rate Model

5.6.1 The Growth Rate Equation Applied to the Batch Crystallization Process.

5.6.2 Test of the Model.

Page No

56 PART II: CONTINUOUS CRYSTALLIZATION

56 5.7 Experimental Procedure

57 5.8 Experiments Performed

57 5.9 Continuous Crystallization Results

5.9.1 Solution of the Continuous Particle Balance Equation

5.9.2 The Dependence of the Growth Rate on the Crystal Size.

5.9.3 Growth Rates Evaluated from the Continuous Crystallizer Experiments

5.9.4 The Growth Rate Equation Applied to the Continuous Crystallization Process.

5.9.5 Test of the Model.

68 PART III: THE RELATIONSHIP BETWEEN THE BATCH AND CONTINUOUS RESULTS

68 5.10 Comparison of the Results

70 5.11 Discussion of the Nucleation Processes

77 CHAPTER VI - A SUMMARY OF THE MAJOR RESULTS

79 APPENDIX A: The Determination of the Cumulative Weight Fraction Particle Size Distribution from the Sedimentation Balance Curve.

84 APPENDIX B: Evaluation of α_1 and α_2 from the Cumulative Weight Distribution Curves of the Crystals.

Page No.

88 APPENDIX C: Batch Crystallization Results

100 APPENDIX D: Continuous Crystallization Results

108 APPENDIX E: Literature Cited.

SYMBOL	MEANING	DIMENSIONS
A	total surface area of the crystals per unit volume of solution	L^{-1}
D	suspension density of the crystals	M/L^3
$M(t)$	total mass of crystals at time t	M
M_I	mass of impurities in a crystal of size ℓ	M
N	nucleation rate per unit volume of solution	$1/\theta L^3$
N_A	number of active sites per unit surface area of the crystals	L^{-2}
N_I	total number of active sites which are completely inhibited against further growth on a crystal of size r	
N_{RE}	Reynold's number	
N_T	number of active sites on a crystal of size r	
N_x	number of active sites which are completely inhibited against further growth, on a crystal of size ℓ	
$Q(t)$	nucleation rate at time t	θ^{-1}
T	average residence time of the crystallizer	θ
u	surface area of the crystals used for nucleation	L^2
V	total volume of the solution in the crystallizer	L^3
V_o	original solution volume for a batch run	L^3

SYMBOL	MEANING	DIMENSIONS
$V(\ell,t)$	cumulative weight fraction of crystals greater than size ℓ at time t	
$W(\ell,t)$	cumulative weight fraction of crystals up to size ℓ at any time t	
$Z(\ell,t)$	defined as $\dfrac{w(\ell,t)}{\int_0^\infty w(\ell,t)d\ell}$	L^{-1}

SYMBOL	MEANING	DIMENSIONS
b	constant:power of crystal size ℓ	
c	solute concentration in the bulk phase	M/L^3
c_{APT}	concentration of impurities in a crystal	M/L^3
c_o	solute concentration of the feed stream	M/L^3
c_i	interfacial solute concentration	M/L^3
c_s	equilibrium saturation solute concentration	M/L^3
c_x	concentration of impurities in the solution	M/L^3
d	diameter of a particle	L
$f(\ell,t)d\ell$	number of crystals having sizes between and $\ell + d\ell$ at any time t	
g	gravitational constant	L/θ^2
$g(\ell)d\ell$	number of crystals per unit volume of solution having sizes between ℓ and $\ell + d\ell$	
$k_o, k_1..k_w$	constants of proportionality	
ℓ	characteristic dimension of a crystal	L
$\overline{\ell}$	average crystal size	L
ℓ_o	critical nuclei size	L
m	mass of a crystal of size ℓ	M
n	constant	
p	growth rate of a crystal of size ℓ	L/θ
p_m	rate of mass increase of a crystal of size ℓ	M/θ

SYMBOL	MEANING	DIMENSIONS
$\bar{p}$	average growth rate	M/θ
p_l	"true" growth rate of a crystal size ℓ	L/θ
q	Laplace transform operator	
s	supersaturation of a solution	
s_N	"threshold" supersaturation	
t	time	θ
u	fluid velocity	L/θ
v	terminal velocity of a particle	L/θ
w	flowrate of the exit stream	L^3/θ
w_o	flowrate of the feed stream	L^3/θ
$w(\ell,t)d\ell$	weight of crystals of sizes between ℓ and $\ell + d\ell$ at any time t	M
x	fraction of the surface of a crystal which is inhibited to further growth	
y	fraction of the total number of sites on which continuous growth takes place	
y_o	original concentration of impurities in the feed solution	

SYMBOL	MEANING	DIMENSIONS
α_1	first moment of $Z(\ell,t)$ i.e. mean with respect to the weight distribution	L
α_2	second moment of $Z(\ell,t)$	L^2
σ	normalised variance of the weight distribution	
δ	Dirac Delta Function	
ρ_s	density of a solid	M/L^3
ρ_L	density of a liquid	M/L^3
γ	variance of the weight distribution	L^2
η	viscosity of a liquid	$M/L\theta$

CHAPTER I

INTRODUCTION

Ammonium paratungstate (APT) is one of the intermediate products in the production of tungsten metal powder from scheelite ($CaWO_4$). It is crystallized from an ammonium tungstate solution by evaporating off ammonia and water. The crystals have a rhombic structure and have the formula: $5(NH_4)_2O \cdot 12WO_3 \cdot 7H_2O$. When obtained from a batch crystallization process they normally range in size from 20 to 130 microns.

The basic process in which APT is involved is as follows: Scheelite which normally consists of approximately 60-70% by weight of WO_3 is converted to crude tungstic acid (H_2WO_4) by the addition of concentrated hydrochloric acid. The crude tungstic acid, which contains most of the impurities present in the original ore, is dissolved in an ammonia solution and the resulting ammonium tungstate solution filtered to remove insoluble material. APT is generally crystallized from this solution in a batch crystallizer. As water and ammonia are driven off by evaporation the solution becomes more concentrated and nucleation takes place. APT crystals are formed and grow under the supersaturated conditions. The crystallization process is carried out until the mother liquor changes to a brownish colour indicating a high concentration of impurities. Crystallization is then stopped in order to prevent considerable trapping of the impurities by the crystals. (Typical analyses of scheelite ore, ammonium tungstate solution and APT crystals are shown in the table below.)

Impurity Content: % by weight of WO_3

Impurity	Scheelite	Ammonium Tungstate Solution	APT
Mo	.803	.302	.031
P	.216	.048	<.0001
Ti	.341	<.001	<.0001
As	.132	<.001	<.0001
Fe	1.751	.003	.002
Cu	.034	.007	.001
Bi	.070	.004	<.0001
Pb	.036	.003	<.0001
Zn	.014	.006	<.0001
Mn	.112	.011	<.0001

The APT crystals are then converted to tungsten trioxide (WO_3) by calcining in air at a temperature of 600°C. Tungsten metal powder is produced by reducing the tungsten trioxide in a stream of hydrogen at 900°C.

It has been established that a linear relationship exists between the grainsize of the tungsten trioxide and the size of the APT crystals from which it was produced. It is also a well-known fact that the grainsize of the tungsten metal powder is dependent on the size of the tungsten trioxide. In the hard metal industry different tungsten metal powder grainsizes are required for different grades of tungsten carbide. It is

therefore important to have a fine control on the tungsten metal powder grainsize during production. In order to achieve this it is obvious that the APT crystal size has to be controlled during the crystallization process.

This work was undertaken to study the growth rate of APT crystals and hence to obtain some information on the nucleation rate. Having established the factors upon which the crystal growth rate is dependent, the crystallization process can be controlled to give the desired crystal product.

This project was put forward and sponsored by Hard Metals Limited, who have been considering converting from a batch to a continuous process, in order to obtain a more uniform final product. It was hoped to predict the performance of a continuous crystallizer from tests done on a batch process, as batch runs are of a much shorter duration and are easier to perform. In this investigation therefore both batch and continuous runs were performed and the results compared.

CHAPTER II

LITERATURE SURVEY

The crystallization of any material from solution involves two basic processes; nucleation and growth. A number of investigators have studied the factors influencing the growth and nucleation rates of various substances. The most relevant and important findings of these investigations are discussed below.

2.1. CRYSTAL GROWTH RATE DETERMINATIONS

The factors influencing the growth rate of crystals have been studied using three different systems. These systems are: experiments with fixed crystals, experiments using fluidised bed crystallizers, and experiments performed in stirred tank vessels where the crystals are freely suspended in the liquid medium.

2.1.1 Experiments with fixed crystals

Garside and Mullin (4) determined the overall growth rate of single crystals of aluminium potassium sulphate, fixed in a moving stream of the aqueous supersaturated solution.

From their results they derived the following equation for the overall crystal growth rate:

$$p = \text{const.}\ u^{0.65}\ \Delta c^{n} \qquad (2\text{-}1)$$

where p = crystal growth rate

u = fluid velocity

Δc = supersaturation

Different values of the power n were obtained for different flow-rates.

They suggested that the velocity effect was due to an

increase in the diffusion rate of the solute from the bulk of the solution to the crystal surface.

Hixon and Knox (7) studied the growth rates of single crystals of copper sulphate pentahydrate and magnesium sulphate heptahydrate. These single crystals were fixed in flowing streams of their corresponding aqueous supersaturated solutions.

According to Hixon and Knox, the overall rate of growth of the copper sulphate pentahydrate crystals followed an equation of the form:

$$p = k_o(c_i - c_s)^2 \qquad (2\text{-}2)$$

For magnesium sulphate heptahydrate the equation was of the form:

$$p = k_o(c_i - c_s) \qquad (2\text{-}3)$$

where: k_o = rate coefficient

c_i = interfacial solute concentration

c_s = equilibrium saturation solute concentration

The relationship between the growth rate and the supersaturation for magnesium sulphate was thus a linear function, whereas for copper sulphate it was found to be non-linear.

Botsaris and Denk (1) measured the growth rates of the (100), (110) and (111) faces of single seed crystals of potassium alum crystals. These crystals were fixed in a flowing stream of the supersaturated mother liquor.

Their results showed that at low supersaturations the growth rates of the (111) faces were linear with supersaturation. In the same region the growth rates of the (100) faces were also linear with supersaturation. Beyond certain transition points, however,

(about 1% supersaturation for the (111) faces and about 5% supersaturation for the (100) faces), the growth rates were no longer linear with supersaturation.

To take into account this non-linearity with supersaturation, they proposed a new growth rate model based on a theory of mono-nuclear two-dimensional nucleation, together with Franks' theory of crystal growth. The resulting expression for the growth rate of a crystal face was:

$$p = k_1 s + k_2 \exp.[-k_3/\ell n(s+1)] \qquad (2\text{-}4)$$

where s, the supersaturation, is defined as:

$$s = \frac{c - c_s}{c_s} \qquad (2\text{-}5)$$

They fitted the above equation (2-4) to their results, and the constants, k_1, k_2 and k_3 were evaluated as given in the table below.

Crystal face	k_1	k_2	k_3
(100)	5.40	3.11	0.280
(110)	1.60	1.72	0.200
(111)	0.41	1.60	0.206

Botsaris and Denk also studied the effect of the liquid velocity on the growth rate of the faces of the crystals. They found that for liquid velocities above 3 in/sec, the velocity had no effect on the growth rate. It was only when the growth rate was bulk diffusion controlled (below 3 in/sec) that it was effected by changes in the liquid velocity. In this region the growth

rate increased with increasing fluid velocity.

2.1.2 Experiments with fluidised bed crystallizers

Garside and Mullin (4) also determined the growth rate of aluminium potassium sulphate crystals in a laboratory scale fluidised bed crystallizer.

They derived the following empirical equation from their practical results:

$$p = \text{const.}\ \bar{\ell}^{0.63}\ \Delta c^{n} \qquad (2\text{-}6)$$

where $\bar{\ell}$ = average size of the crystals.

It should be remembered that in a fluidised bed crystallizer the relative velocity between the crystals and the fluid is dependent on the crystal size. It is thus to be expected that the growth rate will be dependent in some way on the crystal size.

Knapp (10) investigated the effect of certain factors on the growth rate of ammonium sulphate from aqueous supersaturated solutions in a fluidised bed crystallizer.

He found that the overall growth rate followed the relationship:

$$p = k_o(c - c_s) \qquad (2\text{-}7)$$

where c = the solute concentration in the bulk fluid

Rumford and Bain (18) determined the growth rate of sodium chloride crystals from aqueous supersaturated solutions in a fluidised bed crystallizer. The experiments were performed at temperatures ranging from 26°C to 73°C and at supersaturations ranging from 0.185% to 0.925%. Their results are shown in the figure drawn below.

THE RESULTS OF RUMFORD AND BAIN

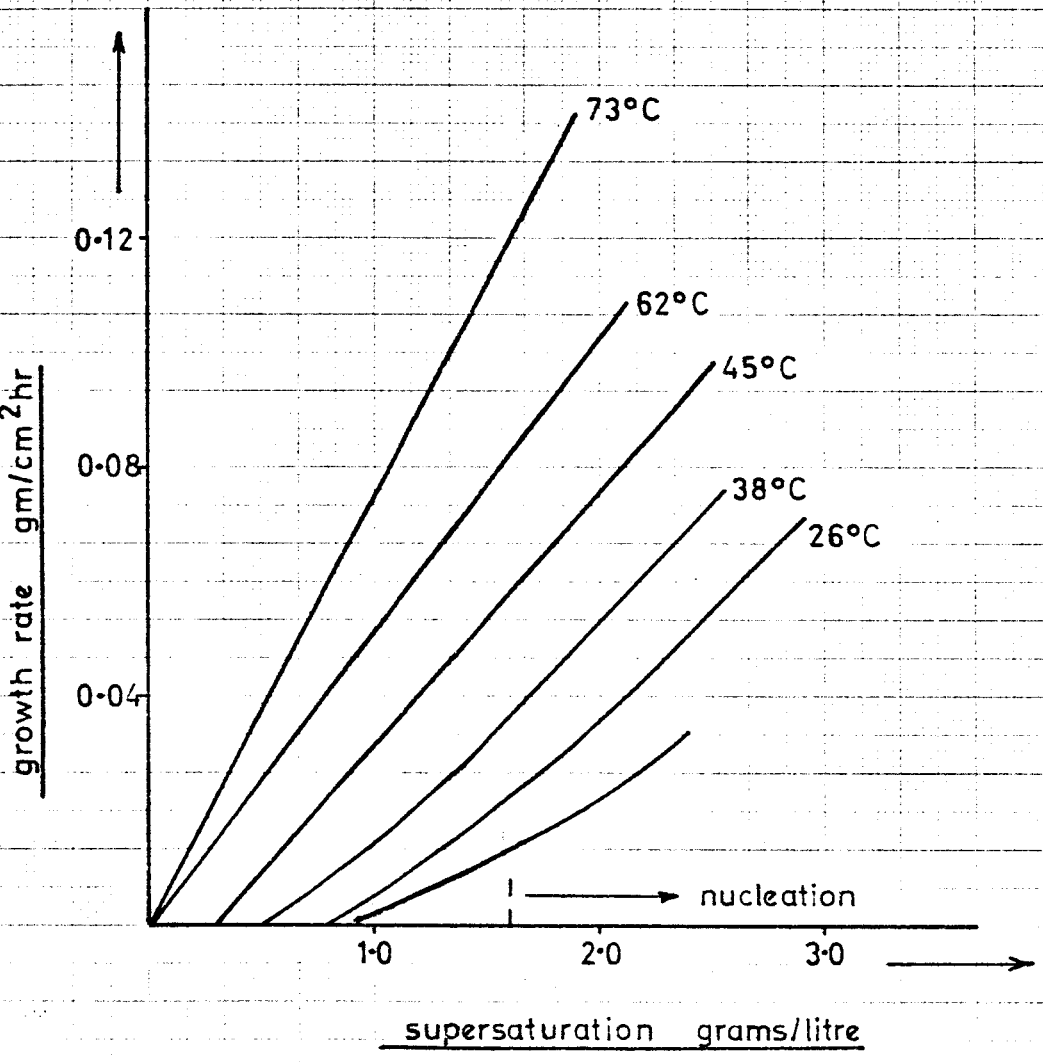

At temperatures above 50°C the relationship follows a straight line through the origin, whereas below 50°C the relationship is non-linear and does not pass through the origin. They suggested that at temperatures above 50°C the crystal growth rate was diffusion controlled, and at temperatures below 50°C the rate of crystal growth was controlled by the surface reaction.

At supersaturations below 0.4 gms/litre, the growth rates were negligible. Rumford and Bain attributed this to some effective "energy barrier" or a temporary blocking of the active sites on the crystal surface by impurities present in the solution.

2.1.3 Experiments performed in stirred tank crystallizers

McCabe and Stevens (12) established that in a mixed suspension batch crystallizer, the growth rate of copper sulphate pentahydrate crystals could be represented by the following empirical equation:

$$p = 0.00177\ \Delta c^{1.8}\ \ell^{1.1} \qquad (2.8)$$

In order to determine whether the crystal size had a direct influence on the crystal growth rate, crystals of different sizes were grown on a retaining screen under similar conditions of temperature and supersaturation. It was established that crystals of the same size grew at different rates when subjected to different fluid velocities, but crystals of different sizes grew at the same rate when subjected to the same fluid velocity.

From this investigation McCabe and Stevens concluded that the crystal growth rate was in fact independent of the crystal size as such. The apparent effect of size resulted from the larger crystals

having a higher settling velocity and hence a larger relative crystal-solution velocity. Since the diffusion resistance and the diffusion boundary layer decrease with increasing velocity, the growth rate of the crystals in a mixed suspension would be expected to increase with size, provided that the growth rate is not reaction controlled.

Watts (22) performed some experiments on magnesium sulphate heptahydrate in a stirred tank crystallizer and arrived at the conclusion that the crystal growth rate was not dependent on the crystal size for the size range studied (73 - 211 microns). He also established that the growth rate for these crystals was linearly dependent on the supersaturation of the solution.

Bransom, Dunning and Millard (3) precipitated cyclonite from nitric acid by the addition of water, in a continuous flow stirred tank crystallizer. Their results indicated that the overall rate of growth of the crystals was not a function of the crystal size.

Larson, Timm and Wolff (11) and Timm and Larson (20) studied the variables affecting the operation of a continuous stirred tank crystallizer, using the following three systems: alum-ethanol-water, ammonium sulphate-methanol-water and sodium chloride-ethanol-water. Their results, for the three systems described, showed that the overall growth rate was not dependent on the crystal size.

The results obtained by the various investigators may be summarised as follows: experiments performed with freely suspended particles in stirred vessels indicate that the crystal growth rate is not a function of the crystal size. However,

the results obtained from experiments with fixed crystals, or where the relative velocity between the crystals and the fluid was dependent upon the crystal size, show that the overall crystal growth rate is a function of the particle size.

Most of the results obtained from the various investigators also indicate that the growth rate is approximately linearly dependent on the supersaturation of the solution.

2.2 NUCLEATION RATE DETERMINATIONS

It is generally accepted that there are two distinct forms of nucleation. Melia and Moffitt (14) suggest that when a solute crystallizes from an aqueous supersaturated solution, two types of nucleation can occur. Primary nucleation occurs on foreign solid bodies present in the solution due to atmospheric (or other) contamination. These primary nuclei develop in the supersaturated solution and give birth to large numbers of new nuclei. This is termed secondary nucleation.

Two main groups of experiments have been performed to ascertain the various factors influencing the nucleation rates of various crystals under various conditions. These groups are: batch experiments performed in stirred vessels and experiments performed in continuous stirred tank crystallizers.

2.2.1. Batch experiments performed in stirred vessels

Mason and Strickland-Constable (13) performed a number of experiments by adding seed crystals of the solute to aqueous supersaturated solutions of magnesium sulphate heptahydrate. They suggest that if crystals, which are growing in a stirred vessel, are free to collide with the walls of the vessel or with

each other, fresh nuclei are readily produced even at low supersaturations and with relatively gentle collisions. Their results further indicated that the nucleation rate was dependent on both the degree of supersaturation of the solution and also on the rate of agitation.

Melia and Moffitt (14) investigated the factors influencing the production of nuclei in aqueous solutions of potassium chloride. Their results can be summarised as follows:

1) The nucleation rate was directly dependent on the degree of agitation of the solution
2) The number of seed crystals introduced into the solution had little or no effect on the number of secondary nuclei produced.
3) Neither the size nor the nature of the surface of the parent crystals had any effect on the number of secondary nuclei produced.

2.2.2. Experiments performed in continuous stirred tank crystallizers

Heeley (6) perfomed a number of experiments in a continuous flow stirred tank crystallizer using magnesium sulphate heptahydrate. He showed that the nucleation rate could be represented by the relationship

$$N = k_N A(s - s_N) \qquad (2.9)$$

where k_N = overall rate coefficient for the nucleation process

s = operating level of supersaturation

s_N = "threshold" supersaturation

A = total surface area of the crystals per unit volume of the solution.

According to Heeley both k_N and s_N were dependent on the hydrodynamic conditions of the system.

Larson, Timm and Wolff (11) investigated the effect of suspension density; i.e. the weight of crystals per unit volume of solution on the size distribution of the crystal product obtained from a continuous flow, mixed product removal, stirred tank crystallizer. They studied the systems: ammonium sulphate - ethanol - water and ammonium sulphate - methanol - water, and their results were correlated to the following equation:

$$N = k_N D^J s^i \qquad (2.10)$$

where k_N = rate coefficient for the nucleation process

D = suspension density, i.e. mass of crystals per unit volume of solution

s = Steady state, operating level of supersaturation

The results showed that the nucleation rate was dependent on the suspension density and the supersaturation.

The values of i and J for the two systems were as follows:

ammonium sulphate - ethanol - water : $i = 1.25$ $J = 1.0$

ammonium sulphate - methanol - water : $i = 4$ $J = 1.0$

Summarising the results of the various investigators it can in general be said that: the nucleation rate is dependent on (i) the supersaturation of the solution (ii) the suspension density of the crystals in the solution and (iii) the hydrodynamic conditions of the system i.e. stirrer speed, power input, etc..

CHAPTER III

APPARATUS AND ANALYTICAL TECHNIQUES

In all the batch and continuous experiments performed, excepting for the seed crystal investigation described in Chapter IV, the same stock solution of ammonium tungstate was used. This stock solution was prepared as follows. Crude tungstic acid, obtained from Hard Metals, was dissolved in a 5,5% aqueous ammonia solution. The insoluble impurities were allowed to settle and the solution then filtered through a Millipore filtration apparatus which removed all foreign particle larger than 0,2 microns. The concentration of this stock solution was arranged to be approximately 90 gm WO_3/litre This value was chosen because an ammonium tungstate solution of this concentration is reasonably stable and can be stored in sealed containers for an indefinite period.

Prior to the commencement of a run, approximately 20 litres of the solution were transferred to a cylindrical PVC container. This container was fitted with a stainless steel coil through which, water at a temperature of 25°C from a constant temperature bath, could be pumped. This ensured that the temperature of the feed solution remained constant at 25°C throughout the run. A stirrer was used to agitate the solution in order to facilitate heat transfer between the coil and the liquid.

The basic apparatus required for the batch and continuous crystallization runs is described below.

3,1 APPARATUS

3.1.1 The Crystallizer

The crystallizer consisted of a jacketed, round-bottomed, cylindrical glass vessel. The dimensions of this vessel are given in Figure 1.

APT crystals have a high settling velocity due to their density

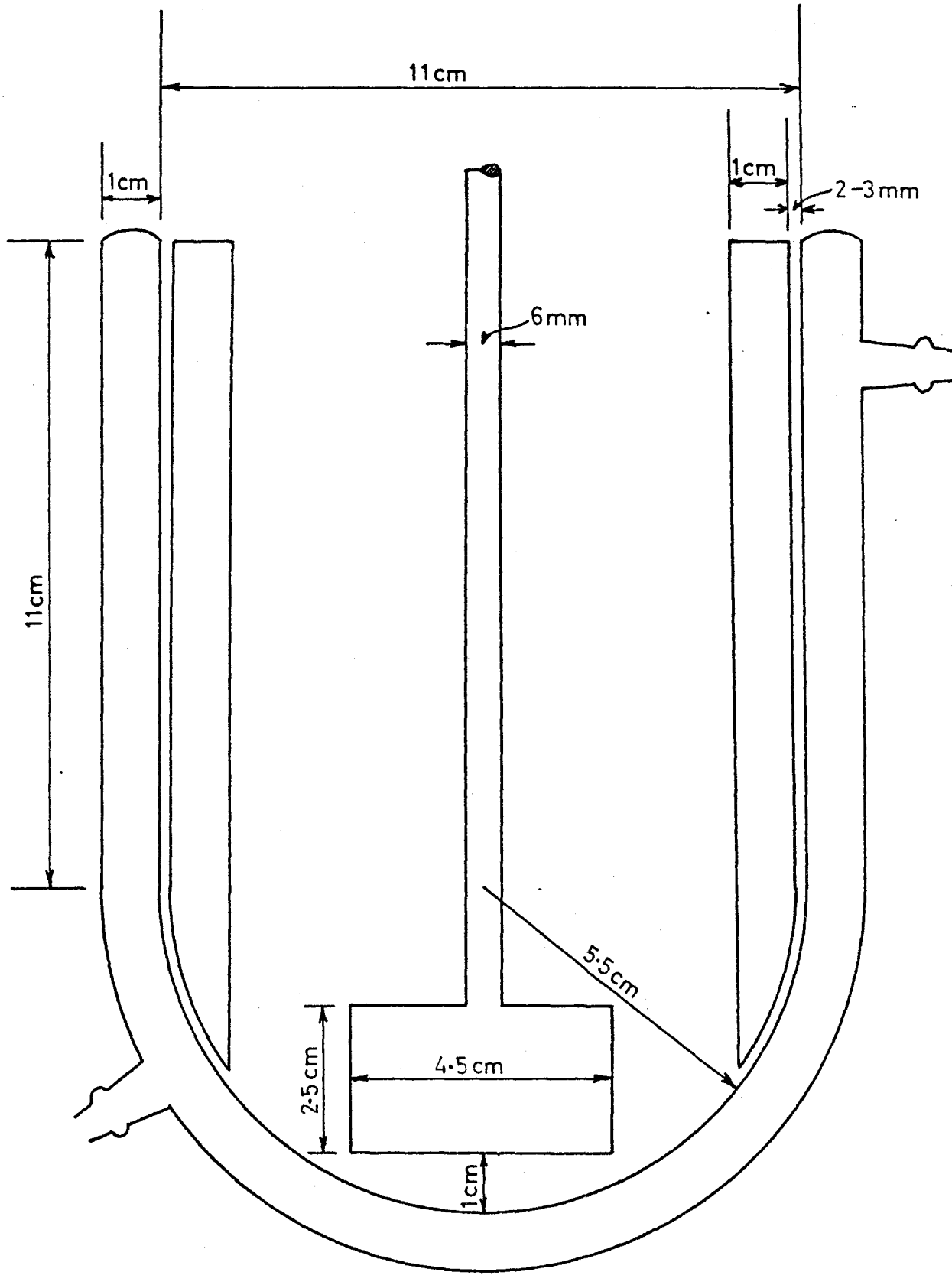

DETAILS OF THE CRYSTALLISER.

FIGURE 1

of 4.6 gms./cc. In order to keep these crystals in suspension it was found necessary to place baffles along the walls of the vessel and to agitate the solution with a flat paddle. Four stainless steel baffles each of width 1 cm. and extending the full length of the wall were placed symmetrically in the crystallizer at right angles to one another. They were set 2 to 3 mm. away from the walls of the vessel in order to prevent entrainment of the crystals between the baffles and the walls of the container.

The stainless steel paddle of width 4.5 cm. and height 2.5 cm. was positioned in such a way that its bottom edge was 1 cm. from the bottom of the crystallizer. The paddle was rotated by a flexible drive connected to a Multifix, constant torque, variable speed motor. It was found in practice that the speed of rotation of this motor never varied by more than 1% from the set point value during a run. The motor was calibrated with the use of a stroboscope.

3.1.2 The Heating Circuit

The evaporation of the ammonium tungstate solution was brought about by circulating glycerol at temperatures ranging from 120°C to 170°C, from a Colora constant temperature bath through the outside jacket of the crystallizer. The constant temperature bath consisted of a closed stainless steel container having a capacity of 15 litres. Heating was produced by three heating coils each having a capacity of 500 watts. An electrical contact thermometer in conjunction with a relay was used to control the temperature of the glycerol. This control mechanism was capable of controlling the bath temperature to ±0.2°C of the desired value. The bath was fitted with a centrifugal pump, which circulated the glycerol at a rate of 15 litres per minute through the outside jacket of the crystallizer.

3.1.3. The Flowrate Control of the Feed Solution

In order to operate a continuous crystallizer under steady state conditions it is essential that the flowrates of the solution to and from the crystallizer remain constant throughout the duration of a run.

The ammonium tungstate solution was continuously pumped into the crystallizer using a variable speed, Bühler Peristaltic Pump. Before entering the crystallizer the solution passed through an over-pressure bottle and a rotameter. The purpose of the over-pressure bottle being to even out any fluctuations in the flow caused by the peristaltic pump and hence allow the rotameter to be read more easily. The rotameter was calibrated over the range of flowrates used in the experiments performed. It was found in practice that the flowrate delivered by the pump did not vary at any stage by more than 1/2% during a run.

3.1.4. The Mixed Product Removal

The mixed product removal from a continuous crystallizer is the most critical step in ensuring operation under steady state conditions. In order to achieve a steady state distribution of crystal sizes in the crystallizer the product removal must be such that (i) the number of crystals removed in the exit stream per unit time must equal the number of crystals produced per unit time by nucleation; and (ii) there must be no classification of crystal sizes in the removal stage, i.e. the distribution of crystal sizes in the exit stream must be identical to the size distribution present in the crystallizer.

Mixed product removal by flowing over a weir has been found by Murray and Larson (15) and others to be unsatisfactory. Their

results showed that this method of removal resulted in classification of the crystals; the larger ones remaining behind in the vessel.

Rushton (19) defined some of the problems associated with sampling of solid material suspended in a liquid stream. According to Rushton, in order to obtain a representative sample, the sampling point must be located where the fluid flow is steady with no sudden changes in either velocity or direction. It is also of importance that the sampling point itself does not disturb the fluid stream. A straight tube with its longitudinal axis parallel to the direction of fluid flow and designed such that the aperture velocity is equal to that of the approaching fluid fulfils these conditions. If the aperture velocity is too high the larger particles tend to remain behind. This is because the larger particles find it more difficult to adapt to a change in velocity and hence get left behind in the fluid stream. The opposite effect is noticed for aperture velocities which are too low.

Removal of the crystal product by means of a suction tube was tested in some preliminary experiments. The suction tube was placed vertically in a position next to one of the baffles and about 1/10" away from the wall of the vessel. In this position the tube was in line with the direction of the fluid velocity.

In order to test the take-off mechanism the following procedure was adopted. A 5.5% ammoniacal solution was continuously pumped into the crystallizer, stirred by the paddle and removed from the vessel by means of a suction tube. Once steady state had been achieved, 40 to 50 grams of lead glass ballotini of density 4.59 gm/cc (same as APT) and varying in size from 10 to 120 microns,

were introduced into the crystallizer. Samples of the ballotini were collected from the outlet stream at different times. At the completion of approximately five residence times the experiment was halted. The ballotini remaining in the crystallizer were then removed. The particle size distributions of the samples obtained at different times were compared with the one obtained for the sample remaining in the crystallizer. If the mixed product removal technique was operating efficiently then all the particle size distributions would be the same.

Suction tubes of different internal diameters were tested and the optimum diameter determined. It was also established that a stirrer speed of 1600 r.p.m. was required to completely fluidize all the particles. All continuous crystallization experiments were thus performed at this stirrer speed. The product removal technique was also tested during a number of actual crystallization runs, and it was found to be operating successfully in all cases.

It should be pointed out that the suction tube method of mixed product removal has another obvious advantage. The liquid level in the crystallizer is automatically kept constant throughout the run.

3.2. ANALYTICAL TECHNIQUES

3.2.1. Crystal Size Analysis

Various methods of particle size analysis were considered in order to establish which would be most suitable for determining the particle size distribution curves of the APT crystals over the size range 20 to 150 microns.

A PHOTOGRAPH OF THE APPARATUS



FIGURE 2

Screening of the crystals using standard screens was found to be unsatisfactory. This was due to the fact that APT crystals, being rather brittle tend to break up into smaller crystals when subjected to harsh treatment such as the abrasive action of the wire mesh on the crystal surface.

The Coulter Counter was considered, but owing to the difficulty of obtaining a suitable liquid capable of keeping the APT crystals in suspension and also satisfying the basic requirements of the apparatus, this method had to be discarded.

The microscopic technique of determining the particle size distribution was considered to be too tedious and time consuming to be of any use for the present application.

Particle size analysis, using a sedimentation technique seemed to be one of the more suitable methods left open. Preliminary work was done using a Sartorius Sedimentation Balance. Inert liquids of various viscosities were tested. Cyclohexanol, at a temperature of 40°C was found to be the most suitable.

In order to test the reproducibility of the balance, a sample of APT crystals was split up into several smaller samples. Each of these were analysed separately on the balance. It was found that the curves obtained did not vary by more than 2% from one another.

It should be noted that Stokes Law, on which all sedimentation processes are based, is only applicable for Reynold's numbers below 0.2.

Considering a particle of density ρ_s and diameter d, settling in a liquid of density ρ_L and viscosity η.

The terminal velocity of this particle is given by:-

$$v = \frac{d^2 g (\rho_s - \rho_L)}{18\eta} \qquad (3.1)$$

where: g = gravitational constant = 981 cm/sec.^{2}

The Reynolds number is defined as:

$$N_{RE} = \frac{v d \rho_L}{\eta} \qquad (3.2)$$

combining the above equations:

$$d^3 = \frac{18\eta^2}{\rho_L g (\rho_s - \rho_L)} N_{RE} \qquad (3.3)$$

Furthermore we have:

Viscosity of cyclohexanol at 40°C η = 20 CP = 0.2 Poise

Density of cyclohexanol ρ_L = 0.962 gm/cc.

Density of APT ρ_s = 4.6 gm/cc.

Replacing these values in equation (3.3) gives

$$d^3 = 2.095 \times 10^{-4} N_{RE} \qquad (3.4)$$

The maximum size of APT crystals for which Stokes Law is applicable is obtained by substituting the limiting condition, N_{RE} = 0.2 in equation (3.4).

This gives:

d_{max} = 347 microns

The minimum size for which Stokes Law is applicable is determined only by the onset of Brownian motion. This occurs below about 5 microns.

The range of applicability of Stokes Law, for APT settling is cyclohexanol at 40°C is between 5 and 347 microns. Since the crystals obtained experimentally ranged in size between 20 and 150 microns, this is more than adequate.

(a) Comparison between the Microscope and the Sedimentation Balance

The sedimentation balance technique analysis was compared with the microscopic technique as follows. The cumulative weight particle size distribution curve of a sample of APT crystals was determined using the sedimentation balance. A number of photographs of the same sample were taken on a microscope at a magnification of 100 times. The length and breadth of each crystal was measured and the actual crystal size taken as the square root of the product. A total of approximately two thousand crystals were measured in this way. The cumulative weight distribution curve was calculated from the results. The two curves obtained are shown in Figure 3.

The curve obtained from the sedimentation analysis compared very favourably with that obtained from the microscopic analysis, the shapes of the curves being practically identical. The shift of the curves with respect to each other, is due to the fact that each method measures a different characteristic size. The microscopic method measures the projected size of the crystal, whereas the sedimentation method gives the equivalent diameter of a sphere whose terminal velocity in the liquid is the same at that of a crystal.

COMPARISON BETWEEN SEDIMENTATION AND MICROSCOPE WEIGHT DISTRIBUTION FUNCTIONS

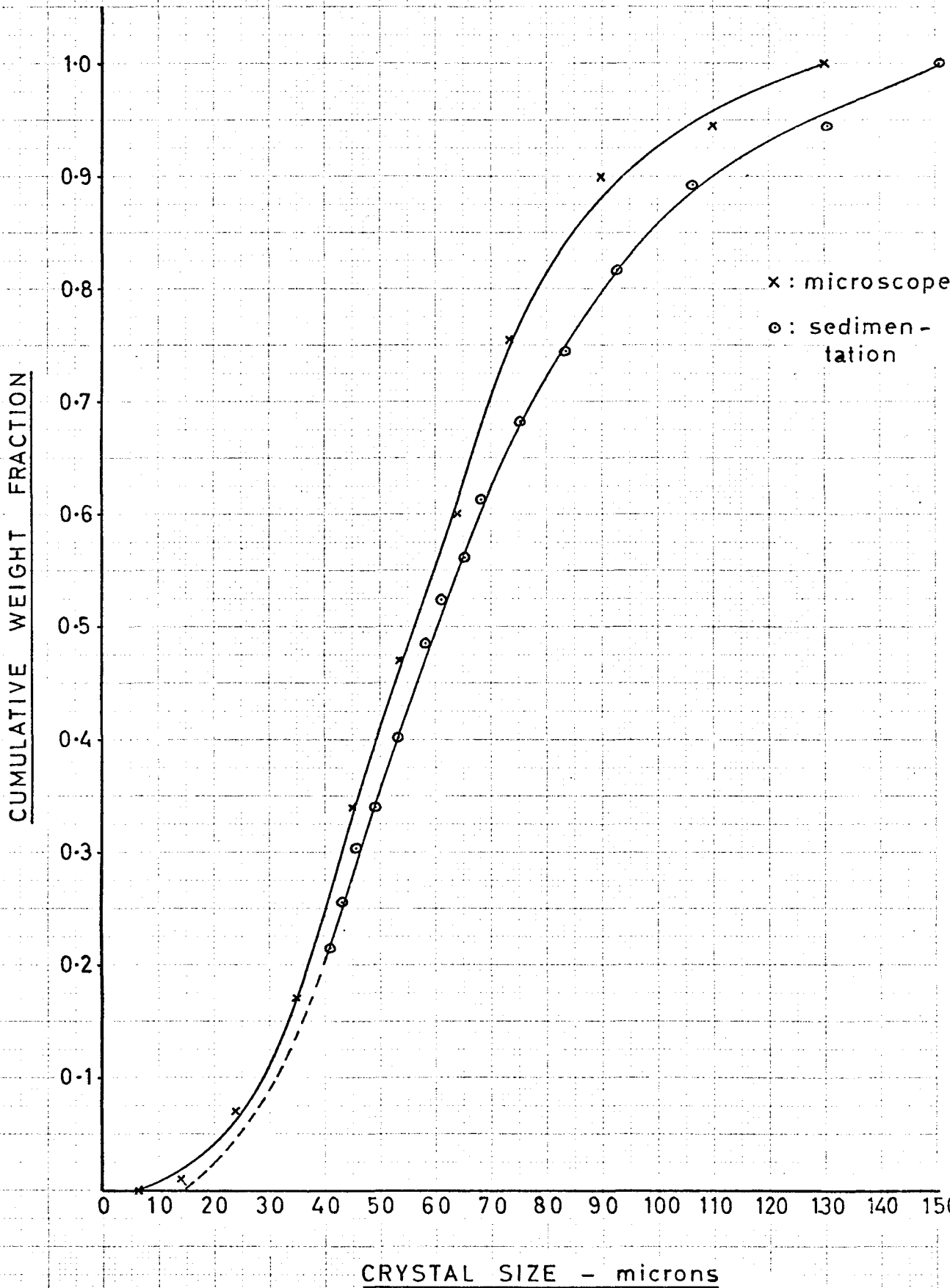

FIG. 3

In view of the fact that the sedimentation and microscopic techniques compared so well, it was decided to use the Sedimentation Balance for all particle size analyses.

If the microscopic size at a particular weight fraction is plotted against the sedimentation size of the same weight fraction (obtainable from Figure 3), the relationship between sedimentation and microscopic size can be obtained. This relationship is shown in Figure 4. to be a linear one.

In this work all sizes obtained from the sedimentation balance were converted to microscopic sizes by the use of Figure 4. By doing this the shape factor for the volume of a crystal of microscopically determined size, ℓ, is unity, as the volume is just ℓ^3.

(b) Description of the Sedimentation Balance

The Sartorius Sedimentation Balance possesses one main beam. A collecting pan is suspended from the right of the beam and into a sedimentation jar. This jar consists of a cylindrical, flat bottomed, jacketed glass container into which the sedimentation liquid is placed. Water is pumped from a constant temperature bath, through the outside jacket of the jar, to keep the liquid at a uniform temperature.

Taring weights are suspended from the left of the balance beam and are used to compensate for the buoyancy of the collecting pan and the differences in buoyancy when using liquids of different densities. The main beam carries in its centre two mirrors which are illuminated by a lamp. The smaller mirror reflects the light onto a groundglass plate. At a deflection of the beam towards the side of the collecting pan, the larger mirror

THE RELATIONSHIP BETWEEN SEDIMENTATION AND MICROSCOPE SIZES

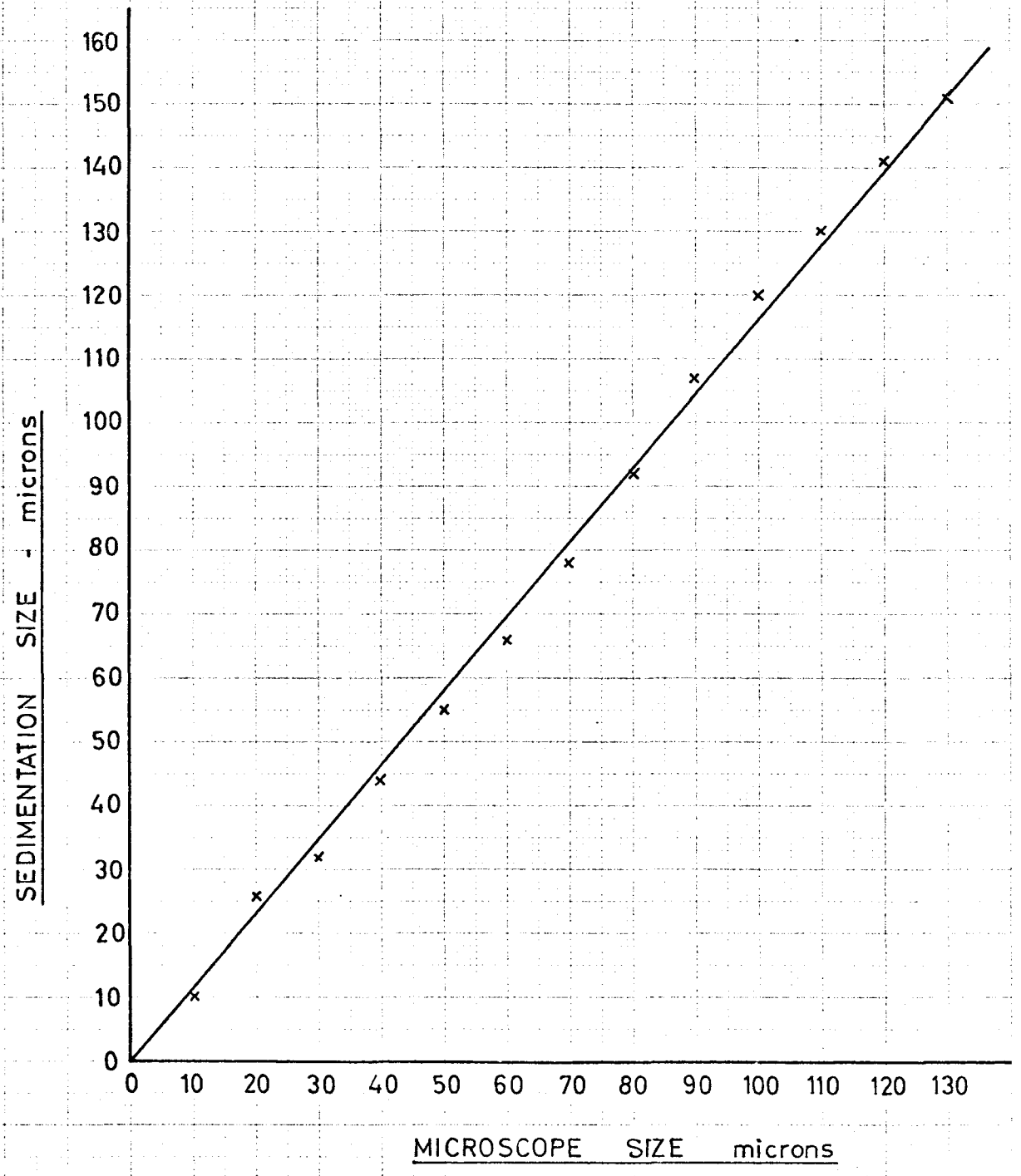

FIG. 4

casts the light through a diaphragm onto a photocell. Upon reaching a certain intensity of illumination a solenoid is activated by means of an amplifier and a relay. This solenoid twists a torsion wire by a determined angle. This wire carries in its centre an auxiliary beam which is attached to the main beam. By torsion of the wire, which is extended between two bearing blocks, the auxiliary beam returns the main beam back to its zero position. This ends the illumination of the photocell and the relay ceases to activate the solenoid. This process is repeated automatically whenever two milligrams of the sample being analysed have sedimented onto the collecting pan.

These steps of 2 mg. are transferred to a recorder pen by means of a recording device. At every step the pen advances horizontally by 0.08 cm. on the chart paper. The curve drawn by the recorder pen is the increase in weight of the sediment against elapsed time. The cumulative weight particle size distribution function of the sample can be readily obtained from this curve (see Appendix A).

3.2.2. Determination of the Solution Concentration

In all experiments performed in this work it was necessary to determine the concentration of the ammonium tungstate solution, as the growth rate of the crystals is dependent thereon. The method employed was the standard determination of tungsten trioxide in solution using hydrochloric acid and a cinchonine solution.

The cinchonine solution was prepared by dissolving 125 grams of cinchonine in a solution consisting of 500 ml. of concentrated hydrochloric acid and 500 ml. of distilled water. The actual determination of the tungsten trioxide in solution was performed as follows.

20 ml. of the ammonium tungstate solution were pipetted into a glass beaker and distilled water added until the total volume of the solution was approximately 150 ml.. 35 ml. of concentrated hydrochloric acid and 15 ml. of the cinchonine solution were then added. This solution was boiled gently for a period of about 30 minutes and then filtered. The filter cake was washed five times with a 1% hydrochloric acid solution and then transferred into a porcelain crucible. The crucible was placed in a calcining furnace at a temperature of 750°C and left there for a period of ten hours. The tungsten trioxide (WO_3) remaining in the crucible was then determined gravimetrically. The solution concentration was thus determined in grams of WO_3 per litre of solution.

CHAPTER IV

THE DEPENDENCE OF THE GROWTH RATE OF APT ON THE CRYSTAL SIZE

4.1 THE PARTICLE BALANCE EQUATIONS

4.1.1 Batch Crystallization

The particle balance equation for a batch crystallizer can be written as

$$\frac{\partial f(\ell, t)}{\partial t} + \frac{\partial [pf(\ell, t)]}{\partial \ell} = Q(t)\ \delta(\ell - \ell_o) \qquad (4\text{-}1)$$

where:

$f(\ell, t)\ d\ell$ = the number of crystals in the crystallizer having sizes between ℓ and $\ell + d\ell$ at any time t.

p = growth rate of a crystal of size ℓ

$Q(t)$ = number of crystals introduced per unit time at time t, due to nucleation

δ = Dirac Delta function

ℓ_o = critical nuclei size

4.1.2 Continuous Crystallization

Doing a particle balance over a continuous, mixed product removal crystallizer operating under steady state conditions, results in the following equation:

$$\frac{d[Vpg(\ell)]}{d\ell} = -wg(\ell) + VN\delta(\ell - \ell_o) \qquad (4\text{-}2)$$

where:

$g(\ell)\ d\ell$ = the number of crystals per unit volume of solution, in the crystallizer having sizes between ℓ and $\ell + d\ell$

V = the volume of the solution.

w = the flowrate of the exit stream.

N = the number of crystals nucleated per unit time - per unit volume of solution.

The derivations of equations (4-1) and (4-2) can be found in Hulburt and Katz (8).

The solutions of the above two differential equations are dependent on the relationship between the growth rate p and the crystal size ℓ. It was therefore necessary to perform some growth rate experiments in order to determine this relationship.

4.2 THE EFFECT OF CRYSTAL SIZE ON THE GROWTH RATE OF APT CRYSTALS

In preliminary crystallization experiments it was established that the majority of APT crystals obtained were in the size range 30 to 100 microns. It was therefore decided to investigate the effect of crystal size on the growth rate, within these limits. Crystals of known sizes were placed in the stirred tank crystallizer and allowed to grow in a supersaturated solution of ammonium tungstate, the concentration of which was kept at a constant level.

4.2.1 Experimental Procedure

APT crystals obtained from previous experiments were screened into various size ranges using Tyler Standard screens. The following size ranges were used in the investigation: <38μ, 38-44 μ, 53-61 μ, and 74-88 μ

An ammonium tungstate solution was prepared as mentioned earlier by the addition of crude tungstic acid to an ammonium solution. Stock solutions of three different concentrations in the range 130-170 gms $W\emptyset_3$/litre were made up, each by adding approximately 300 gms of crude tungstic acid to 1000 ml of a 5.5% ammoniacal solution and then stirring the mixture until the desired solution density, which is directly related to the solution concentration, was obtained. Due to the solution being unstable at these high concentrations, it was found necessary to store it under conditions of vacuum.

400 ml of the ammonium tungstate solution were poured into the crystallizer and glycerol circulated through the outside jacket of the vessel at a temperature of 150°C. The stirrer motor was switched on and the paddle allowed to rotate at 1600 rpm. A 5.5% aqueous ammonia solution was continuously pumped into the crystallizer at a rate equal to the evaporation rate of the solution. This meant that the solution volume remained constant throughout the run. The solution concentration also remained virtually constant due to the fact that only a small amount of ammonium tungstate was used for growth of the seed crystals. Ten grams of one of the size ranges of the crystals mentioned earlier were introduced into the crystallizer and allowed to grow under these controlled conditions for a definite period of time.

At the completion of each run the crystals together with the solution were removed from the crystallizer by means of a suction tube and immediately separated by filtration through a millipore membrane filter. The crystals were then washed with a small quantity of distilled water and then dried.

The solution concentration was determined prior to the commencement of each run and also on completion of the run. The average of these two concentrations was taken to be the solution concentration for the run.

The cumulative weight particle size distributions of the crystals both before and after growth, were determined using the sedimentation balance. Analysis of the sedimentation curves after growth showed that practically no crystals smaller than the smallest crystal detected on the cumulative weight distribution before growth was obtained. This indicated that essentially no nuclei were being formed and that only growth on the crystals originally injected into the crystallizer was taking place.

The growth rate of the crystals was evaluated as follows: The particle balance equation for the case where no nucleation occurs is:

$$\frac{\partial f(\ell,t)}{\partial t} + \frac{\partial\{pf(\ell,t)\}}{\partial \ell} = 0 \qquad (4\text{-}3)$$

Since the crystals were allowed to grow by only a small amount (i.e approximately 10 microns), and the average growth rate $\bar{p}$ for the run was required, equation (4-3) can be approximated by:

$$\frac{\partial f(\ell,t)}{\partial t} + \bar{p}\,\frac{\partial f(\ell,t)}{\partial \ell} = 0 \qquad (4\text{-}4)$$

Multiplying each term of equation (4-4) by ℓ^4 and integrating with respect to ℓ between the limits 0 and ∞ results in:

$$\frac{d}{dt}\int_0^\infty \ell^4 f(\ell,t)d\ell + \bar{p}\{f(\ell,t)\ell^4\}_0^\infty$$

$$- 4\bar{p}\int_0^\infty \ell^3 f(\ell,t)d\ell = 0 \qquad (4\text{-}5)$$

Substituting the boundary condition as $\ell \to \infty$ $f(\ell,t) \to 0$ into the above equation gives:

$$\frac{d}{dt}\int_0^\infty \ell^4 f(\ell,t)d\ell = 4\bar{p}\int_0^\infty \ell^3 f(\ell,t)d\ell \qquad (4\text{-}6)$$

The mean with respect to the weight distribution α_1, is defined as:

$$\alpha_1 = \frac{\int_0^\infty \rho_s \ell^4 f(\ell,t)d\ell}{\int_0^\infty \rho_s \ell^3 f(\ell,t)d\ell} \qquad (4\text{-}7)$$

and the mass of the crystals at any time t is

$$M(t) = \int_0^\infty \rho_s \ell^3 f(\ell,t)d\ell \qquad (4\text{-}8)$$

Replacing for M(t) and α_1 from equations (4-7) and (4-8) into equation (4-6) gives:

$$\frac{d}{dt}\{\alpha_1 M(t)\} = 4\bar{p}M(t) \qquad (4\text{-}9)$$

Integrating with respect to t between the limits t_1 and t_2 results in:

$$\alpha_1 M(t)/_{t=t_2} - \alpha_1 M(t)/_{t=t_1} = 4\bar{p} \int_{t_1}^{t_2} M(t)dt \qquad (4\text{-}10)$$

The values of α_1 at $t = t_1$ and $t = t_2$ were obtained from the cumulative weight fraction distribution curves of the crystals. M(t) was known by weighing the crystals before and after each run and because the increase in mass of the crystals during a run was relatively small the integral under the M(t) versus t curve was evaluated by assuming a linear relationship between the crystal mass and time. The growth rate $\bar{p}$ could therefore be calculated directly using equation (4-10).

4.2.2 Results

The results obtained from this investigation were plotted on a graph in the form growth rate versus crystal size at a particular concentration. This is shown in Figure 5. For each level of concentration it can be seen that the growth rate is independent of the crystal size.

This result can be examined using a theoretical approach as follows. If one considers growth to take place by the addition of crystalline material at dislocations on the crystal surface, then the rate of mass increase of a crystal is proportional to the total number of dislocations present.

It is a well established fact that the dislocation density can be considered to be relatively constant over the whole of the crystal surface. The rate of mass deposition onto a crystal is thus proportional to its surface area.

THE EFFECT OF CRYSTAL SIZE ON THE GROWTH RATE OF APT.

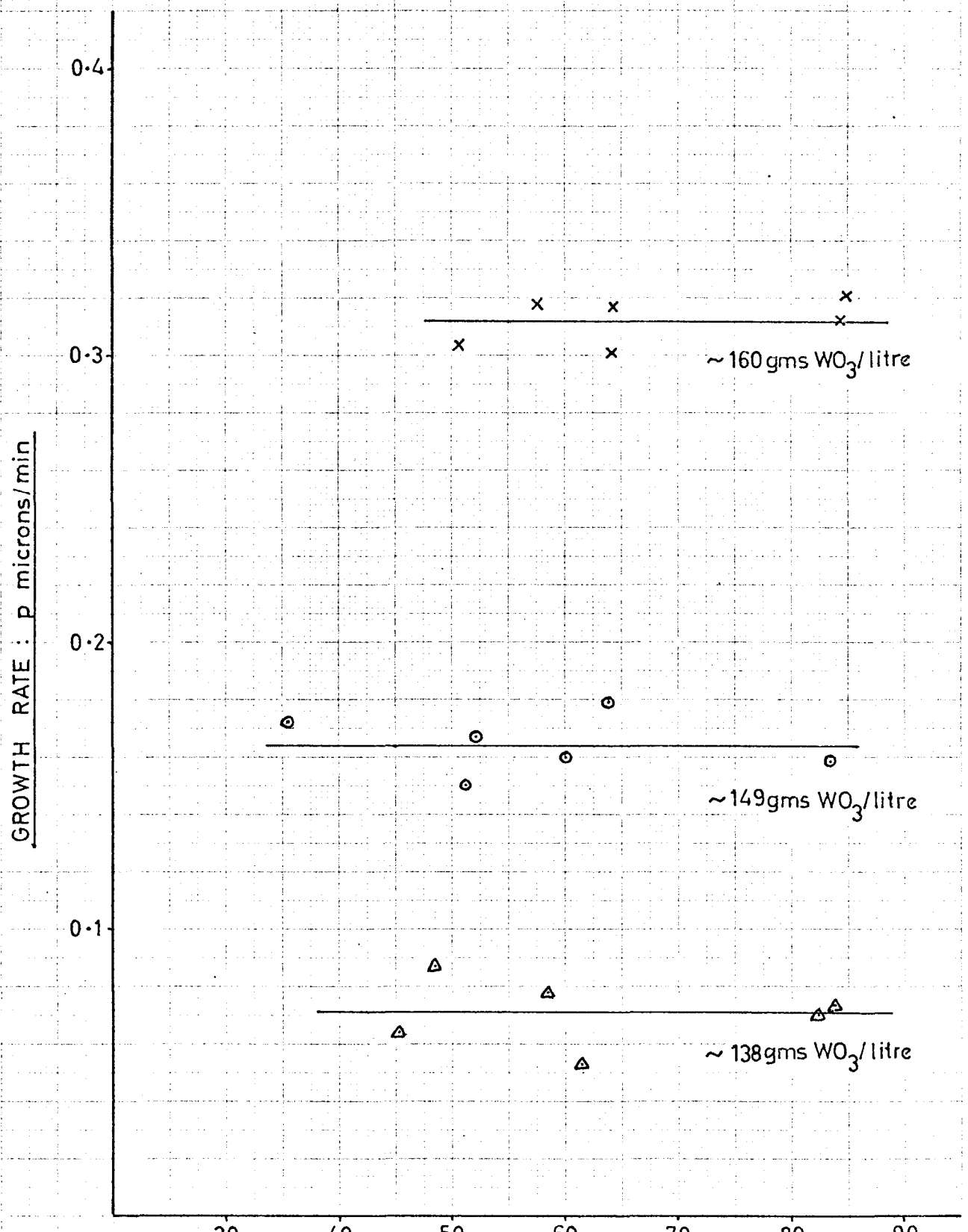

FIG. 5

Considering a crystal of mass m and size ℓ we have that

$$m = \text{constant} \quad \ell^3 \tag{4-11}$$

The rate of mass increase of this crystal is given by

$$p_m = \frac{dm}{dt} = \text{constant } \ell^2 \frac{d\ell}{dt} \tag{4-12}$$

or

$$p_m = \text{constant } \ell^2 p \tag{4-13}$$

where p is the growth rate of a crystal of size ℓ.

Since it has been shown that p_m is proportional to the crystal surface area, ℓ^2, p itself must be independent of the size ℓ; which is the result that was obtained from the experimental investigation.

At the stage when this investigation was carried out the effect of the impurity concentration on the crystal growth rate was not realized and hence the impurity concentration in the three different solutions were not noted. For this reason it is not possible to use these results to establish the relationship between growth rate and solution concentration or in fact to compare the actual growth rate values with those obtained from the batch and continuous experiments performed at a latter date. The only information that can be derived from this investigation is that at a particular concentration of the solution and of impurities in the solution, the growth rate is independent of the crystal size.

CHAPTER V

THE GROWTH RATE MODEL

Part I. Batch Crystallization

5.1 EXPERIMENTAL PROCEDURE

In all the batch experiments performed the following procedure was adopted. The concentration of the ammonium tungstate solution was determined in duplicate before the start of each run. The constant temperature bath was heated to a particular temperature depending on the heating rate required for the run. The circulation pump was switched on 15 minutes prior to the commencement of each run and glycerol allowed to flow through the outside jacket of the crystallizer. This was done to ensure that there were no dead volume regions present in the circuit.

600 ml of the ammonium tungstate solution were then poured into the crystallizer. The stirrer motor was immediately switched on and the paddle allowed to rotate at the required speed. It was observed that, immediately preceding the appearance of the first crystals, the solution suddenly became opalescent. This easily detectable point was taken as time zero for crystallization. The crystallization was then allowed to proceed for a predetermined time depending on the experiment being performed. At the completion of each run, the solution together with the crystals were removed from the crystallizer by means of a suction tube, and immediately separated by filtration. The total volume of this solution was measured and its concentration determined.

The crystals were washed with distilled water and then dried. The total weight of these crystals was determined as well as their cumulative weight particle size distribution function.

5.2 EXPERIMENTS PERFORMED

Batch experiments were performed at three different heating rates corresponding to temperatures of 120°C, 130°C and 140°C in the outside jacket of the crystallizer. Four runs, each for a different total crystallization time, were performed for each of these heating rates. This was done to investigate the dependence of the growth rate on the supersaturation of the solution. A stirrer speed of 1600 r.p.m. was used in all these experiments.

Further experiments were performed at three different stirrer speeds (250, 800 and 1600 r.p.m.) using a heating rate corresponding to an outside jacket temperature of 140°C. In this way the effect of the stirrer speed on the growth rate could be established.

5.3 BATCH CRYSTALLIZATION RESULTS

5.3.1 The Critical Nuclei Size of APT Crystals

In the experiments performed at the three different stirrer speeds, but at the same heating rate (140°C), the conditions in the crystallizer were identical in all cases. This meant that the variation of the mass of the crystals, the solution concentration and the solution volume, with crystallization time were the same for the three stirrer speeds. The dependence of these three variables on the crystallization time is shown in Figures 6, 7 and 8. It should be noted that these three variables are interdependent and that the mass versus time curve as presented in Figure 6 is probably the least accurate due to physical losses during the drying and weighing procedures of the crystals, after each run.

VARIATION OF THE CRYSTAL MASS WITH CRYSTALLIZATION TIME

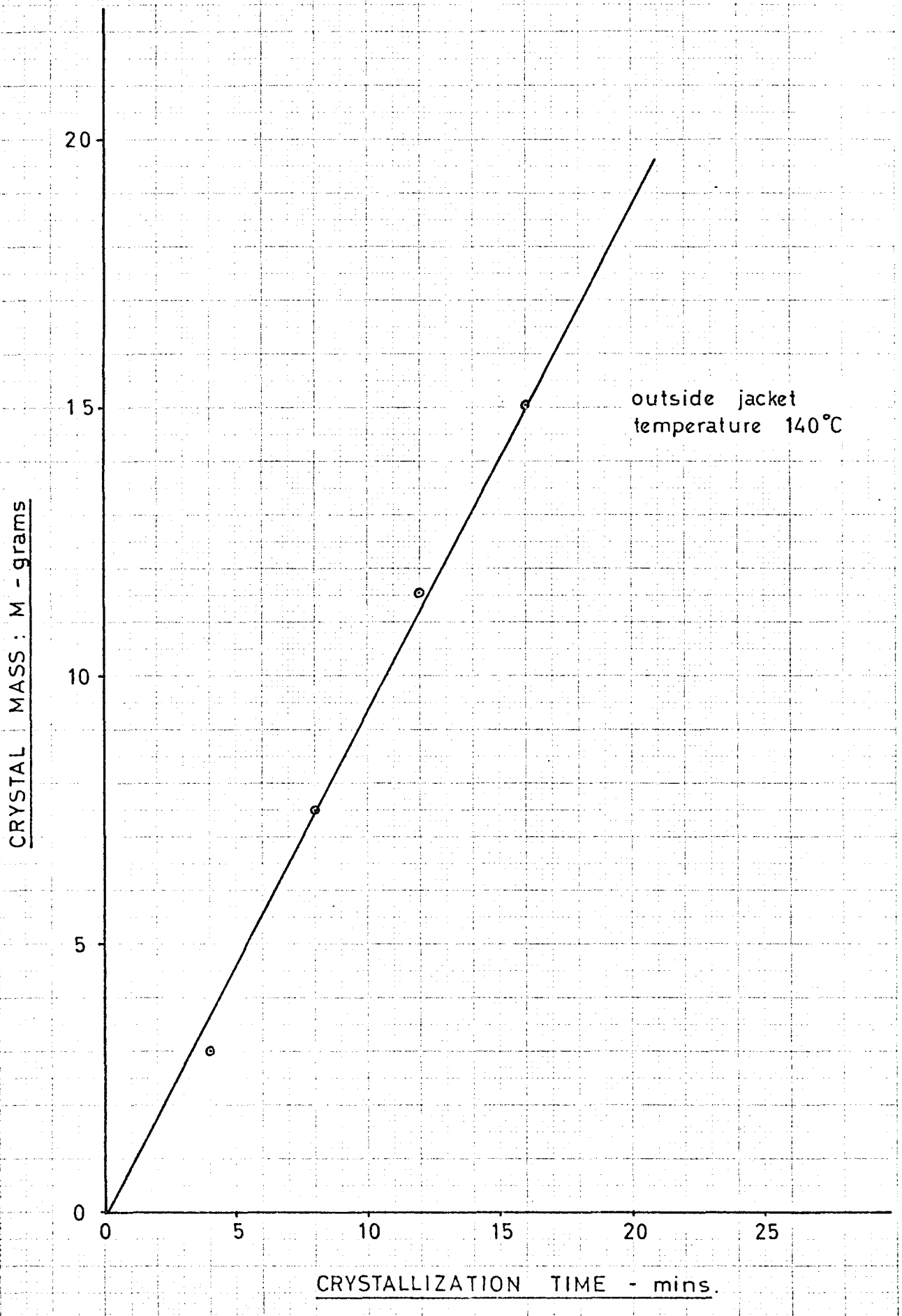

VARIATION OF THE SOLUTION CONCENTRATION WITH TIME

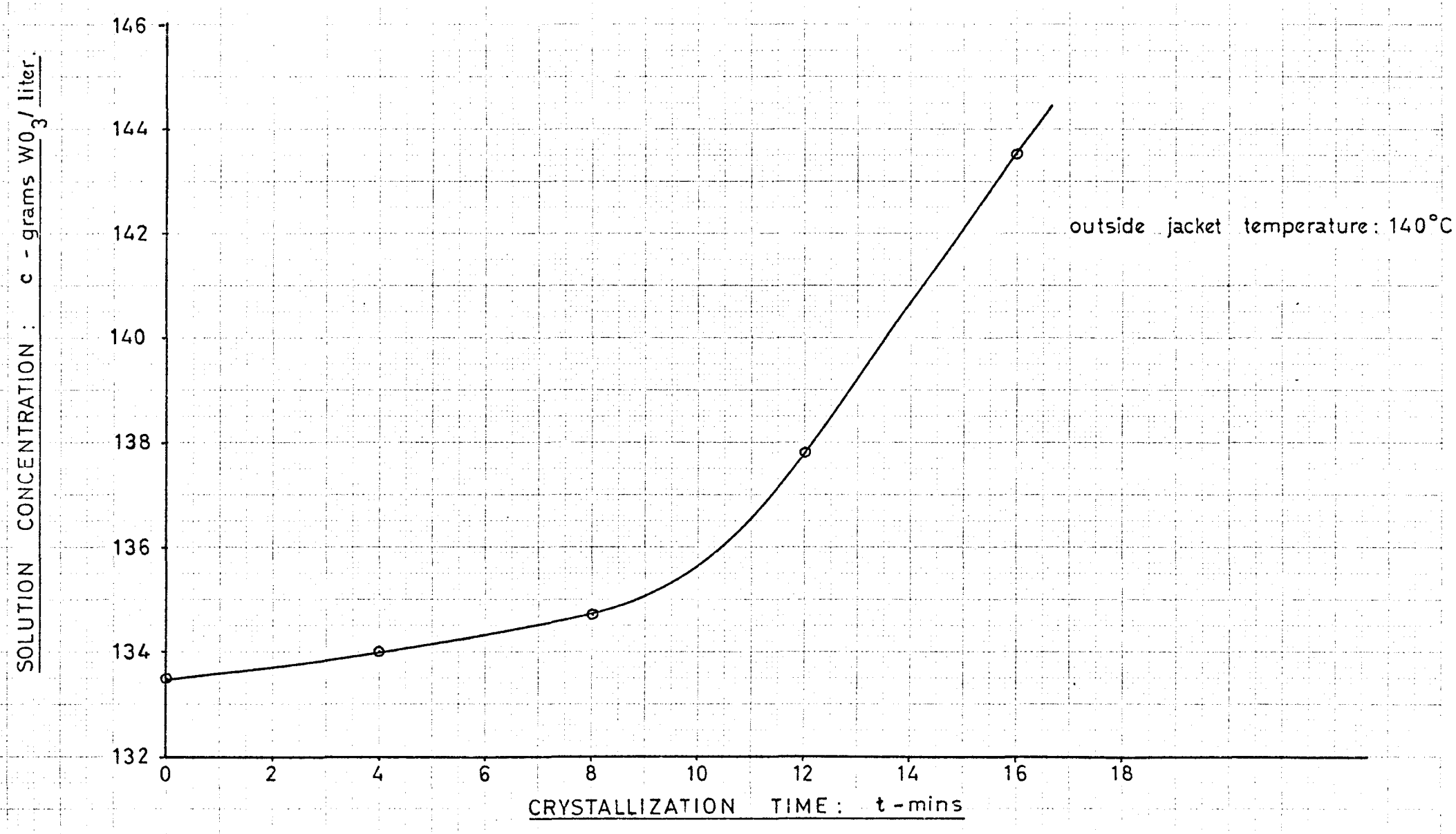

FIG. 7

VARIATION OF THE SOLUTION VOLUME WITH TIME

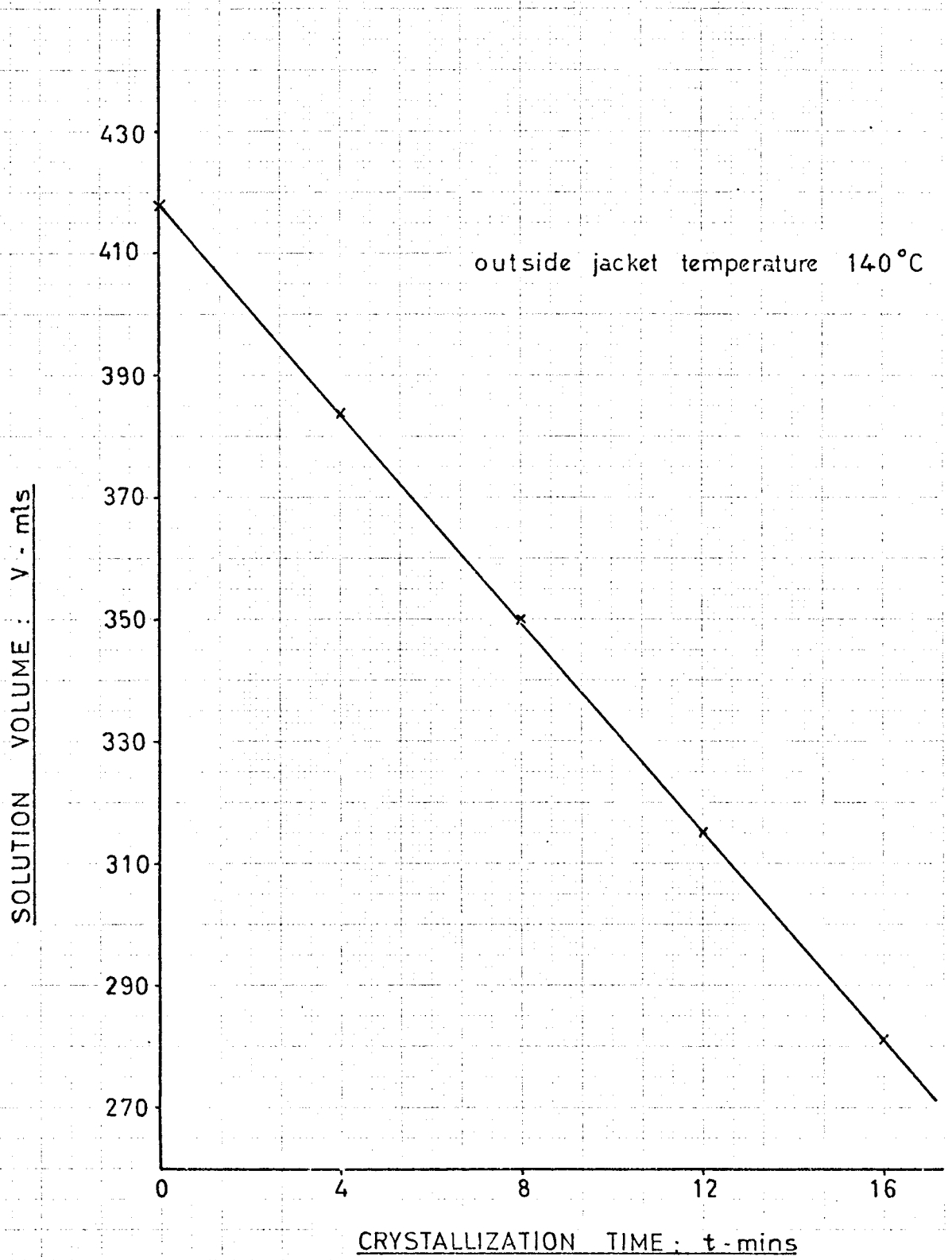

FIG. 8

The mean α_1, of the cumulative weight distribution curve at a particular time, was evaluated for the three stirrer speeds (see Appendix B). The relationship between α_1 and time, as shown in Figure 9 closely approximates to a linear function. The second moment of the weight distribution, α_2 was also evaluated at different times and for each of the three stirrer speeds (see Appendix B). The normalized variance σ was calculated with the use of the following equation.

$$\sigma = \frac{\alpha_2}{\alpha_1^2} - 1 \qquad (5\text{-}1)$$

The results are shown in Figure 10. It is seen that σ is not a function of time but is dependent only on the stirrer speed

i.e. $\sigma = n$ (5-2)

where n is a constant for a particular stirrer speed.

Furthermore it was noticed by examining the cumulative weight distribution curves of the crystals as shown in Figure 11, that the smallest crystal detected by the sedimentation analysis was of the order of 25 microns. Similarly for the runs performed at 800 r.p.m. and 250 r.p.m. (shown in Figures 12 and 13 respectively), the smallest crystals detected by the sedimentation analyses were 40 microns and 52 microns respectively. This result seems to indicate that the size at which crystals are nucleated is of the order 20-60 microns, depending on the stirrer speed.

VARIATION OF α_1 WITH TIME

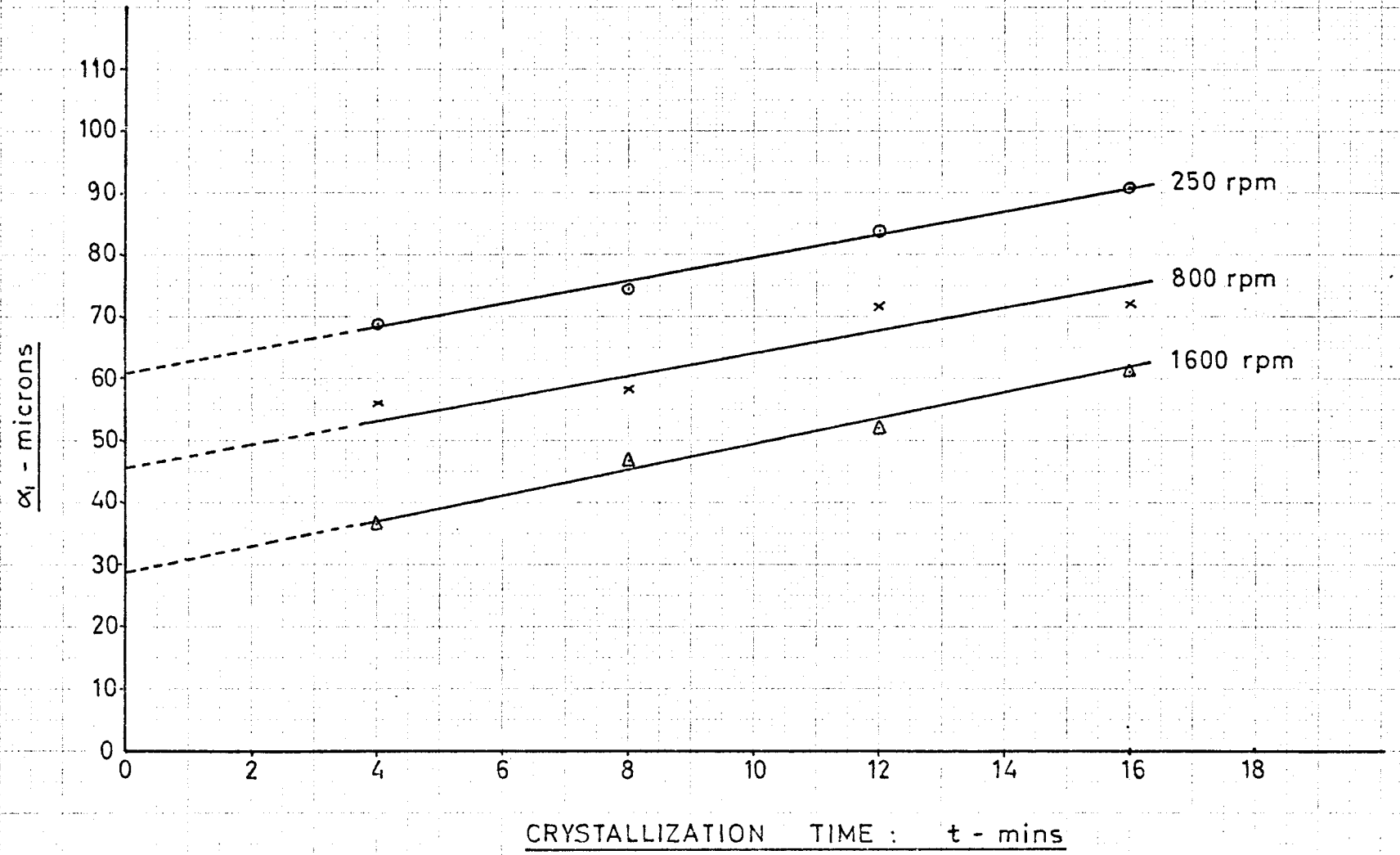

FIG. 9

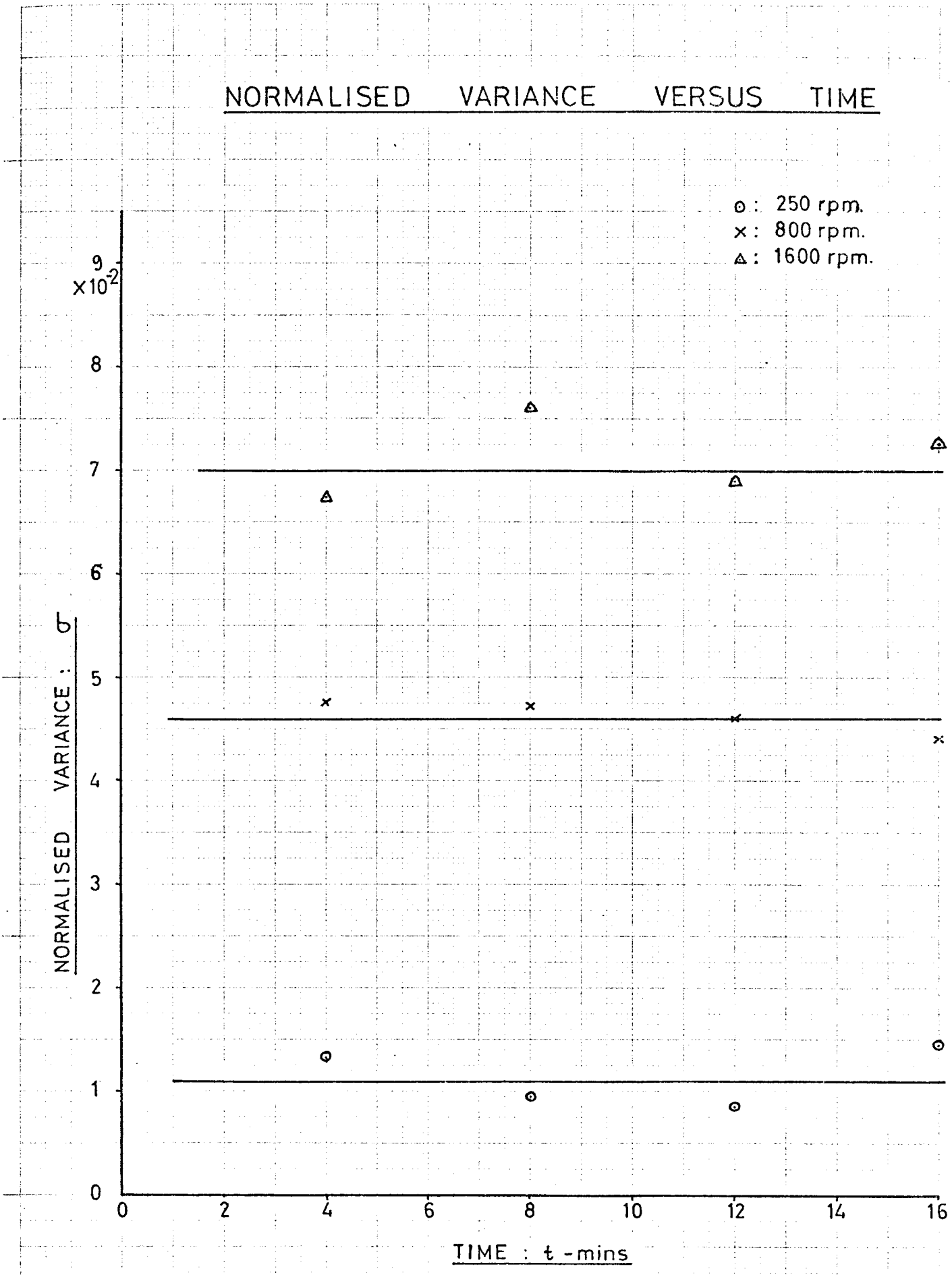
NORMALISED VARIANCE VERSUS TIME
o : 250 rpm.
× : 800 rpm.
△ : 1600 rpm.
9
×10⁻²
8
7
6
5
4
3
2
1
0
NORMALISED VARIANCE : σ
0
2
4
6
8
10
12
14
16
TIME : t - mins

FIG. 10

VARIATION OF THE CUMULATIVE WEIGHT FRACTION WITH CRYSTAL SIZE

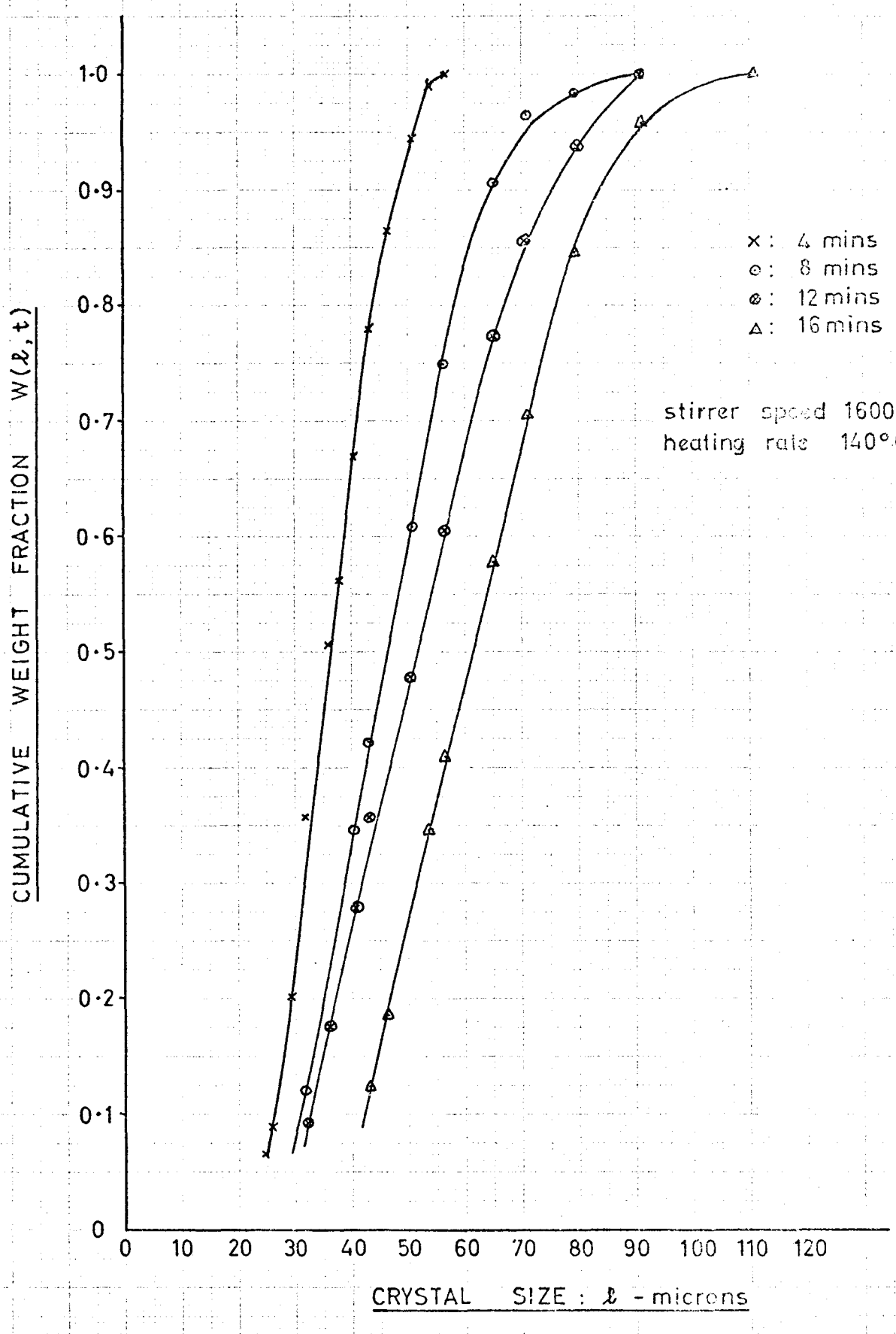

FIG. 11

VARIATION OF THE CUMULATIVE WEIGHT FRACTION WITH CRYSTAL SIZE

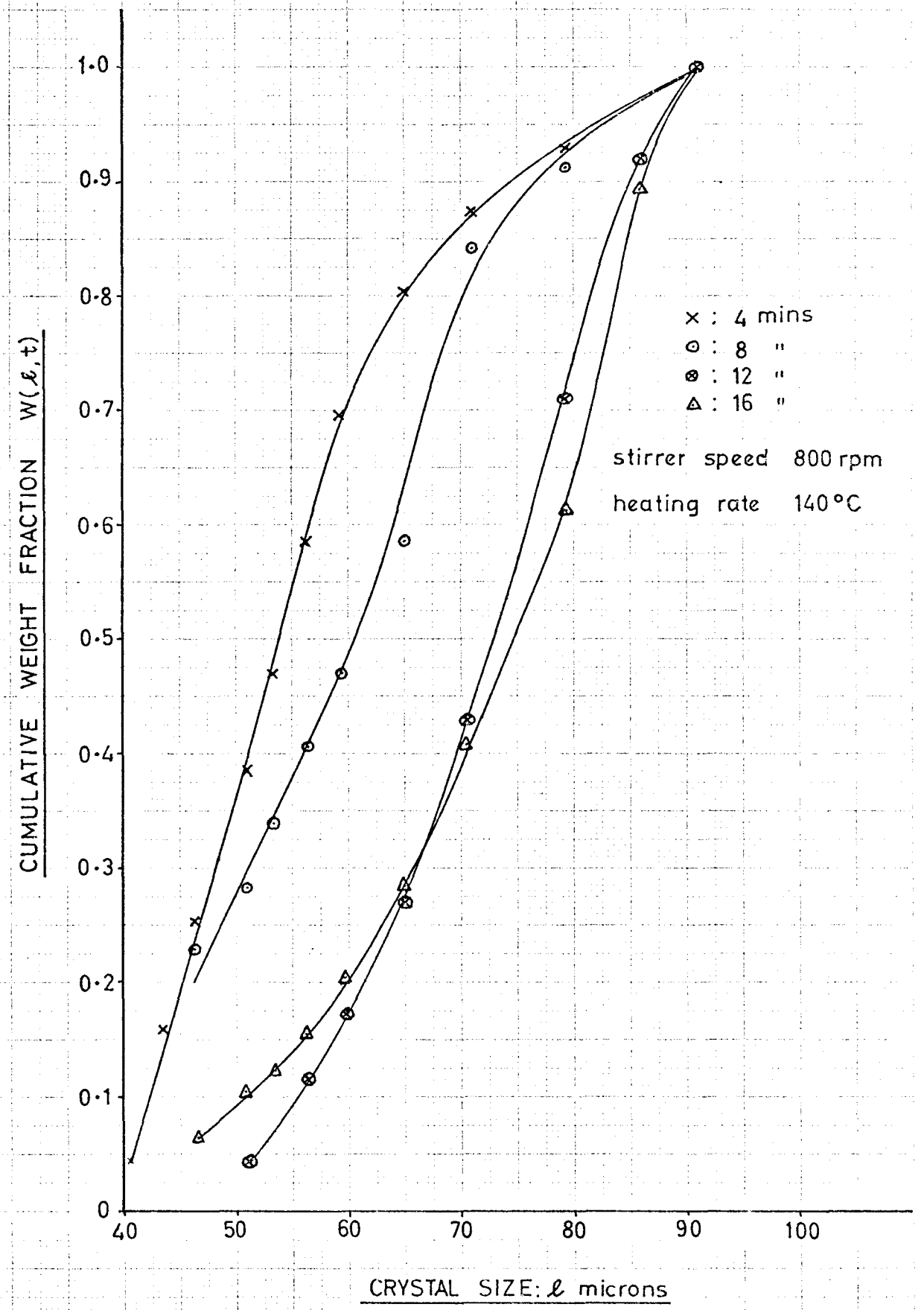

FIG 12

VARIATION OF THE CUMULATIVE WEIGHT FRACTION WITH CRYSTAL SIZE

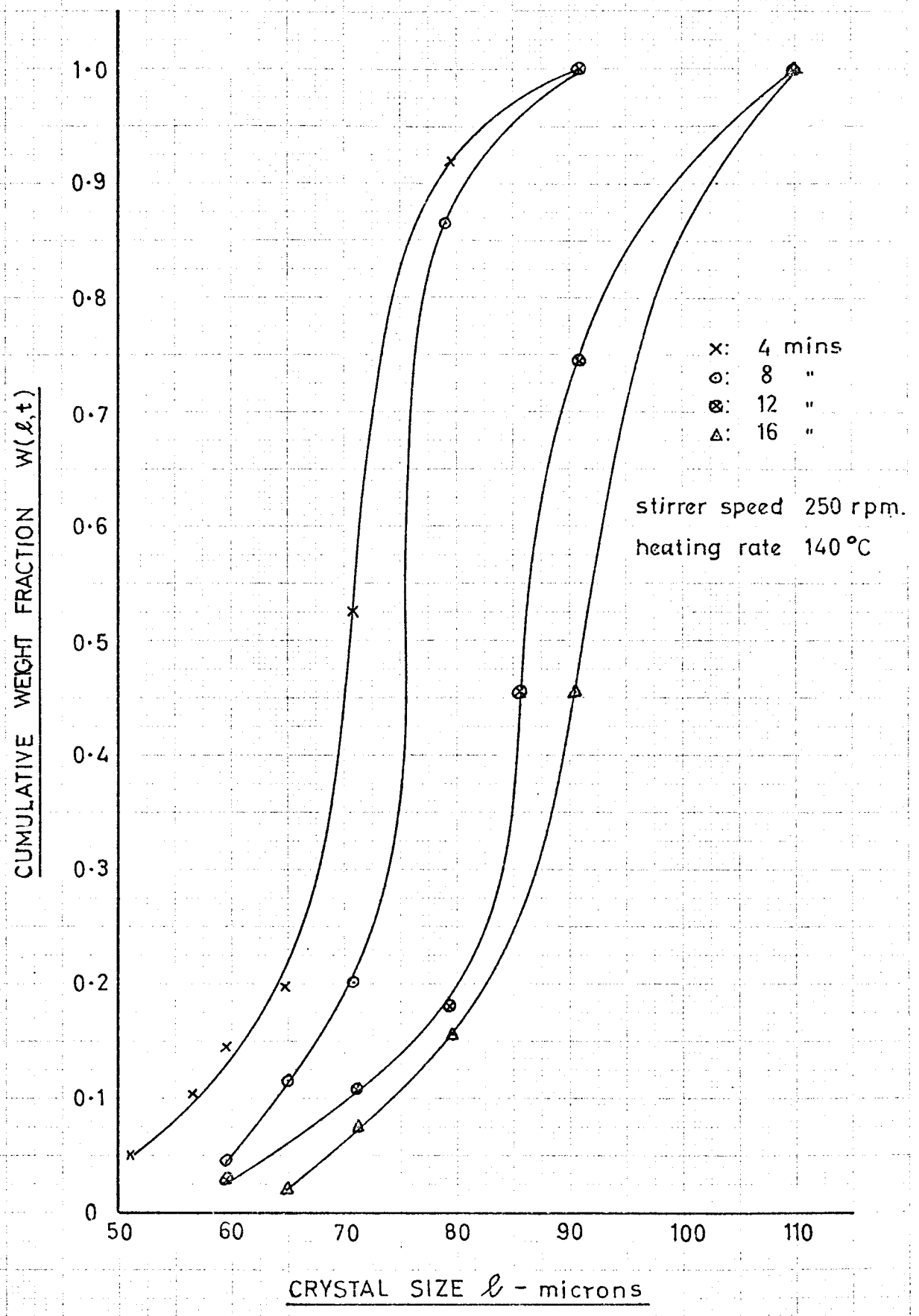

FIG. 13

In addition, the particle size distribution curves for the runs performed at 120°C and 130°C and at a stirrer speed of 1600 r.p.m. showed that the smallest crystal size was 24 microns in both cases. In order to substantiate this result even further the following experimental investigation was performed.

Three runs, each at a temperature of 140°C in the outside jacket of the crystallizer, but each at one of the three above mentioned stirrer speeds were carried out as before. At the stage where the first crystals could be visually detected in the solution, the run was halted and the crystals together with the solution removed from the crystallizer and separated by filtration through a millipore membrane filter. After drying these crystals were examined under a microscope at a magnification of 100 times. At a stirrer speed of 1600 r.p.m. these crystals were observed to be in the range of 25-30 μ; at 800 r.p.m. the range was 45-50 μ and at 250 r.p.m. 60-65 μ.

If the straight lines obtained in Figure 9 (α_1 versus time curve) are extrapolated backwards to time t = 0 when crystallization has just commenced, the smallest crystal size (or nuclei size) obtained agrees rather well with that obtained from both the sedimentation analyses and the microscopic examination mentioned above. This comparison is shown in the table below.

Table I Comparison of critical nuclei size values

Stirrer Speed r.p.m.	ℓ_o Sedimentation Analysis microns	ℓ_o Microscope Examination microns	ℓ_o Extrapolation of α_1 versus t microns
1600	25- 24- 24	25-30	29
800	40	45-50	46
250	52	60-65	61

It can therefore be concluded that the size at which the first crystals appear in the solution i.e. the critical nuclei size, is much larger than is normally the case and further that this size is dependent on the stirrer speed. This result is not as surprising as it seems at first, if one examines the actual situation in the crystalliser.

Using the terminology of Turnbull and his associates (21) in their article on the transient nucleation in phase transformations in solids, where particles of the new phase which exceed the critical size for continuous growth are called nuclei, whereas particles which are of sub-critical size are termed embryos, the following argument can be developed.

The concentrations at which crystallization occured in the batch experiments were in the range of 128-144 gms WO_3/litre compared to the saturation concentration of 43.5 gms WO_3/litre, measured at the crystallization temperature (see Section 5.3.3). This is somewhat exceptional

in itself as in most cases crystallization occurs readily at concentrations which are 2-10% in excess of the saturation concentration. However, bearing in mind the exceptionally large size of the APT molecule $\{5(NH_4)_2O \cdot 12WO_3 \cdot 7H_2O\}$, there is every likelihood that it is difficult for the various molecules and ions to arrange themselves correctly to form complete molecular structures. The result of this is that the concentration of the solution increases and greatly exceeds the range of supersaturation where crystallization would normally occur. At these high supersaturations it is possible that the WO_3 groups combine in solution to form long polymer-like chains or embryos. Nucleation of a number of these chains followed by rapid growth by addition of further chains could result in relatively large critical nuclei sizes. This theory is supported by the opalescent nature of the solution which is observed immediately prior to the appearance of the first crystals.

As seen in Table I the experimental results showed that the nuclei size decreased with increasing stirrer speed. If we postulate that immediately before nucleation the solution contains embryos of semi-ordered solute molecules, then the formation of large embryos will be inhibited by the increased shearing action of the fluid. The embryo size distribution also appears to be affected as indicated by the dependence of the variance σ on the stirrer speed.

5.3.2 Solution of the Batch Particle Balance Equation

In the previous chapter it was established that the growth rate of APT crystals was independent of the crystal size. Equation (4-1) can therefore be rewritten as follows:

$$\frac{\partial f(\ell,t)}{\partial t} + p\,\frac{\partial f(\ell,t)}{\partial \ell} = Q(t)\,\delta(\ell - \ell_o) \qquad (5\text{-}3)$$

It is impossible even to attempt to solve the above partial differential equation analytically as the boundary conditions are not known with any degree of certainty. However, the growth rate of the crystals at any time during a batch run can be evaluated using the cumulative weight distribution curve of the crystals at that time.

Multiplying each term of the above equation by ℓ^4 and integrating with respect to ℓ between the limits 0 and ∞ results in:

$$\int_0^\infty \ell^4 \frac{\partial f(\ell,t)}{\partial t}\cdot d\ell + p\int_0^\infty \ell^4 \frac{\partial f(\ell,t)}{\partial \ell}\cdot d\ell$$

$$= Q(t)\int_0^\infty \ell^4 \delta(\ell - \ell_o)\,d\ell \qquad (5\text{-}4)$$

or

$$\frac{d}{dt}\int_0^\infty \ell^4 f(\ell,t)\,d\ell + p\{f(\ell,t)\ell^4\}_0^\infty$$

$$- 4p\int_0^\infty \ell^3 f(\ell,t)\,d\ell = Q(t)\ell_o^4 \qquad (5\text{-}5)$$

Substituting the boundary condition:

as $\ell \to \infty$, $f(\ell,t) \neq 0$ into the above equation yields:

$$\frac{d}{dt}\int_0^\infty \ell^4 f(\ell,t)d\ell - 4p\int_0^\infty \ell^3 f(\ell,t)d\ell = Q(t)\ell_o^4 \qquad (5\text{-}6)$$

Similarly by multiplying each term of equation (5-3) by ℓ^5 and integrating with respect to ℓ between the limits 0 and ∞, the following result is obtained:

$$\frac{d}{dt}\int_0^\infty \ell^5 f(\ell,t)d\ell - 5p\int_0^\infty \ell^4 f(\ell,t)d\ell = Q(t)\ell_o^5 \qquad (5\text{-}7)$$

Defining $w(\ell,t)d\ell$ to be the weight of crystals of sizes between ℓ and $\ell + d\ell$ at any time t, we have:

$$w(\ell,t) = \rho_s \ell^3 f(\ell,t) \qquad (5\text{-}8)$$

The mean with respect to the weight distribution is:

$$\alpha_1 = \frac{\int_0^\infty \ell w(\ell,t)d\ell}{\int_0^\infty w(\ell,t)d\ell} \qquad (5\text{-}9)$$

The second moment of the weight distribution is given by:

$$\alpha_2 = \frac{\int_0^\infty \ell^2 w(\ell,t)d\ell}{\int_0^\infty w(\ell,t)d\ell} \qquad (5\text{-}10)$$

replacing for $w(\ell,t)$ from equation (5-8) into equations (5-9) and (5-10) results in:

$$\alpha_1 = \frac{\int_0^\infty \ell^4 f(\ell,t)d\ell}{\int_0^\infty \ell^3 f(\ell,t)d\ell} \qquad (5\text{-}11)$$

$$\alpha_2 = \frac{\int_0^\infty \ell^5 f(\ell,t)d\ell}{\int_0^\infty \ell^3 f(\ell,t)d\ell} \qquad (5\text{-}12)$$

The total mass of the crystals at any time t is given by:

$$M(t) = \rho_s \int_0^\infty \ell^3 f(\ell,t)d\ell \qquad (5\text{-}13)$$

Replacing equation (5-13) into equations (5-11) and (5-12) yields:

$$\alpha_1 = \frac{\rho_s}{M(t)} \cdot \int_0^\infty \ell^4 f(\ell,t)d\ell \qquad (5\text{-}14)$$

$$\alpha_2 = \frac{\rho_s}{M(t)} \int_0^\infty \ell^5 f(\ell,t)d\ell \qquad (5\text{-}15)$$

Equations (5-6) and (5-7) can therefore be rewritten as:

$$\frac{d}{dt}\left\{\frac{\alpha_1 M(t)}{\rho_s}\right\} - 4p\frac{M(t)}{\rho_s} = Q(t)\ell_o^4 \qquad (5\text{-}16)$$

$$\frac{d}{dt}\left\{\frac{\alpha_2 M(t)}{\rho_s}\right\} - 5p\alpha_1\frac{M(t)}{\rho_s} = Q(t)\ell_o^5 \qquad (5\text{-}17)$$

By solving the above equations simultaneously, the nucleation rate term Q(t) can be eliminated. The resulting expression is as follows:

$$\frac{d}{dt}\{\alpha_2 M(t)\} - \ell_o\frac{d}{dt}\{\alpha_1 M(t)\} = pM(t)\{5\alpha_1 - 4\ell_o\} \qquad (5\text{-}18)$$

From the experimental results presented earlier the normalized variance σ was found to be a constant dependent only on the stirrer speed. Combining equations (5-1) and (5-2) gives:

$$\alpha_2 = (n + 1)\alpha_1^2 \qquad (5\text{-}19)$$

Replacing this value of α_2 in equation (5-18), and solving for the growth rate p, the following expression is obtained:

$$p = \frac{M(t).\frac{d\alpha_1}{dt}[2(n+1)\alpha_1 - \ell_o] + \frac{dM(t)}{dt}[(n+1)\alpha_1^2 - \ell_o\alpha_1]}{M(t)[5\alpha_1 - 4\ell_o]} \qquad (5\text{-}20)$$

As M(t) and α_1 are both known functions of time p can be evaluated.

The growth rates for the experiments performed at the same heating rate, corresponding to a temperature of 140°C in the outside jacket of the crystallizer, and at the three different stirrer speeds were calculated using the above equation.

The critical nuclei size ℓ_o was taken as the value obtained from the extrapolation of the mean particle size (α_1) versus time curve in Figure 9, as it was felt that this was the most accurate value.

It should be noted that in doing this the value of ℓ_o is based on the mean of the weight distribution, whereas in fact the mean based on the number distribution should be used. However, if the size distribution of nuclei is narrow, the mean based on the weight distribution will not differ much

from the mean based on the number distribution. As an example if nucleation occurs as a Dirac Delta function there is no difference at all between the means of the two distributions. From Figures 11, 12 and 13 it is seen that at low values of t the size distributions are fairly narrow. In any event it was found subsequently (Table II) that the growth rate was not particularly sensitive to the value of ℓ_o used.

The results are shown in Figure 14 which is a plot of crystal growth rate versus time for the stirrer speeds of 250, 800 and 1600 r.p.m. There is no significant difference between the growth rates at the different stirrer speeds showing that the growth rate of APT crystals is independent of the stirrer speed.

5.3.3 The Dependence of the Crystal Growth Rate on the Supersaturation

In order to evaluate the solution supersaturation during a batch run it was necessary to determine the equilibrium concentration of the ammonium tungstate solution at the crystallization temperature of 93°C. A saturated solution of ammonium tungstate was made up by dissolving APT crystals in an ammonia solution. An ammonia solution was poured into a 100 ml flask which was kept at the required temperature by immersing it in a constant temperature bath. An excess of APT crystals was added to the solution and the mixture continuously stirred for a period of about 10 hours.

GROWTH RATE AS A FUNCTION OF TIME

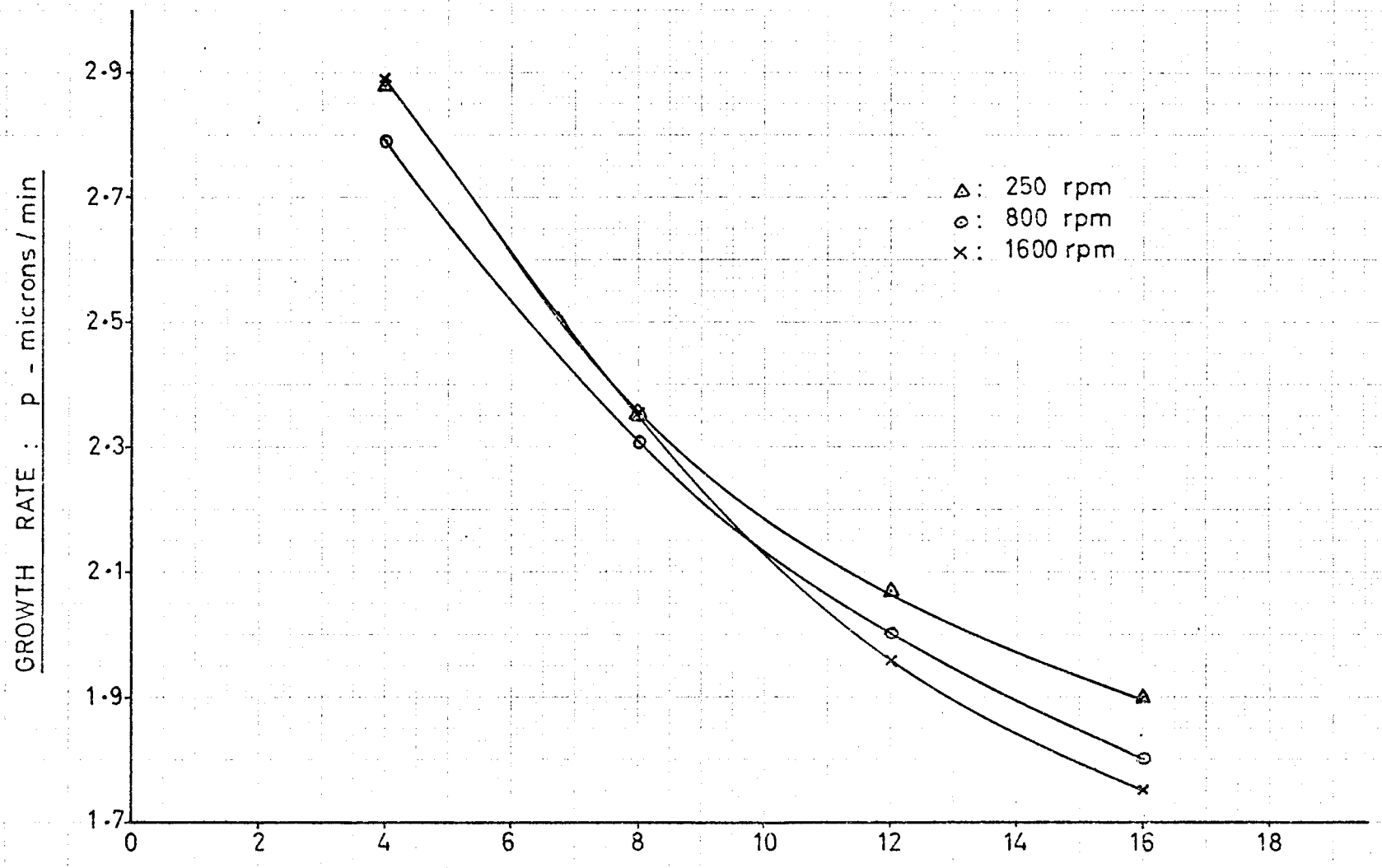

FIG. 14

The concentration of this solution was then determined in the normal way. It was found that the saturation concentration was dependent on the pH of the solution i.e. the ammonia content. It was therefore necessary to determine the saturation point for solutions of different pH values. This was done and the variation of the equilibrium saturation concentration with pH is given in Figure 15.

In order to establish how the saturation concentration varied throughout a batch run, the pH of the ammonium tungstate solution was measured at different times during the run. This was done for all runs performed under the different conditions. It was found that the maximum variation of the solution pH for all runs, during the crystallization period was from pH 7.55 to pH 7.82. From Figure 15 it can be seen that this variation in pH resulted in a change of the saturation concentration from 44.5 to 42.5 gm WO_3/litre. Since this change was small it was decided to use an average value of 43.5 gm WO_3/litre for all the runs. The change of the solution concentration with time had been measured for all batch runs, and hence the supersaturation of the solution at any time could be evaluated from the equation:

$$s = c - c_s = c - 43.5 \qquad (5\text{-}21)$$

It is generally accepted (1,7, 10, 22) that the crystal growth is linearly dependent on the supersaturation of the solution.

VARIATION OF SATURATION CONCENTRATION WITH SOLUTION PH

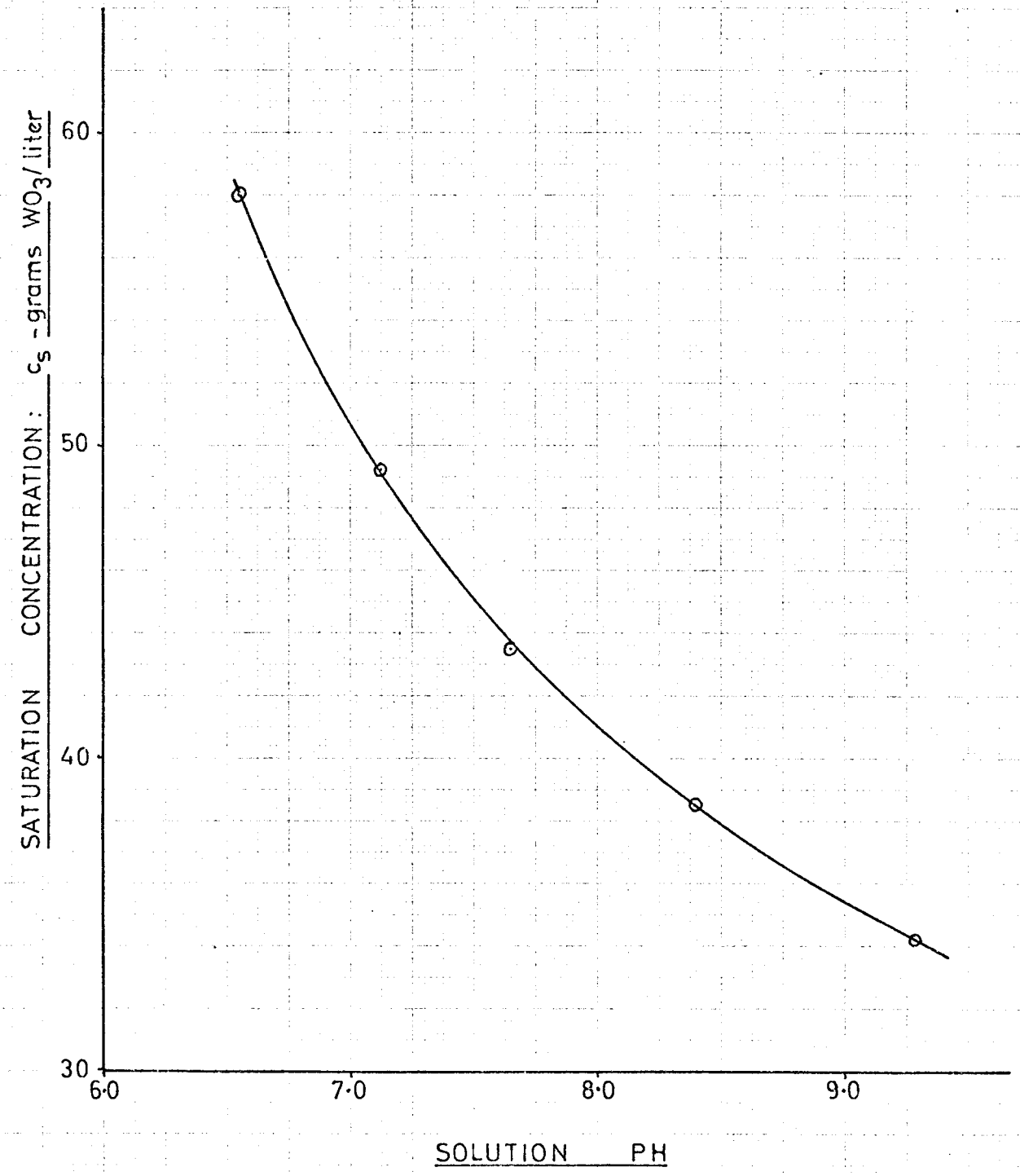

FIG. 15

i.e.

$$p = k_4(c - c_s) \qquad (5\text{-}22)$$

In order to establish whether this relationship also holds for APT crystals growing in a supersaturated solution in the batch crystallization experiments, the growth rate of the crystals at a particular time during a run was evaluated using equation (5-20) and the supersaturation at the same time calculated using (5-21) above. The results for the experiments performed at 120°, 130°C and 140°C are shown in Figure 16.

It is immediately apparent from these results that the growth rate decreases with increasing supersaturation. As this was a somewhat strange and unexpected result it was decided to check on the basic equation used for the calculation of the growth rate; namely equation (5-20). i.e.

$$p = \frac{M(t)\frac{d\alpha_1}{dt}[2(n+1)\alpha_1 - \ell_o] + \frac{dM(t)}{dt}[(n+1)\alpha_1^2 - \ell_o\alpha_1]}{M(t)[5\alpha_1 - 4\ell_o]} \qquad (5\text{-}20)$$

Let us have a look at this equation to see how sensitive the growth rate is to the value of ℓ_o used. This was done with three different values of ℓ_o; the results are presented in the Table below.

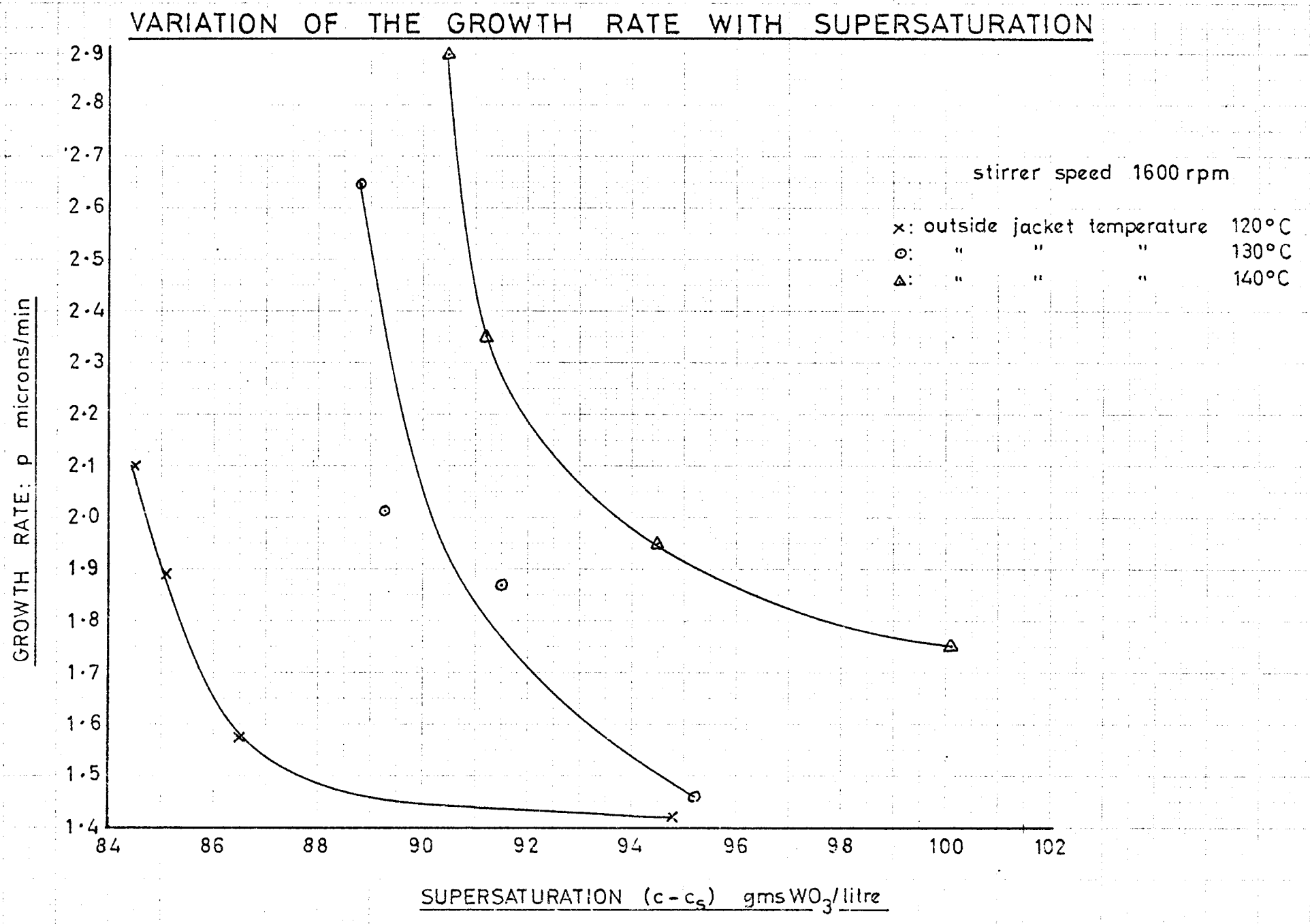
VARIATION OF THE GROWTH RATE WITH SUPERSATURATION
stirrer speed 1600 rpm
×: outside jacket temperature 120°C
⊙: " " " 130°C
△: " " " 140°C
GROWTH RATE: ρ microns/min
2·9
2·8
2·7
2·6
2·5
2·4
2·3
2·2
2·1
2·0
1·9
1·8
1·7
1·6
1·5
1·4
84
86
88
90
92
94
96
98
100
102
SUPERSATURATION (c - c_s) gms WO3/litre

FIG 16

Table II. Sensitivity of the growth rate p to the critical nuclei size ℓ_o

Stirrer speed: 1600 r.p.m.
Outside jacket temperature: 140°C

Time, t mins	GROWTH RATE p: microns/min		
	ℓ_o = 29	ℓ_o = 20	ℓ_o = 10
4	2.89	2.87	2.57
8	2.35	2.20	2.10
12	1.96	1.89	1.83
16	1.75	1.76	1.71

Examination of the above table shows that the growth rate p is not particularly sensitive to the value of ℓ_o used. Of greater importance is the fact that in all three cases p decreases with increasing crystallization time i.e. it might be thought that p is a decreasing function of supersaturation.

It must therefore be concluded that some termination process was taking place which tended to slow down the growth of the crystals even though the driving force for crystallization was increasing. Equation (5-22) must be modified to:

$$p = \phi(t).(c - c_s) \qquad (5\text{-}23)$$

where $\phi(t)$ is some strongly decreasing function of time and is a measure of the termination process. This termination

in the growth could possibly result from either one or both of the following two occurences:

(i) Break up of larger crystals into smaller ones due to collisions with the stirrer and the walls of the vessel, and (ii) impurities on the surface of the crystals blocking various growth or addition sites and in this way reducing the growth rate of the crystals.

It has been well established that crystal growth can be inhibited by impurities being present on the crystal surface at sites where growth normally takes place. For example substances such as tannin, dextrin or sodium hexametaphosphate when added in small quantities to boiler feed water, prevent nucleation and growth of calcium carbonate crystals and therefore reduce scaling. Similarly the addition of 0.1% HCl and 0.1% $PbCl_2$ will prevent the growth of sodium chloride crystals. According to Nabarro (16) and others, only very small quantities of impurities need be adsorbed at the growth step on the surface of a crystal in order to inhibit the growth of the whole face of that crystal.

In order to establish which of the two above mentioned termination processes was occuring, the following investigation was carried out.

5.4 CRYSTAL BREAK-UP INVESTIGATION

The cumulative weight particle size distribution curve of a sample of APT crystals was determined using the sedimentation

balance. This sample was then split up into several smaller samples of 15 grams each. A saturated solution of APT in water at the crystallization temperature of 93°C was made up by dissolving APT crystals in a flask of distilled water kept in a constant temperature bath. 400 ml of this saturated solution were then poured into the crystallizer. Glycerol was circulated through the outside jacket of the vessel at a temperature of 140°C and the paddle was then switched on and allowed to rotate at the required speed. One of the smaller samples of the APT crystals was introduced into the crystallizer and allowed to remain there for a period of about twenty minutes. During this time the crystals were subjected to the same mechanical forces as was the case in the normal batch run. At the completion of the run the crystals together with the solution were removed from the vessel by means of a suction tube and separated by filtration. The crystals were then dried and their particle size weight distribution curve determined. This procedure was adopted for the three different stirrer speeds of 250, 800 and 1600 r.p.m. respectively.

For each of the stirrer speeds the weight distribution curve of the crystals after the run was compared to that before the run. The results are shown in Figure 17. It is seen that in all three cases virtually no change in the cumulative weight distribution curves could be detected. This therefore indicated that crystal break-up due to collisions was not taking place to any measurable extent and hence could not account for the slowing down of the crystal growth with increasing time in the batch crystallizer.

CRYSTAL BREAK-UP INVESTIGATION

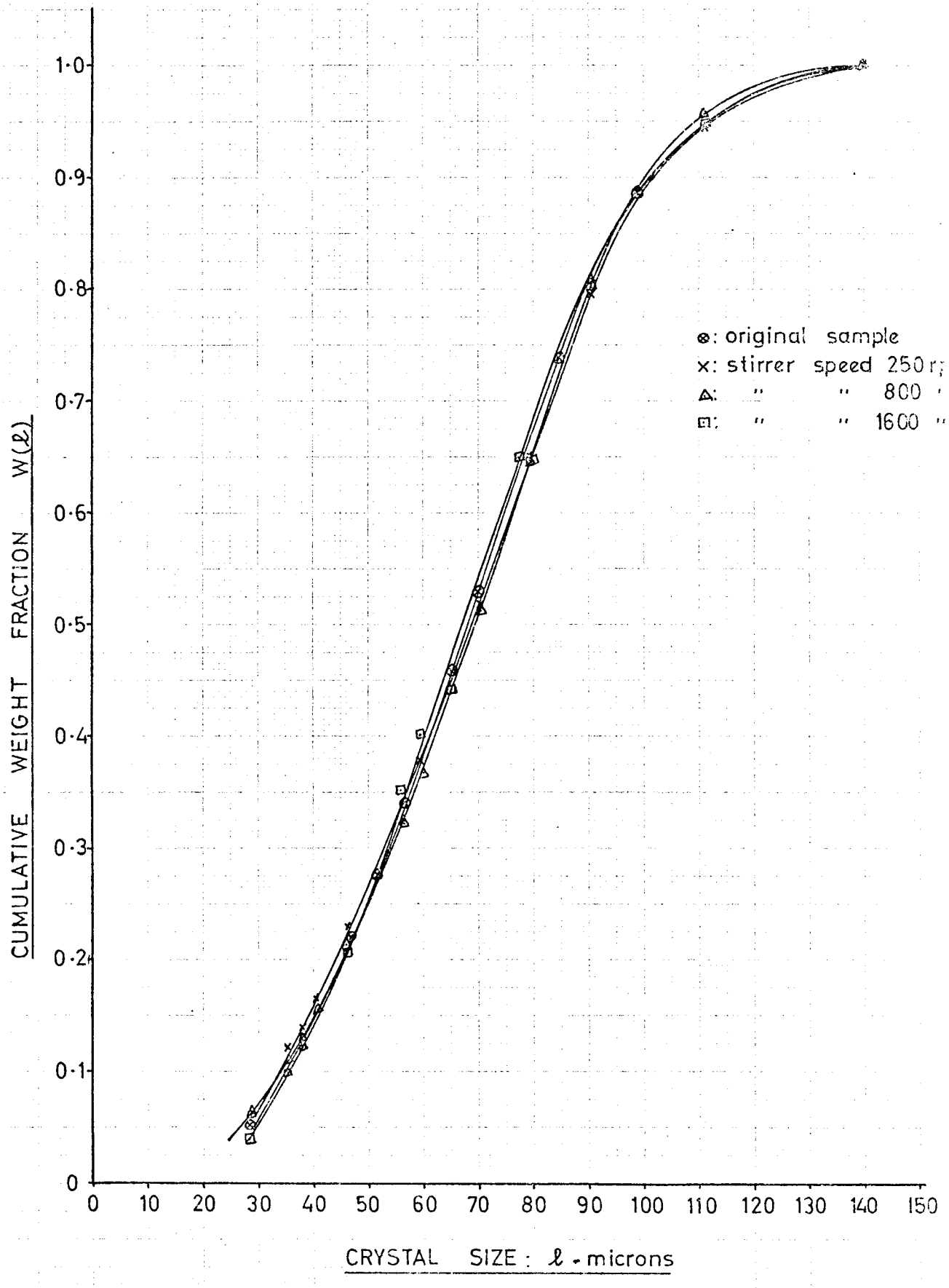

FIG. 17

5.5 THE EFFECT OF IMPURITIES ON THE CRYSTAL GROWTH RATE

As the crystals were not breaking up in the crystallizer, the only other possible explanation seems to be growth retardation in the presence of impurities on the crystal surface. Botsaris and Denk (1) in their study of the growth rates of potassium alum crystals found that their results were considerably lower than those reported earlier by Mullin and Garside (4). They, however, used reagent grade alum and distilled water whereas Mullin and Garside worked with recrystallized alum and deionized water. They therefore offered the explanation that the difference in growth rates between their study and that performed by Mullin and Garside was due to the presence of impurities which inhibited the crystal growth rate.

It has been established by Gorshtein and Baliner (5), that when ammonium paratungstate is crystallized by evaporation of an ammoniacal solution of crude tungstic acid as was done in all experiments performed in this investigation, certain impurities are present in the crystals.

Gorshtein and Baliner studied the fractionation of the Cu^{2+}, Fe^{3+}, Co^{2+} and Mn^{2+} impurities during the crystallization of APT from the mother liquor. Their results showed that the separation factor k_{cr} for washed crystals in the separation of the copper impurity was only 3-6 as compared with an ideal separation factor of 800; where k_{cr} was defined as the ratio of the impurity concentration (relative to WO_3) in the original solution to that in the crystals. This indicated that a fairly

considerable trapping of the copper impurity by the solid phase was taking place. They further showed that appreciably no separation of the Fe^{3+} impurity from the APT crystals takes place, as the experimentally determined value of k_{cr} was very close to unity. The separation factors for Co^{2+} and Mn^{2+} were 20 and 70 respectively, indicating that a fairly high purification effect was obtained in relation to these impurities.

It is therefore apparent that either the Cu^{2+} or the Fe^{3+} ions are more likely to be the cause of the termination in the growth of the APT crystals than the Co^{2+} and Mn^{2+} ions. It is only necessary that either of these ions attach themselves onto the surface of a growing crystal, at a site such as a growth step in order to retard the further growth of that crystal.

A table of their results obtained on the fractionation of the Cu^{2+} impurity, on which most of their experimentation was performed, is presented below.

Table III. The results of Gorshtein and Baliner

Concentration of Cu^{2+} in the solution: gm/litre c_x	Concentration of Cu^{2+} in the crystals gm/gm APT c_{APT}	$\frac{c_{APT}}{c_x}$
1.46×10^{-4}	2.22×10^{-7}	1.64×10^{-3}
2.25×10^{-3}	3.40×10^{-6}	1.51×10^{-3}
1.86×10^{-3}	2.41×10^{-6}	1.30×10^{-3}
2.24×10^{-2}	3.40×10^{-5}	1.52×10^{-3}

It is seen from the above table that the distribution coefficient c_{APT}/c_x is approximately the same for the four cases indicating that the concentration of the Cu^{2+} ion in the APT crystals is proportional to the concentration of the Cu^{2+} ion in the ammonium tungstate solution.

This can be written mathematically as:

$$c_{APT} = k_5 c_x \qquad (5\text{-}24)$$

This result is not unexpected as this relationship can be derived from thermodynamics for a dilute distribution of impurities between two phases.

Unfortunately Gorshtein and Baliner performed only one experiment on the trapping of the Fe^{3+} ion by APT crystals and it is thus not possible to establish whether the same conclusion holds for the Fe^{3+} ion. It is however, reasonable to suppose that a similar relationship might exist for the Fe^{3+} impurity.

An analysis of the crystals obtained from two different batch experiments is presented in the table below.

Table IV. Impurity concentration in the crystals gm/gm APT

Impurity	Sample 1	Sample 2
Mo	2×10^{-4}	2×10^{-4}
P	$<1.0 \times 10^{-6}$	$<1.0 \times 10^{-6}$
Ti	$<1.0 \times 10^{-6}$	$<1.0 \times 10^{-6}$
As	$<1.0 \times 10^{-6}$	$<1.0 \times 10^{-6}$
Fe	3×10^{-5}	3×10^{-5}
Cu	1×10^{-5}	2×10^{-5}
Bi	$<1.0 \times 10^{-6}$	$<1.0 \times 10^{-6}$
Pb	$<1.0 \times 10^{-6}$	$<1.0 \times 10^{-6}$
Zn	$<1.0 \times 10^{-6}$	$<1.0 \times 10^{-6}$
Mn	$<1.0 \times 10^{-6}$	$<1.0 \times 10^{-6}$

It is seen from the above table that the Mo, Cu and Fe impurities are present in greater quantities than the others and hence are more likely to be instrumental in causing blocking of active sites on the crystal surface. However, as the structure of the molybdates and tungstates are very similar it is unlikely that Mo will inhibit crystal growth. On the other hand Cu and Fe could very well block growth sites and so lower the growth rate p.

5.6 THE GROWTH RATE MODEL

Previously it was assumed that the growth rate of the crystals was dependent only on the supersaturation of the solution. However, if the growth of a crystal is being inhibited by the presence of impurities on the surface, this equation can no longer be applied as some termination term is now necessary. Consider a crystal in contact with its mother liquor in the crystalliser. This crystal has certain impurities present on its surface. Some of these will completely stop growth on a certain part of the crystal surface, others will only retard the growth on a part of the surface and others will not affect the growth rate at all. It is difficult to describe this situation mathematically. However, this can be overcome by considering the retardation of the crystal growth as an on-off process.

If we consider a crystal of size ℓ and mass m, let us define x to be the fraction of the surface of this crystal that is completely inhibited due to impurities and hence cannot grow further. (Alternatively x can be defined as the fraction of the total number of active sites on the crystal surface that are completely inhibited by the presence of impurities).

The total area of this crystal onto which further growth can take place is thus proportional to $\ell^2(1 - x)$.

The rate of mass transfer to this crystal is thus:

$$p_m = \frac{dm}{dt} = k_6(1 - x)\ell^2(c - c_s) \qquad (5\text{-}25)$$

But from equation (4-12) we have:

$$p_m = \text{constant}.\ell^2.p \qquad (4\text{-}12)$$

Combination of equations (4-12) and (5-25) yields

$$p = k_7(1 - x)(c - c_s) \qquad (5\text{-}26)$$

k_7 being a constant.

It is to be expected that x, the fraction of the total number of active sites which are completely inhibited against further growth, will be dependent in some way on the concentration of the impurities in the solution in which crystallization is taking place.

Let us take a crystal, which has grown to a size ℓ in the solution, and consider it at any point in time when it has reached an intermediate size r between o and ℓ. It is a well established fact that the density of active sites on a crystal surface is a constant.

Thus defining N_A to be the number of active sites per unit surface area of the crystal, the total number of active sites on a crystal of size r is given by

$$N_T = \text{constant}.N_A.r^2 \qquad (5\text{-}27)$$

Since N_A is constant, the above equation can be rewritten as:

$$N_T = k_8 r^2 \tag{5-28}$$

The total number of sites on the crystal surface which are completely inhibited against further growth

$$N_I = x k_8 r^2 \tag{5-29}$$

Consider the same crystal when it has reached a size ℓ.

The mass of this crystal is

$$m \propto \rho \ell^3$$

where ρ is the density

Since ρ is a constant independent of the crystal size this can be rewritten as:

$$m = k_9 \ell^3 \tag{5-30}$$

The concentration of impurities in a crystal has been defined as: c_{APT} gm impurity/gm APT

Therefore the total mass of impurities in this crystal is:

$$M_I = m c_{APT}$$

$$= k_9 \ell^3 c_{APT}$$

Assuming that it requires only one impurity ion to attach itself onto an active site on the crystal surface and so inhibit further growth on that site, then the total number of sites which have been inhibited in the whole crystal, is given by

$$N_x = \int_0^{\ell} N_I dr \tag{5-32}$$

$$= \int_0^{\ell} x k_8 r^2 dr \tag{5-33}$$

The total mass of these impurity ions is thus

$$M_I = k_{10} \int_0^{\ell} x k_8 r^2 dr \tag{5-34}$$

where k_{10} is a constant.

Combining equations (5-31) and (5-34) gives

$$M_I = k_9 \ell^3 c_{APT} = k_{10} \int_0^{\ell} x k^8 r^2 dr \tag{5-35}$$

It is reasonable to assume that x, the fraction of the total number of sites that is completely inhibited to further growth, will be dependent on the external environment of the crystals and not on the crystal size.

Applying this assumption, the above equation can be differentiated with respect to ℓ giving.

$$3k_9 \ell^2 c_{APT} = k_{10} k_8 \ell^2 x \tag{5-36}$$

or

$$x = k_{11} c_{APT} \tag{5-37}$$

Based on the results of Gorshtein and Baliner

$$c_{APT} = k_5 c_x \tag{5-24}$$

Combining equations (5-24) and (5-37), and putting $k_{12} = k_{11} k_5 =$ constant, yields

$$x = k_{12} c_x \tag{5-38}$$

From the above equation it can be concluded that x, the fraction of the crystal surface which is inhibited is proportional to the concentration of the impurities in the solution, c_x. Replacing for x from equation (5-38) into the growth rate equation (5-26) results in

$$p = k_7(1 - k_{12}c_x)(c - c_s) \qquad (5\text{-}39)$$

5.6.1 The Growth Rate Equation applied to the Batch Crystallization process

The batch crystallization runs were started by pouring a volume V_o, of the ammonium tungstate solution into the crystalliser. This volume of solution contained a certain concentration of impurities capable of blocking growth steps on the crystal surface. Let this impurity concentration by y_o.

As the volume of the solution in the crystalliser decreases, due to evaporation, the impurity concentration increases. This impurity concentration at any time during a batch run is given by:

$$c_x = \frac{y_o V_o}{V} \qquad (5\text{-}40)$$

where V is the solution volume at any time t.

Replacing this expression into equation (5-39) yields:

$$p = k_7(1 - \frac{k_{12}y_o V_o}{V})(c - c_s) \qquad (5\text{-}41)$$

Since the same stock solution was used for all runs performed, y_o is a constant, and the above equation can be simplified by putting

$$k_{13} = k_{12}y_o V_o \qquad (5\text{-}42)$$

Hence resulting in the following growth rate equation

$$p = k_7(1 - \frac{k_{13}}{V})(c - c_s) \qquad (5\text{-}43)$$

5.6.2 Test of the Model

In order to test the growth rate model, the results obtained from the batch crystallization runs were plotted on a graph in the form: $p/(c - c_s)$ against $1/V$.

This was done for all experiments performed. The result is shown in Figure 18. It is seen that a good straight line can be drawn through the experimentally determined points, indicating that the proposed growth rate model fits the results reasonably well.

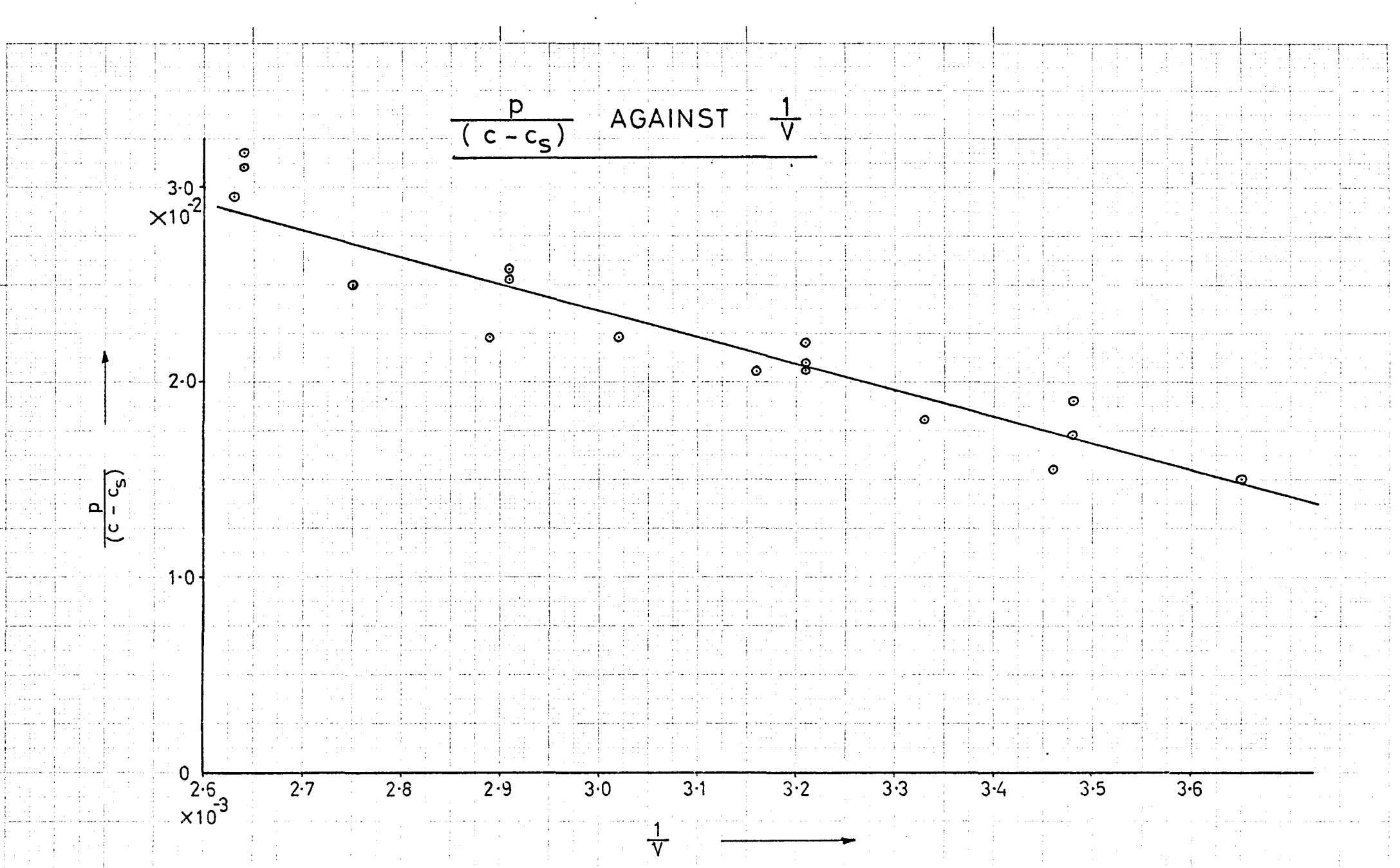
p / (c - cs) AGAINST 1/V
3·0
×10-2
2·0
1·0
0
p / (c - cs)
2·6
×10-3
2·7
2·8
2·9
3·0
3·1
3·2
3·3
3·4
3·5
3·6
1/V

FIG. 18

Part II. Continuous Crystallization

Crystallization experiments in a continuous mixed product removal crystallizer were performed in order to substantiate the results obtained from the batch experiments.

5.7 EXPERIMENTAL PROCEDURE

Thirty minutes prior to the commencement of a run, the circulation pump was switched on and glycerol at the required temperature circulated through the outside jacket of the crystalliser. 400 ml of the ammonium tungstate solution were poured into the vessel and the stirrer rotated at 1600 r.p.m. The feed solution was pumped into the crystallizer at a constant rate and the suction tube allowed to operate. The crystallization was carried on for a period corresponding to at least ten residence times in order to ensure steady state operation. Liquid samples were taken from the outlet stream at various times and their concentration determined. The flow-rate of the exit stream of the crystallizer was measured volumetrically.

At the completion of the run the crystals and the mother liquor were removed from the vessel and separated by filtration. The solution concentration was determined and the cumulative weight distribution curve of the crystals found by means of the sedimentation balance. The total mass of the crystals in the crystallizer was also determined.

5.8 EXPERIMENTS PERFORMED

Experiments were performed at five different heating rates. These corresponded to outside jacket temperatures of 130°C, 140°C 150°C, 160°C and 170°C. Different feed solution flow-rates were used for each of these heating rates. In this way a fairly large variation in the residence time of the crystallizer was achieved. In all the experiments performed the total volume of crystals and solution was 400 ml.

As mentioned in Section 3.4.1, it was not possible to use stirrer speeds lower than 1600 r.p.m. as the take off mechanism for the mixed product removal did not then operate efficiently. Neither was it possible to use higher stirrer speeds as the solution then tended to splash out of the crystallizer. For this reason all continuous runs were performed at a stirrer speed of 1600 r.p.m.

5.9 CONTINUOUS CRYSTALLIZATION RESULTS

It was found by examining the cumulative weight distribution curves of the crystals removed from the continuous crystallizer that no crystals smaller than 25 to 30 microns were present. This figure agrees very well with that obtained from the batch runs performed at the same stirrer speed.

5.9.1 Solution of the Continuous Particle Balance Equation

The particle balance equation as presented in Chapter IV is:

$$\frac{d[Vpg(\ell)]}{d\ell} + wg(\ell) = VN\delta(\ell - \ell_o) \qquad (4\text{-}2)$$

In order to use the continuous crystallization results to verify that the growth rate is independent of the crystal size, it is important to examine how the solution of the above equation changes if p is made to be a function of the crystal size ℓ.

Branson (2) suggested a relationship of the form:

$$p = k_{14}\ell^{b} \tag{5-44}$$

Where the ℓ^{b} term was derived from considerations of the relative velocity between the solution and the crystals. Using this relationship for the growth rate and incorporating it into the particle balance equation gives.

$$\frac{d[Vk_{14}\ell^{b}g(\ell)]}{d\ell} + wg(\ell) = VN\delta(\ell - \ell_{o}) \tag{5-45}$$

Since the solution volume V, is independent of ℓ the above equation reduces to

$$\frac{d}{d\ell}[g(\ell)\ell^{b}] + \frac{g(\ell)}{Tk_{14}} = \frac{N}{k_{14}}\delta(\ell - \ell_{o}) \tag{5-46}$$

where: $\frac{w}{V} = \frac{1}{T}$

Rearrangement of this equation gives:

$$\frac{dg(\ell)}{d\ell} + g(\ell)\{b\ell^{-1} + \frac{\ell^{-b}}{Tk_{14}}\} = \frac{N}{k_{14}}\ell^{-b}\delta(\ell - \ell_{o}) \tag{5-47}$$

This is a linear first order differential equation whose integrating factor is:

$$\exp[\int(b\ell^{-1} + \frac{\ell^{-b}}{Tk_{14}})d\ell] = \ell^{b}\exp(\frac{\ell^{1-b}}{Tk_{14}(1 - b)}) \tag{5-48}$$

The solution is therefore:

$$g(\ell)\ \ell^{b}\ \exp\left(\frac{\ell^{1-b}}{Tk_{14}(1-b)}\right) = \int \ell^{b}\exp\left\{\frac{\ell^{1-b}}{Tk_{14}(1-b)}\right\}\ \frac{N}{k_{14}}\ \ell^{-b}\delta(\ell-\ell_{o}).d\ell$$

$$+ \text{constant} \qquad (5\text{-}49)$$

$$= \frac{N}{k_{14}} \exp\left\{\frac{\ell_{o}^{1-b}}{Tk_{14}(1-b)}\right\} + \text{constant} \qquad (5\text{-}50)$$

The Boundary condition is:

when $\ell = \ell_{o}$, $g(\ell) = g(\ell_{o})$

Replacing this in equation (5-50) gives:

$$g(\ell_{o})\ell_{o}^{b}\exp\frac{\ell_{o}^{1-b}}{Tk_{14}(1-b)} = \frac{N}{k_{14}}\exp\frac{\ell_{o}^{1-b}}{Tk_{14}(1-b)} + \text{constant} \qquad (5\text{-}51)$$

In order to evaluate the constant the following procedure is adopted

In a continuous crystallizer, operating under steady state conditions, the total number of crystals in the crystallizer must be the same at all times. This means that the rate of nucleation of the crystals must equal the rate of removal of crystals in the exit stream.

i.e.

$$N = \frac{W}{V}\int_{\ell_{o}}^{\infty} g(\ell).d\ell$$

$$= \frac{1}{T}\int_{\ell_{o}}^{\infty} g(\ell).d\ell \qquad (5\text{-}52)$$

Replacing for $g(\ell)$ from equation (5-50) gives

$$N = \frac{1}{T} \int_{\ell_o}^{\infty} \frac{N \exp\{\frac{\ell_o^{1-b}}{Tk_{14}(1-b)}\} + \text{const.}}{k_{14}\, \ell^b \exp \frac{\ell^{1-b}}{Tk_{14}(1-b)}} \, d\ell \qquad (5\text{-}53)$$

Performing the integration results in:

$$N = N + \text{const.}\ k_{14} \exp\{\frac{-\ell_o^{1-b}}{Tk_{14}(1-b)}\} \qquad (5\text{-}54)$$

The only way in which the left hand side of equation (5-54) can equal the right hand side is that:

constant = 0

Replacing this in equations (5-50) and (5-51)

$$g(\ell) = \frac{N}{k_{14}} \ell^{-b} \exp\{\frac{-\ell^{1-b}}{Tk_{14}(1-b)}\} \exp\{\frac{\ell_o^{1-b}}{Tk_{14}(1-b)}\} \qquad (5\text{-}55)$$

$$g(\ell_o)\ell_o^{\,b} = \frac{N}{k_{14}} \qquad (5\text{-}56)$$

For the case b = 0, i.e. the growth rate is independent of the crystal size:

$$p = k_{14}$$

and the solution becomes:

$$g(\ell) = \frac{N}{p} \exp(\frac{-\ell}{Tp}) \exp(\frac{\ell_o}{Tp}) \qquad (5\text{-}57)$$

Examination of the above equation shows that if log $g(\ell)$ is plotted against ℓ a straight line of slope $-1/Tp$ will be obtained. However, if the growth rate is a function of crystal size, then from equation (5-55) it can be seen that a plot of log $g(\ell)$ versus ℓ will not yield a straight line. The continuous results can therefore be used to verify that the growth rate is independent of the crystal size by making use of this plot.

5.9.2 The Dependence of the Growth Rate on the Crystal Size

In order to obtain $g(\ell)$ and hence log $g(\ell)$ from the cumulative weight distribution curve of the crystal product the following procedure was adopted

For a continuous crystallizer operating under steady state conditions, the weight fraction of crystals up to size ℓ is given by:

$$W(\ell) = \frac{\int_{\ell_o}^{\ell} \ell^3 g(\ell) d\ell}{\int_{\ell_o}^{\infty} \ell^3 g(\ell) d\ell} \qquad (5\text{-}58)$$

The total mass of the crystals in the crystallizer is:

$$M = \rho_s V \int_{\ell_o}^{\infty} \ell^3 g(\ell) d\ell \qquad (5\text{-}59)$$

Combining equations (5-58) and (5-59) above gives

$$\int_{\ell_o}^{\ell} \ell^3 g(\ell) d\ell = \frac{M}{V\rho_s} W(\ell) \quad . \tag{5-60}$$

Differentiating both sides of this equation with respect to ℓ:

$$\ell^3 g(\ell) = \frac{M}{V\rho_s} \cdot \frac{dW(\ell)}{d\ell} \tag{5-61}$$

or

$$g(\ell) = \frac{M}{V\rho_s} \cdot \frac{1}{\ell^3} \cdot \frac{dW(\ell)}{d\ell} \tag{5-62}$$

$g(\ell)$ can thus be obtained from the cumulative weight distribution curve using (5-62) above.

Rearranging (5-62)

$$\frac{1}{\ell^3} \cdot \frac{dW(\ell)}{d\ell} = \frac{V\rho_s}{M} \cdot g(\ell) \tag{5-63}$$

and replacing for $g(\ell)$ from (5-57) we get

$$\frac{1}{\ell^3} \frac{dW(\ell)}{d\ell} = \frac{V\rho_s}{M} \cdot \frac{N}{p} \exp\left(\frac{-\ell}{Tp}\right) \exp\left(\frac{\ell_o}{Tp}\right) \tag{5-64}$$

For any individual run we may write

$$\frac{V\rho_s}{M} \cdot \frac{N}{p} \exp\left(\frac{\ell_o}{Tp}\right) = \text{constant} \tag{5-65}$$

$$= k_{15}$$

Therefore

$$\frac{1}{\ell^3} \cdot \frac{dW(\ell)}{d\ell} = k_{15} \exp\left(\frac{-\ell}{Tp}\right) \tag{5-66}$$

Taking logs on both sides of the equation

$$\log\left[\frac{1}{\ell^3} \cdot \frac{dW(\ell)}{d\ell}\right] = \log k_{15} - \frac{\ell}{Tp} \qquad (5\text{-}67)$$

Converting to logs to the base 10

$$\log_{10}\left[\frac{1}{\ell^3} \cdot \frac{dW(\ell)}{d\ell}\right] = \log_{10} k_{15} - \frac{\ell}{2.303\ Tp} \qquad (5\text{-}68)$$

A plot of $\log_{10}\left[\frac{1}{\ell^3} \cdot \frac{dW(\ell)}{d\ell}\right]$ versus ℓ should therefore yield a straight line of slope: $-1/2.303Tp$

All the continuous results were examined in this way. It was found that for all the runs performed the plot mentioned above yielded a good straight line. This is shown in Figures 19 to 25. This confirms the result obtained earlier that the growth rate of APT crystals is independent of the crystal size.

5.9.3 Growth rates evaluated from the Continuous Crystallizer experiments

It was found that in all the continuous runs no matter how the heating rate and the inlet flow rate of the feed solution were adjusted, the steady state concentration of the ammonium tungstate solution in the crystallizer always remained the same. This concentration was 167 ± 3 gm WO_3/litre. The pH of this solution was found to be $7.7 \pm .05$ in all the experiments done. This meant that the saturation concentration of the ammonium tungstate solution was the same as for the batch runs, i.e.

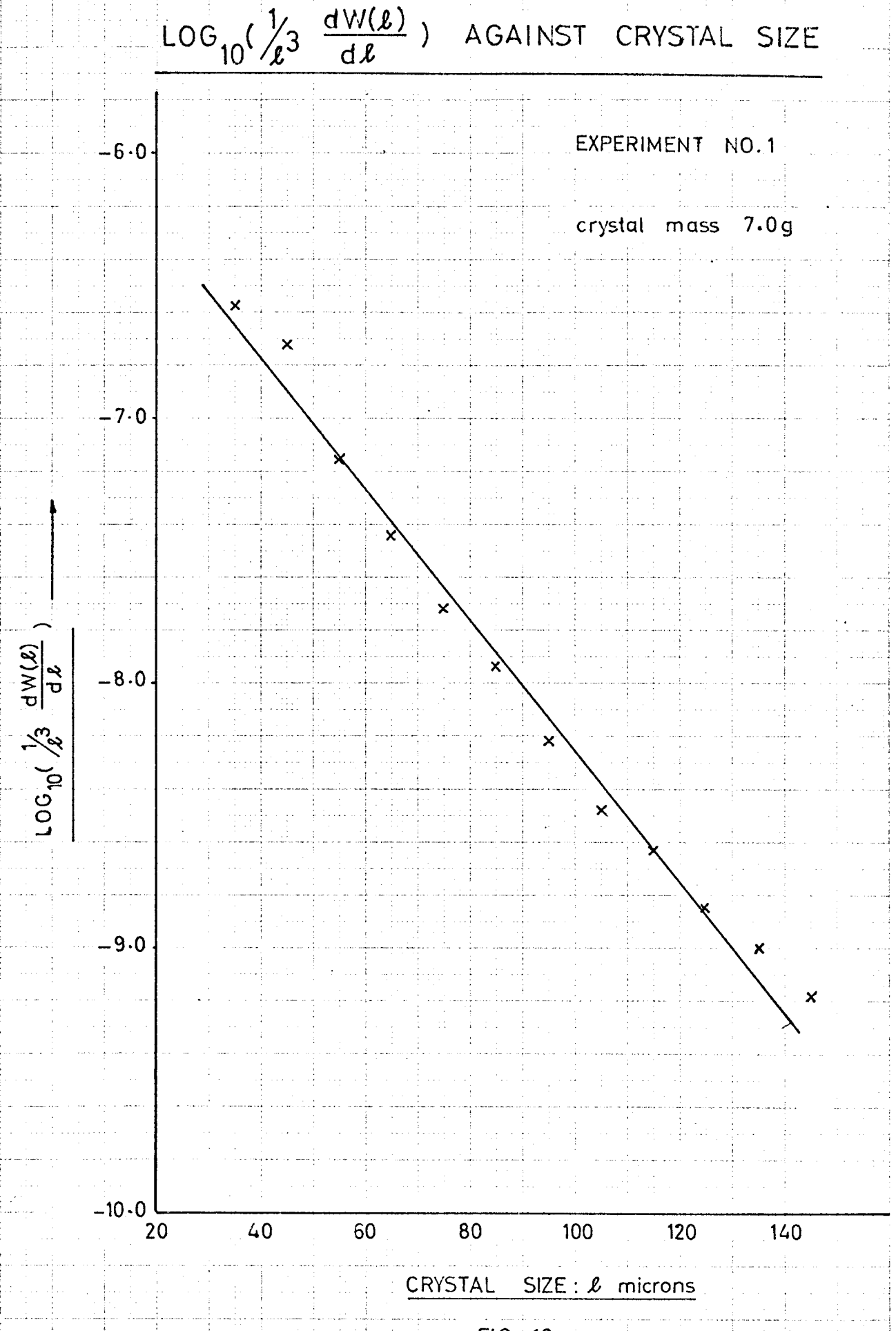
$\log_{10}(\frac{1}{\ell^3}\frac{dW(\ell)}{d\ell})$ AGAINST CRYSTAL SIZE
EXPERIMENT NO.1
crystal mass 7.0g
-6.0
-7.0
-8.0
-9.0
-10.0
$\log_{10}(\frac{1}{\ell^3}\frac{dW(\ell)}{d\ell})$
20
40
60
80
100
120
140
CRYSTAL SIZE : ℓ microns

FIG. 19

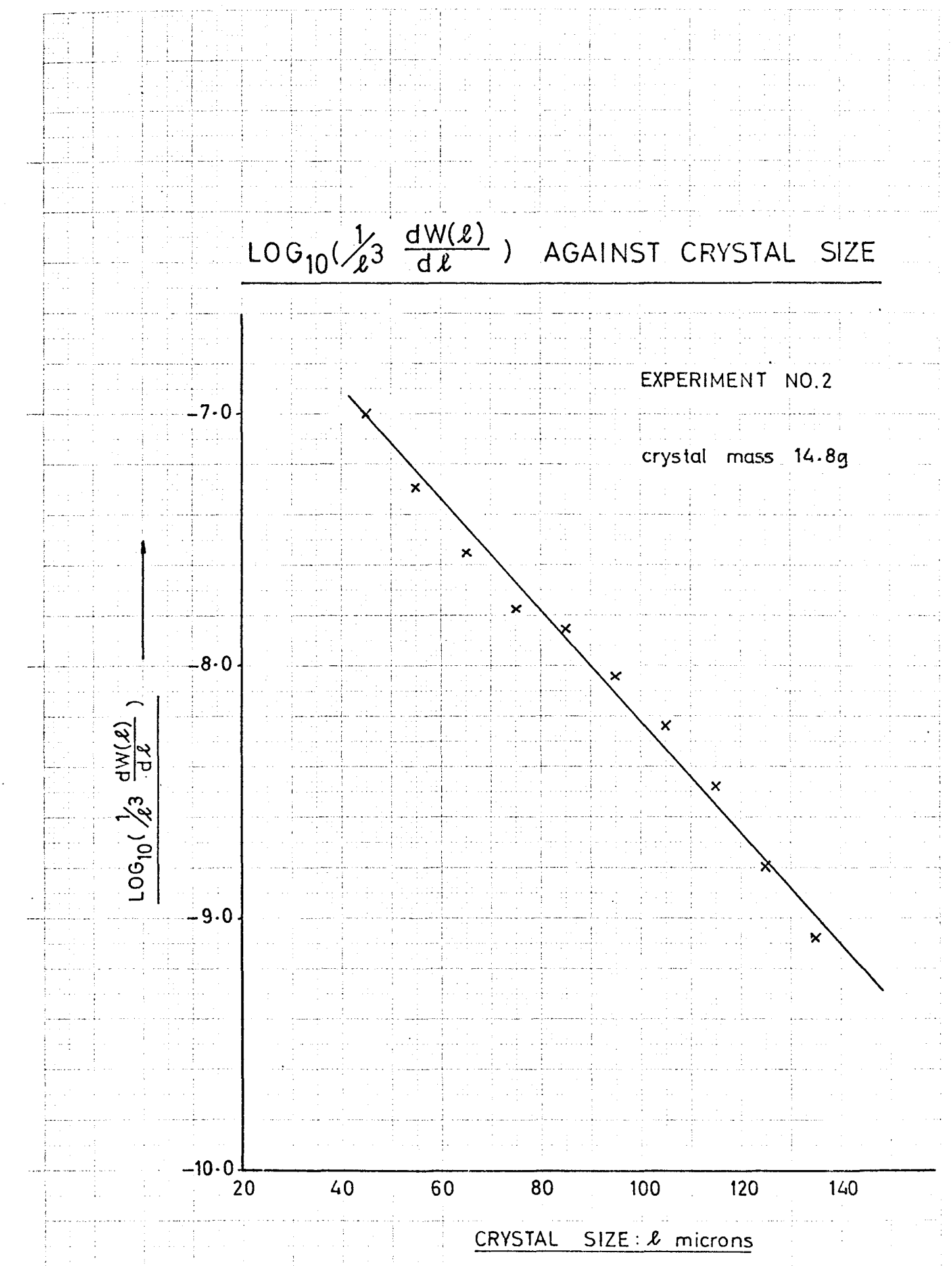
$LOG_{10}(\frac{1}{\ell^3}\frac{dW(\ell)}{d\ell})$ AGAINST CRYSTAL SIZE
EXPERIMENT NO.2
crystal mass 14.8g
$LOG_{10}(\frac{1}{\ell^3}\frac{dW(\ell)}{d\ell})$
-7·0
-8·0
-9·0
-10·0
20
40
60
80
100
120
140
CRYSTAL SIZE : ℓ microns

FIG. 20

$\log_{10}\left(\frac{1}{\ell^3}\frac{dW(\ell)}{d\ell}\right)$ AGAINST CRYSTAL SIZE

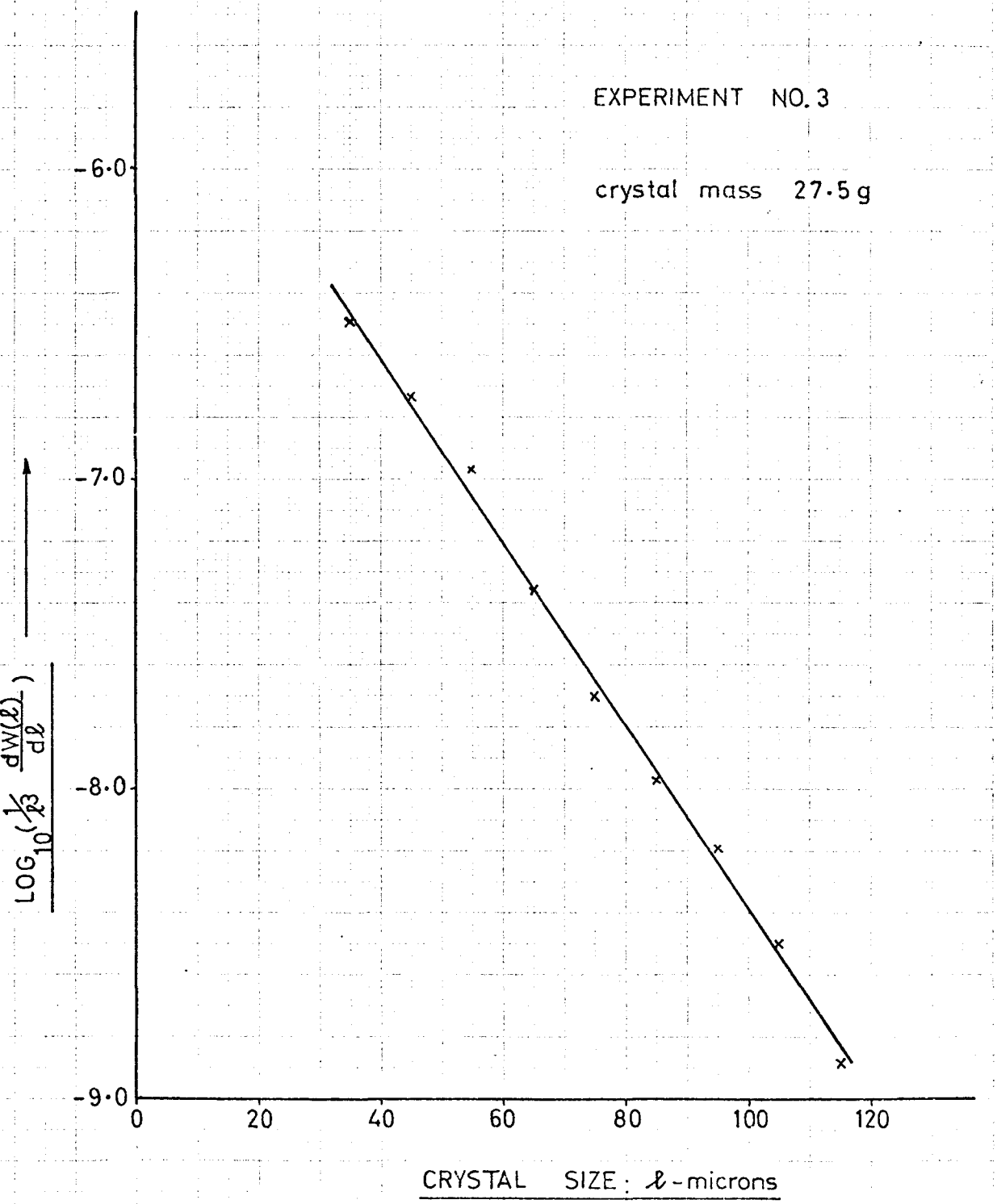

FIG. 21

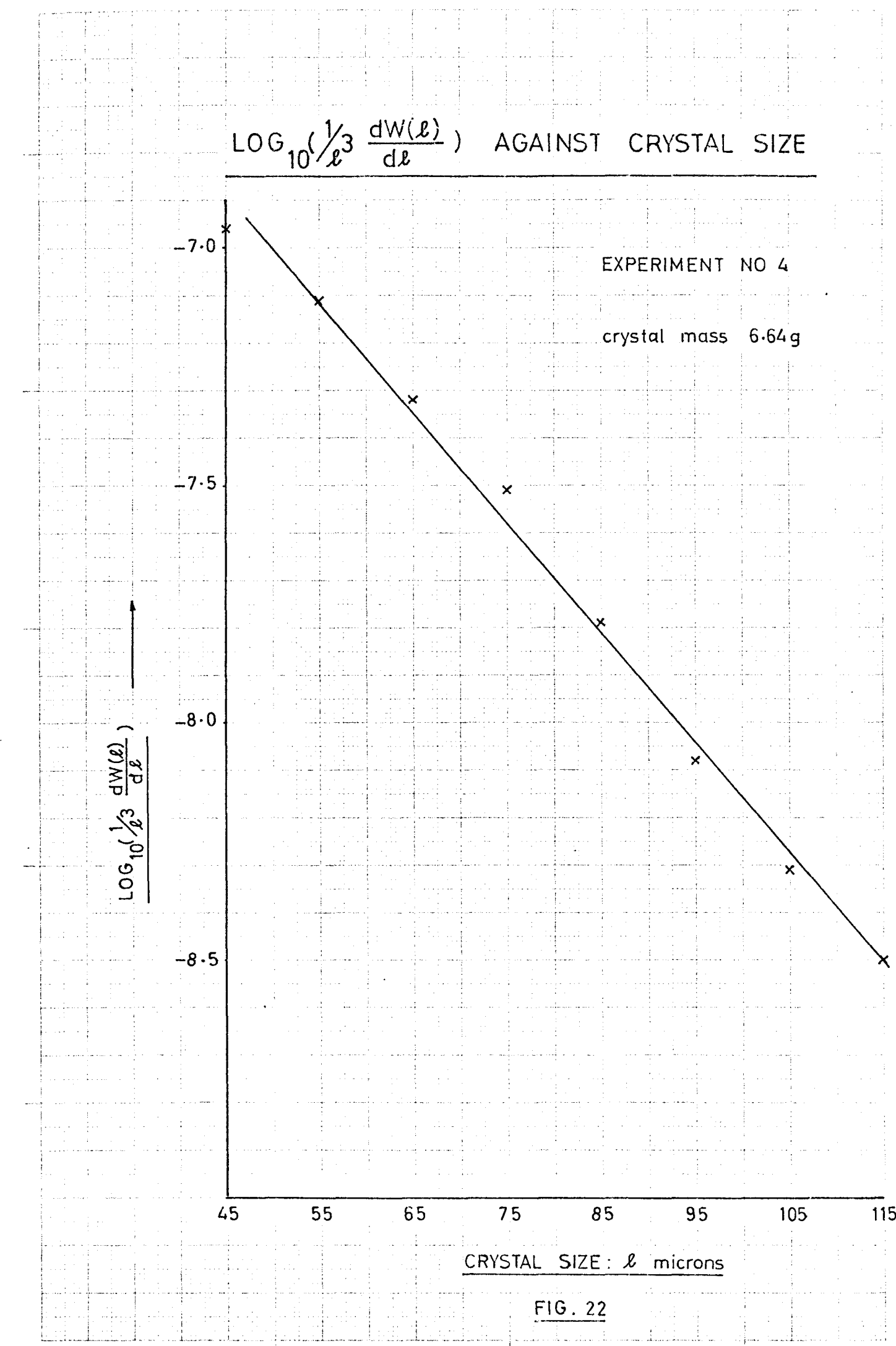
LOG10(1/ℓ3 dW(ℓ)/dℓ) AGAINST CRYSTAL SIZE
EXPERIMENT NO 4
crystal mass 6·64g
-7·0
-7·5
-8·0
-8·5
LOG10(1/ℓ3 dW(ℓ)/dℓ)
45
55
65
75
85
95
105
115
CRYSTAL SIZE : ℓ microns

FIG. 22

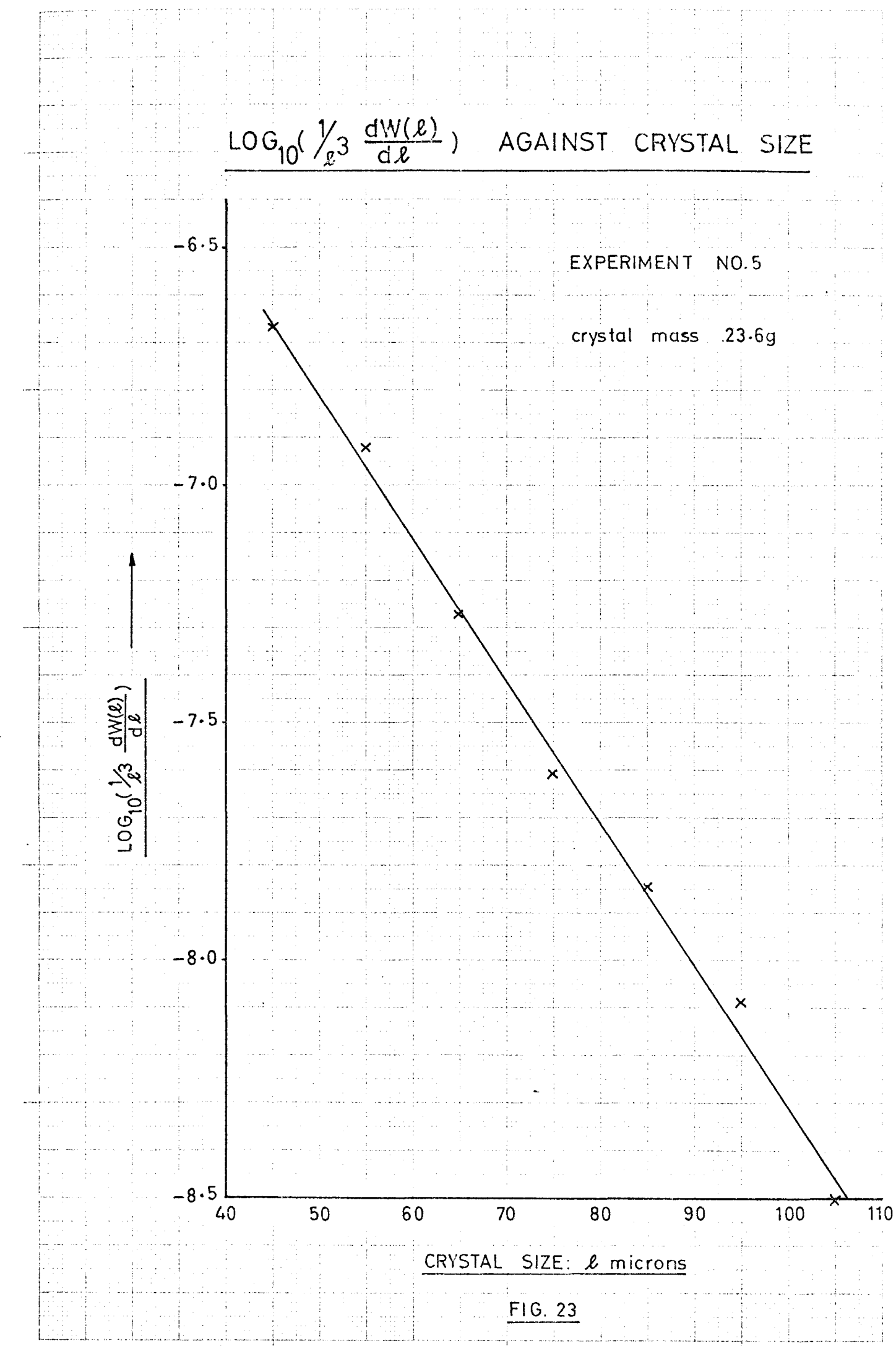
$LOG_{10}(\frac{1}{\ell^3}\frac{dW(\ell)}{d\ell})$ AGAINST CRYSTAL SIZE
EXPERIMENT NO. 5
crystal mass .23·6g
-6·5
-7·0
-7·5
-8·0
-8·5
$LOG_{10}(\frac{1}{\ell^3}\frac{dW(\ell)}{d\ell})$
40
50
60
70
80
90
100
110
CRYSTAL SIZE: ℓ microns

FIG. 23

$LOG_{10}(\frac{1}{\ell^3}\frac{dW(\ell)}{d\ell})$ AGAINST CRYSTAL SIZE

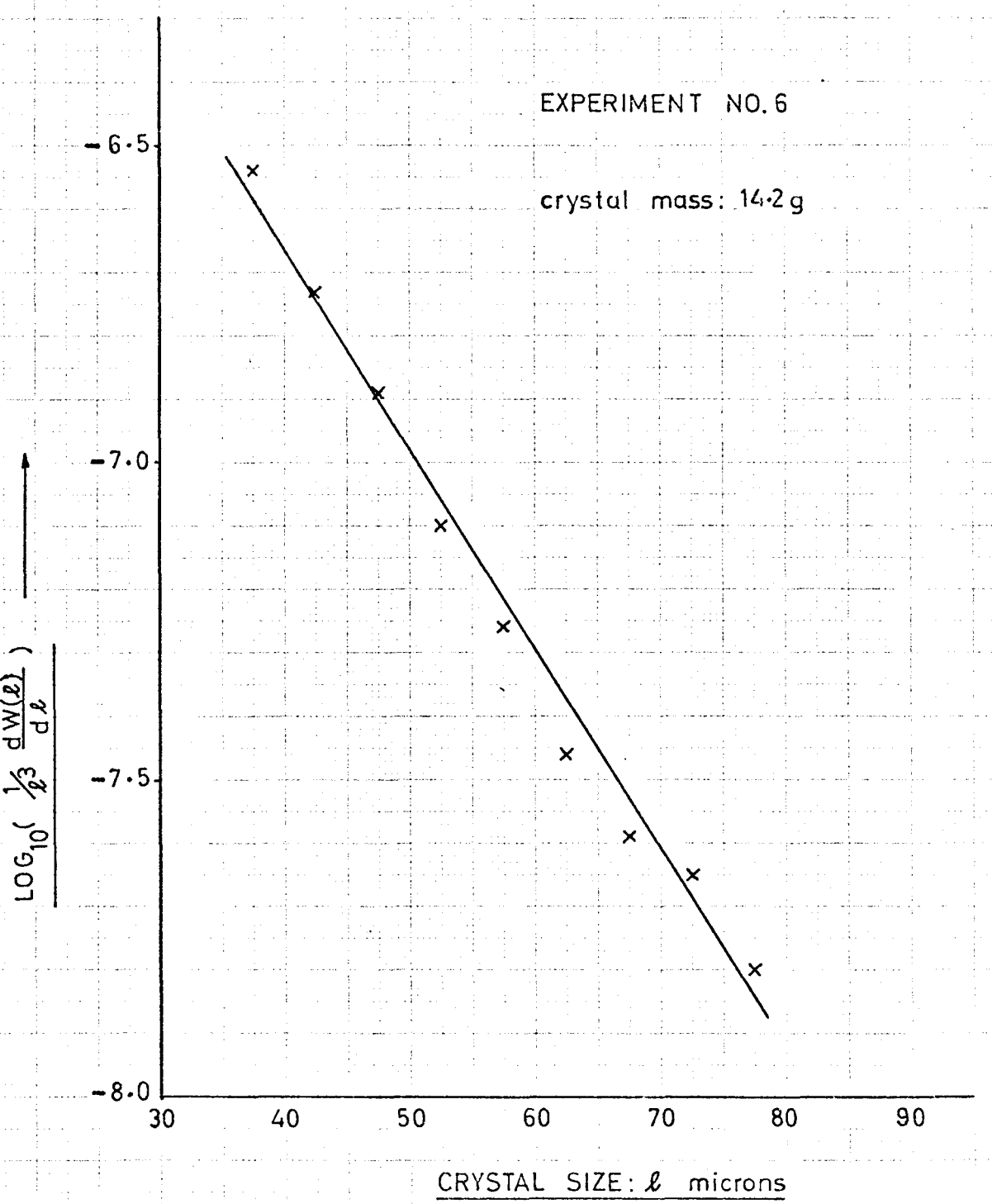

FIG. 24

$\text{LOG}_{10}\left(\frac{1}{\ell^3}\frac{dW(\ell)}{d\ell}\right)$ AGAINST CRYSTAL SIZE

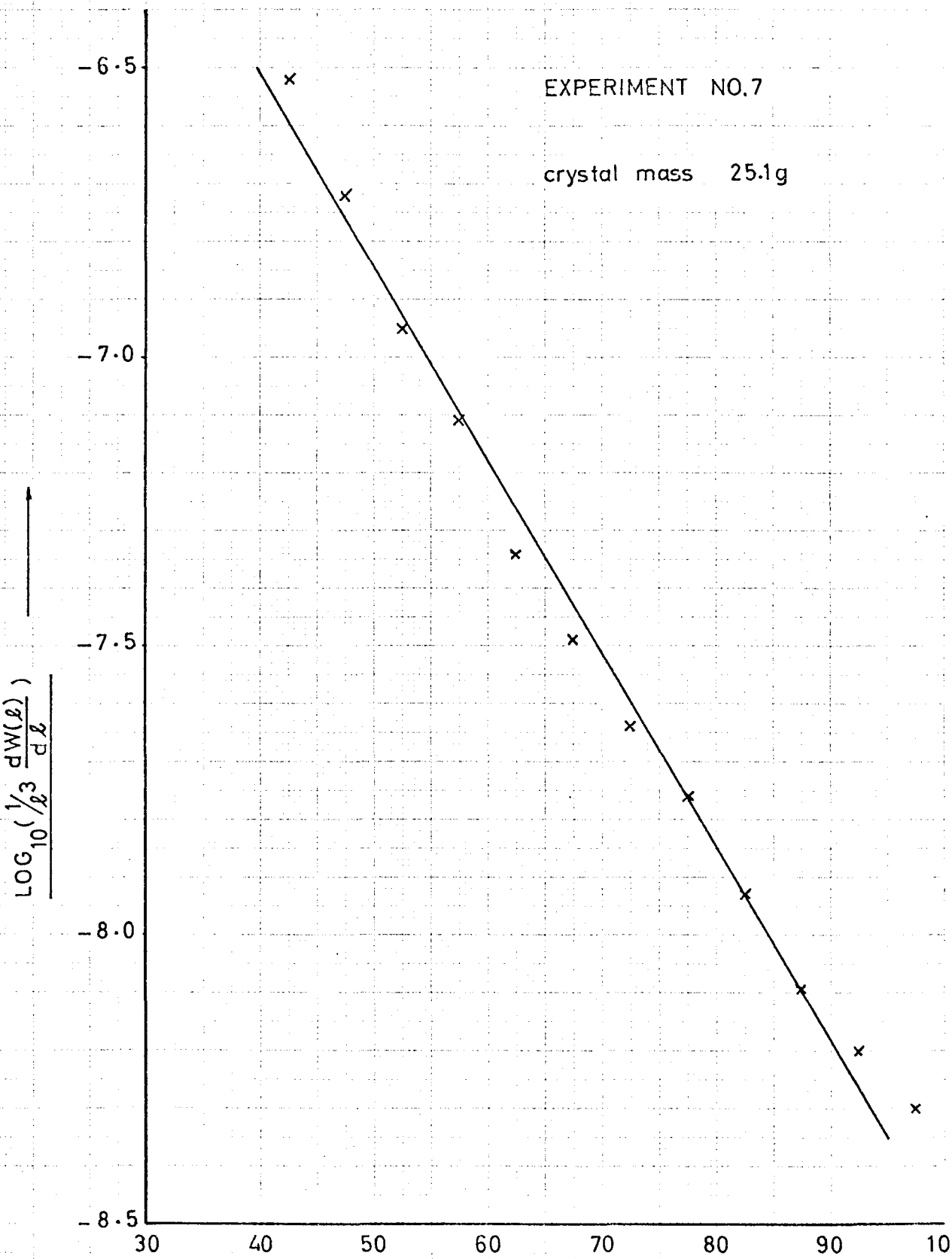

FIG. 25

43.5 gm WO_3/litre. The supersaturation of the solution was therefore the same for all the runs performed.

The growth rate of the crystals for each run were evaluated from the slopes of Figures 19 to 25. The results are presented in the table below.

Table VI. Growth rates obtained for the continuous crystallization experiments

Expt No	p, microns/min
1	.433
2	.384
3	.242
4	.377
5	.314
6	.257

It is seen that p differs considerably for the experiments performed, although the supersaturation of the solution was the same in all cases. Therefore it must be concluded that, as in the batch case, some other mechanism such as growth retardation due to the presence of impurities on the crystal surface is occuring.

5.9.4 The Growth Rate Equation applied to the Continuous Crystallization process

The continuous results were used to further test the proposed growth rate model as follows:

The feed solution to the continuous crystallizer was the same as that used for the batch runs and hence had the same impurity concentration y_o.

Letting c_x be the impurity concentration in the continuous crystallizer and doing an impurity mass balance over the crystallizer, we get:

Under steady state conditions, the mass rate of entry of the impurities is equal to the mass rate of removal of impurities,

i.e. $$y_o w_o = w c_x \tag{5-69}$$

where w_o = inlet flowrate of the feed solution

w = exit flowrate of the solution,

Rearranging equation (5-69)

$$c_x = \frac{y_o w_o}{w} \tag{5-70}$$

Replacing for c_x into equation (5-39) gives:

$$p = k_7(1 - k_{12}\frac{y_o w_o}{w})(c - c_s) \tag{5-71}$$

As mentioned earlier, the supersaturation $(c - c_s)$ was a constant for all runs performed,

Equation (5-71) can therefore be rewritten as:

$$p = k_{16}\{1 - \frac{k_{12} y_o w_o}{w}\} \tag{5-72}$$

putting $k_{17} = k_{12}y_o$ (5-73)

results in:

$$p = k_{16}\{1 - \frac{k_{17}w_o}{w}\} \qquad (5\text{-}72a)$$

5.9.5 Test of the model

Examination of equation (5-72a) shows that if p is plotted against w_o/w a straight line of slope $- k_{16}k_{17}$ should be obtained. The experimental results were plotted in this way (see Figure 26). It is seen that the experimentally determined points lie reasonably well along a straight line indicating that the growth rate model fits the continuous crystallization results.

The constants k_{16} and k_{17} were evaluated from the slope of Figure 26 and by considering any point on the graph. The results were as follows.

$$k_{16} = 1.230$$

$$k_{17} = .319$$

Replacing for k_{17} into equation (5-73) gives

$$k_{17} = k_{12}y_o = .319 \qquad (5\text{-}73a)$$

From equation (5-38)

$$x = k_{12}c_x \qquad (5\text{-}38)$$

i.e. the fraction of the crystal surface which is completely inhibited by impurities is proportional to the concentration of the impurities in the solution.

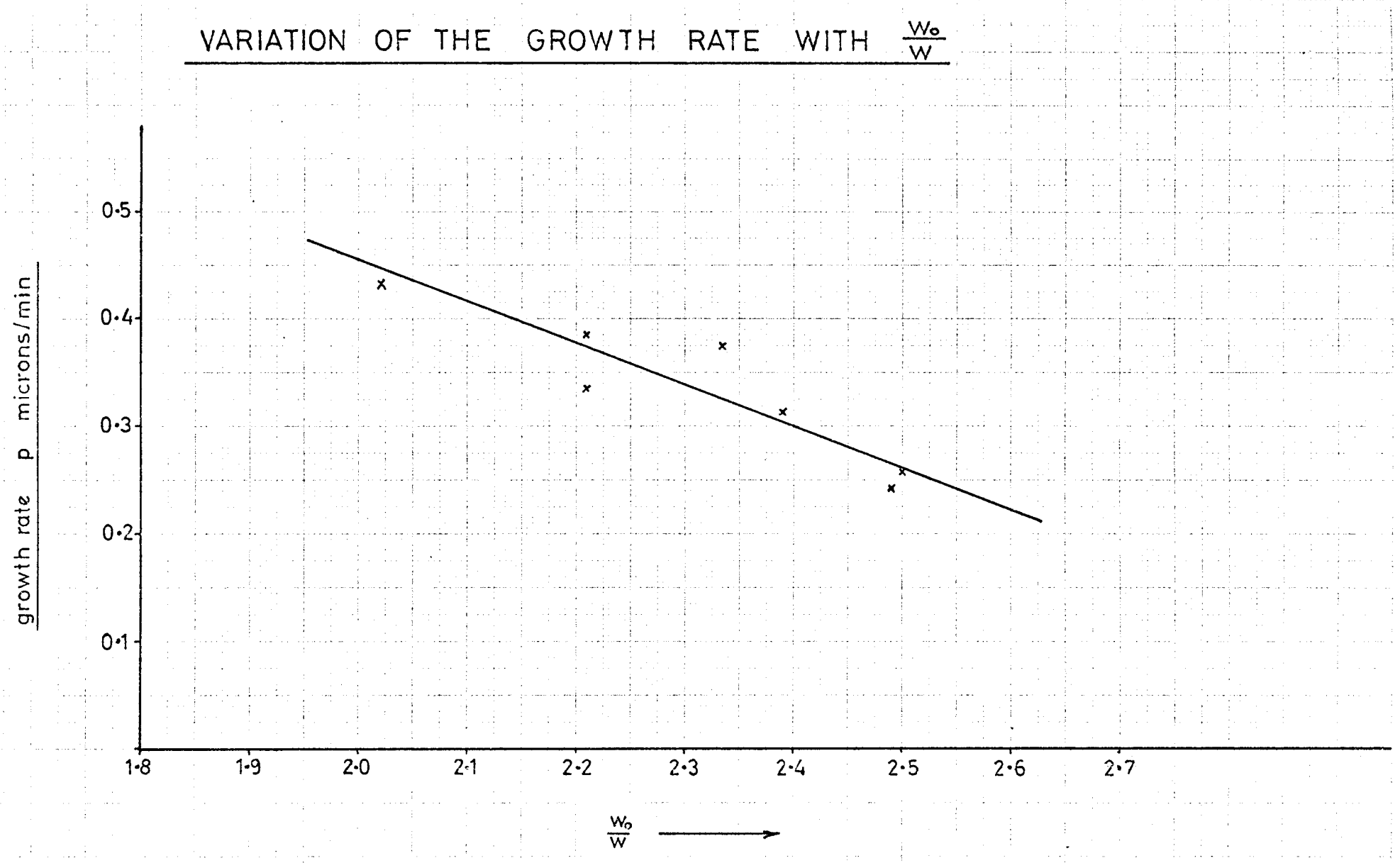
VARIATION OF THE GROWTH RATE WITH $\frac{W_o}{W}$
growth rate p microns/min
0·5
0·4
0·3
0·2
0·1
1·8
1·9
2·0
2·1
2·2
2·3
2·4
2·5
2·6
2·7
$\frac{W_o}{W}$

FIG. 26

If the same impurity mechanism is operating in both the batch and continuous crystallization processes then the constant k_{12} should be the same for both cases.

From the slope of Figure 18 (batch results) we have:

$$k_7 k_{13} = 13.45 \qquad (5\text{-}74)$$

k_7 was evaluated by considering any point on the straight line:

The result was:

$$k_7 = 6.38 \times 10^{-2} \qquad (5\text{-}75)$$

$$k_{13} = 211 \qquad (5\text{-}76)$$

From equation (5-42)

$$k_{13} = k_{12} y_o V_o \qquad (5\text{-}42)$$

and since V_o, the original volume of the solution was 600 ml, for all batch runs performed

$$k_{12} y_o = 0.351 \qquad (5\text{-}77)$$

Since y_o, the concentration of impurities in the starting solution was the same for both the batch and continuous experiments, it can be seen from equations (5-73a) and (5-77) that the two values obtained for k_{12} do not differ by more than 10%. Taking into account the experimental error involved these values can be regarded as being the same.

It must therefore be concluded that the growth rate model and in particular the proposed impurity effect on the growth rate is an excellent representation of what is actually taking place in the crystallizer.

Part III. The Relationship between the Batch and Continuous Results

5.10 COMPARISON OF THE RESULTS

The growth rates obtained from the batch and the continuous crystallization results can be compared by adopting the following procedure.

The growth rate equations for the batch and continuous crystallization processes as derived previously, are:

$$\text{Batch:} \qquad p = k_7\{1 - \frac{k_{12}y_o V_o}{V}\}(c - c_s) \tag{5-41}$$

$$\text{Continuous:} \quad p = k_7\{1 - \frac{k_{12}y_o w_o}{w}\}(c - c_s) \tag{5-71}$$

It is seen that the batch and continuous equations are analogous, with V_o/V in the batch case being replaced by w_o/w in the continuous case.

The constants k_7 and $k_{12}y_o$ were previously evaluated from the batch crystallization results, the numerical values being.

$$k_7 = 6.38 \times 10^{-2} \tag{5-75}$$

$$k_{12}y_o = 0.351 \tag{5-77}$$

Replacing these values in equation (5-71) together with $c_s = 43.5$ gm WO_3/litre gives

$$p = 6.38 \times 10^{-2}\{1 - .351\frac{w_o}{w}\}(c - 43.5) \tag{5-78}$$

This equation should be capable of predicting the experimentally determined continuous results. This was done for

various values of w_o/w and the curve obtained for the growth rate p as a function of w_o/w was compared with the experimentally determined curve of Figure 26. This comparison is shown in Figure 27.

It is immediately apparent from Figure 27 that the results as predicted from equation (5-78) are completely different from the experimentally determined values, being much higher than the experimental results, for the range of w_o/w used.

It is of interest to note that Randolph and Rajagopal (17) obtained a similar result when comparing their work on the growth rate of potassium sulphate crystals with that done by Ishii (9) at a previous date.

Ishii performed experiments with single crystals of potassium sulphate. His experiments were arranged in such a way that the growth rate of the crystals was dependent only on the surface rate. However, he also developed a diffusion correlation and Randolph and Rajagopal used this to estimate the diffusion resistance for the crystals obtained from a continuous crystallizer in their investigation. They found that by adding this diffusion resistance in series, to the surface limiting rate of Ishii, the overall rate constant was lowered by 12%, whereas their experimentally determined rate was 54% lower than that of Ishii.

The results of Randolph and Rajagopal further showed that the nucleation rate was dependent on the solids concentration in the solution and hence a secondary nucleation mechanism was taking place. In order to explain why their results were lower

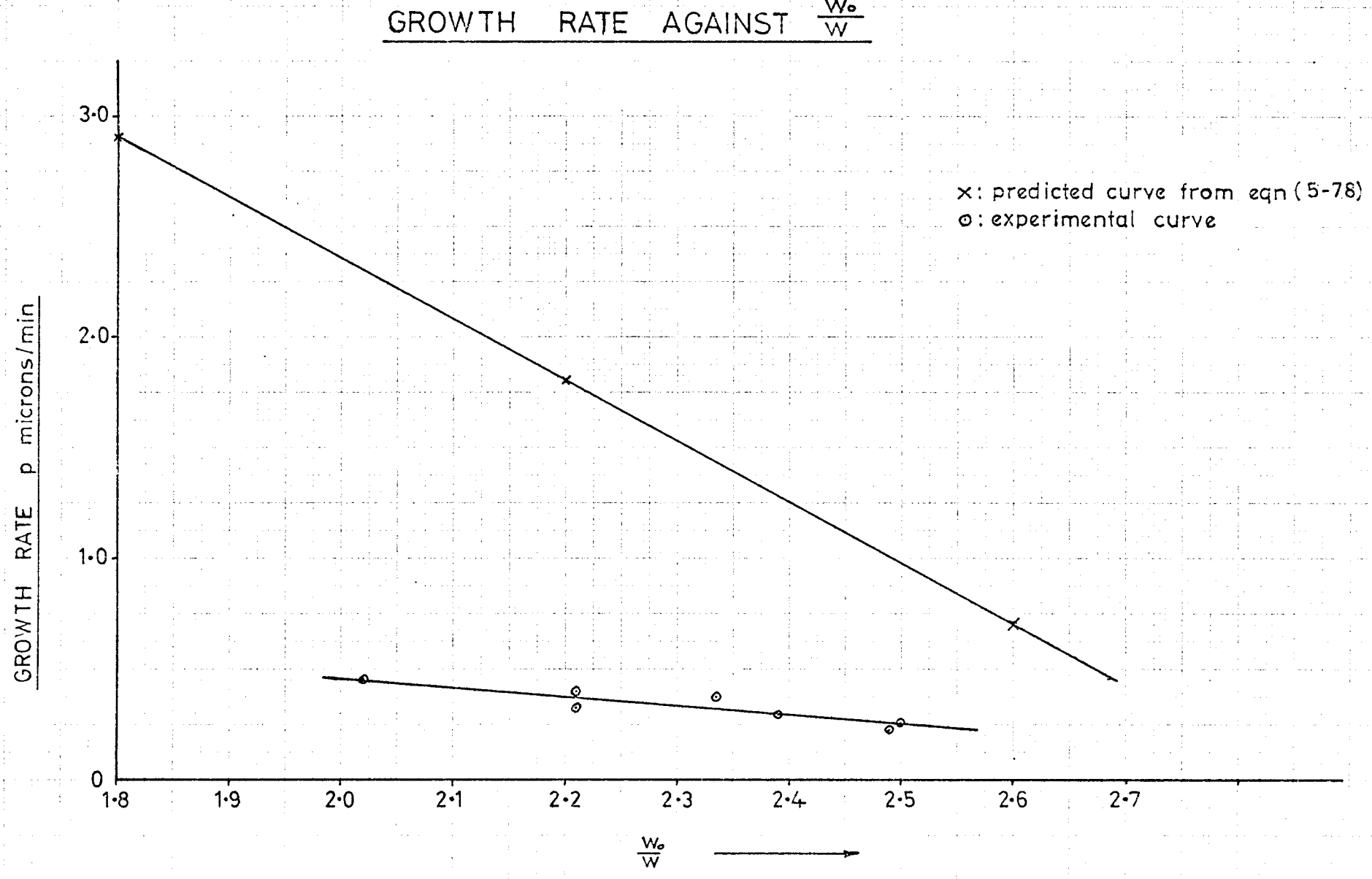
GROWTH RATE AGAINST $\frac{W_o}{W}$
GROWTH RATE p microns/min
3·0
2·0
1·0
0
1·8
1·9
2·0
2·1
2·2
2·3
2·4
2·5
2·6
2·7
$\frac{W_o}{W}$
x: predicted curve from eqn (5-78)
o: experimental curve

FIG. 27

than those obtained by Ishii, they proposed that nucleation was in fact occuring on active sites on the crystal surface and that it was inhibited at high rates of crystal growth. They therefore suggested that nucleation and growth were competing for active sites on the crystal surface.

Based on the above conclusion drawn by Randolph and Rajagopal, it would appear that the difference between the batch and the continuous growth rates, obtained in this investigation , could possibly be explained by the difference in nucleation mechanisms between the batch and continuous crystallization experiments. These nucleation mechanisms will now be discussed in more detail.

5.11 DISCUSSION OF THE NUCLEATION PROCESSES

The nucleation rate Q(t) for the batch crystallization process can be evaluated directly from equation (5-16) which is:

$$\frac{d}{dt}\left\{\frac{\alpha_1 M(t)}{\rho_s}\right\} - \frac{4pM(t)}{\rho_s} = Q(t)\ell_o^4 \qquad (5\text{-}16)$$

as all the other terms in the equation are known.

Q(t) was calculated, as a function of crystallization time, for the runs performed at a heating rate, corresponding to an outside jacket temperature of 140°C. The results for the three stirrer speeds are shown in Figures 28, 29 and 30. In addition the sensitivity of the nucleation rate as evaluated from the above equation was tested in order to establish how much reliance could be placed on the shapes of these curves. This was done for the case of the stirrer speed of 250 r.p.m. using different values

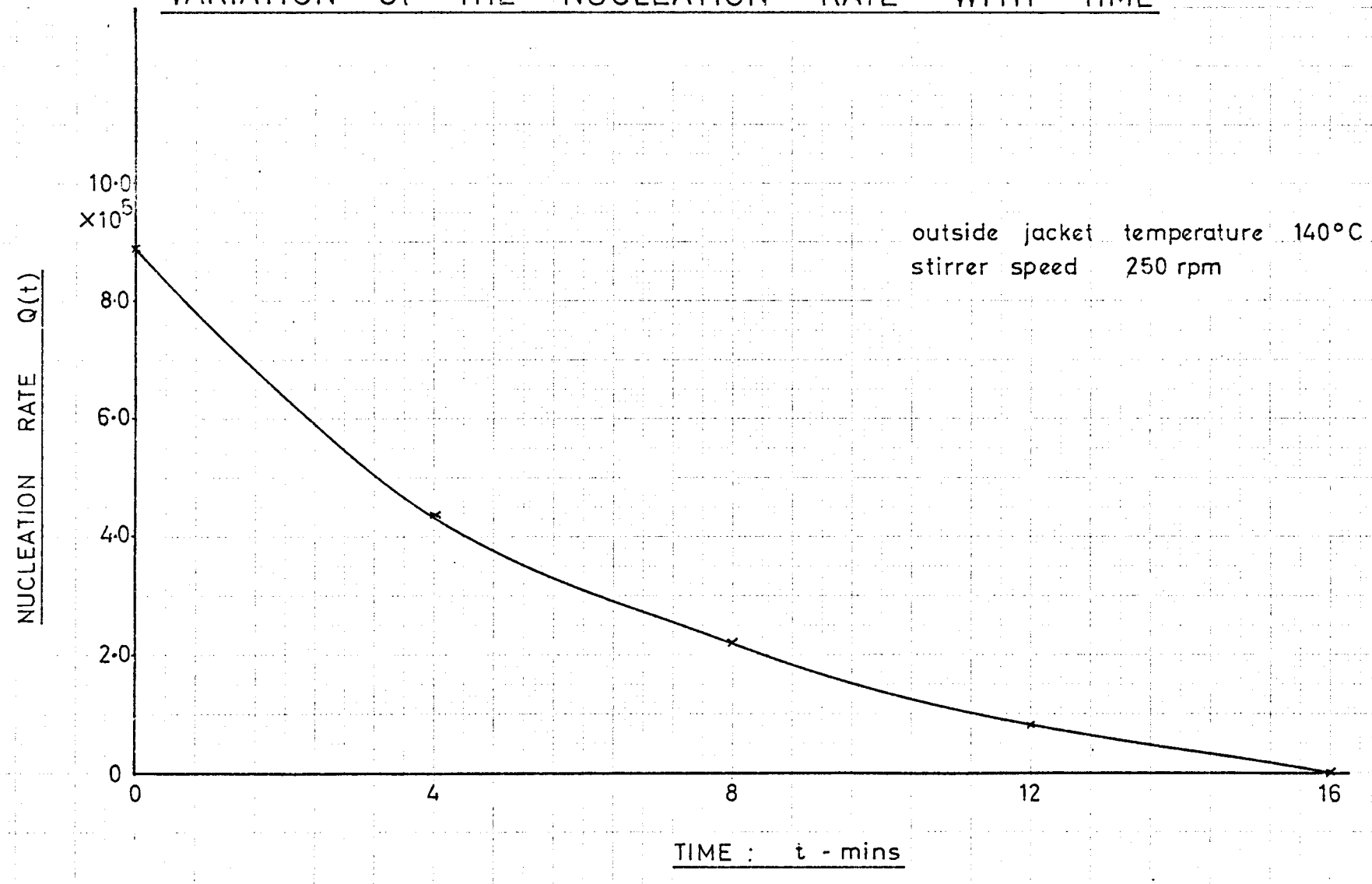
VARIATION OF THE NUCLEATION RATE WITH TIME
NUCLEATION RATE Q(t)
10·0
×10⁵
8·0
6·0
4·0
2·0
0
0
4
8
12
16
TIME : t - mins
outside jacket temperature 140°C
stirrer speed 250 rpm

FIG. 28

VARIATION OF THE NUCLEATION RATE WITH TIME

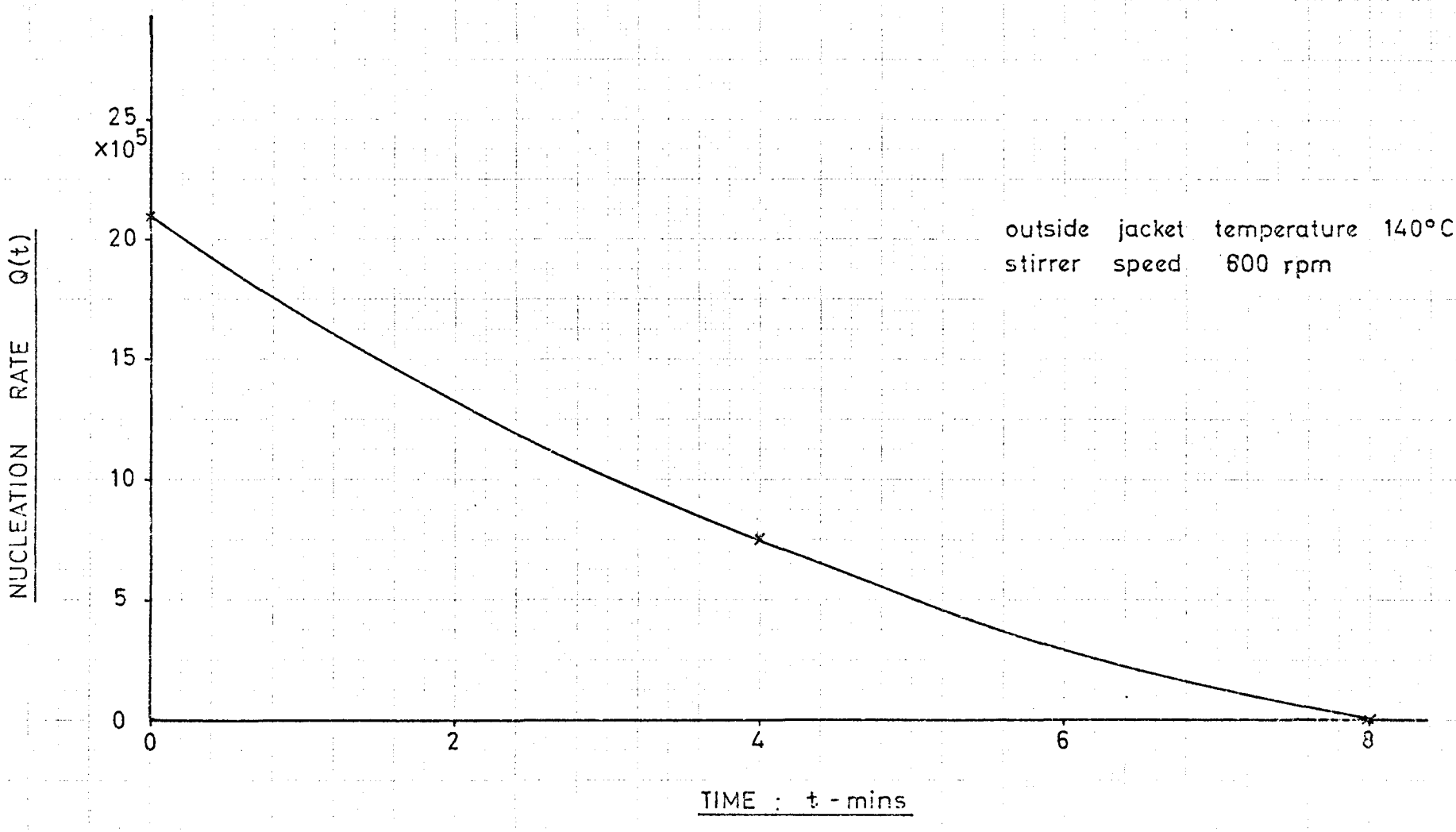

FIG. 29

VARIATION OF THE NUCLEATION RATE WITH TIME

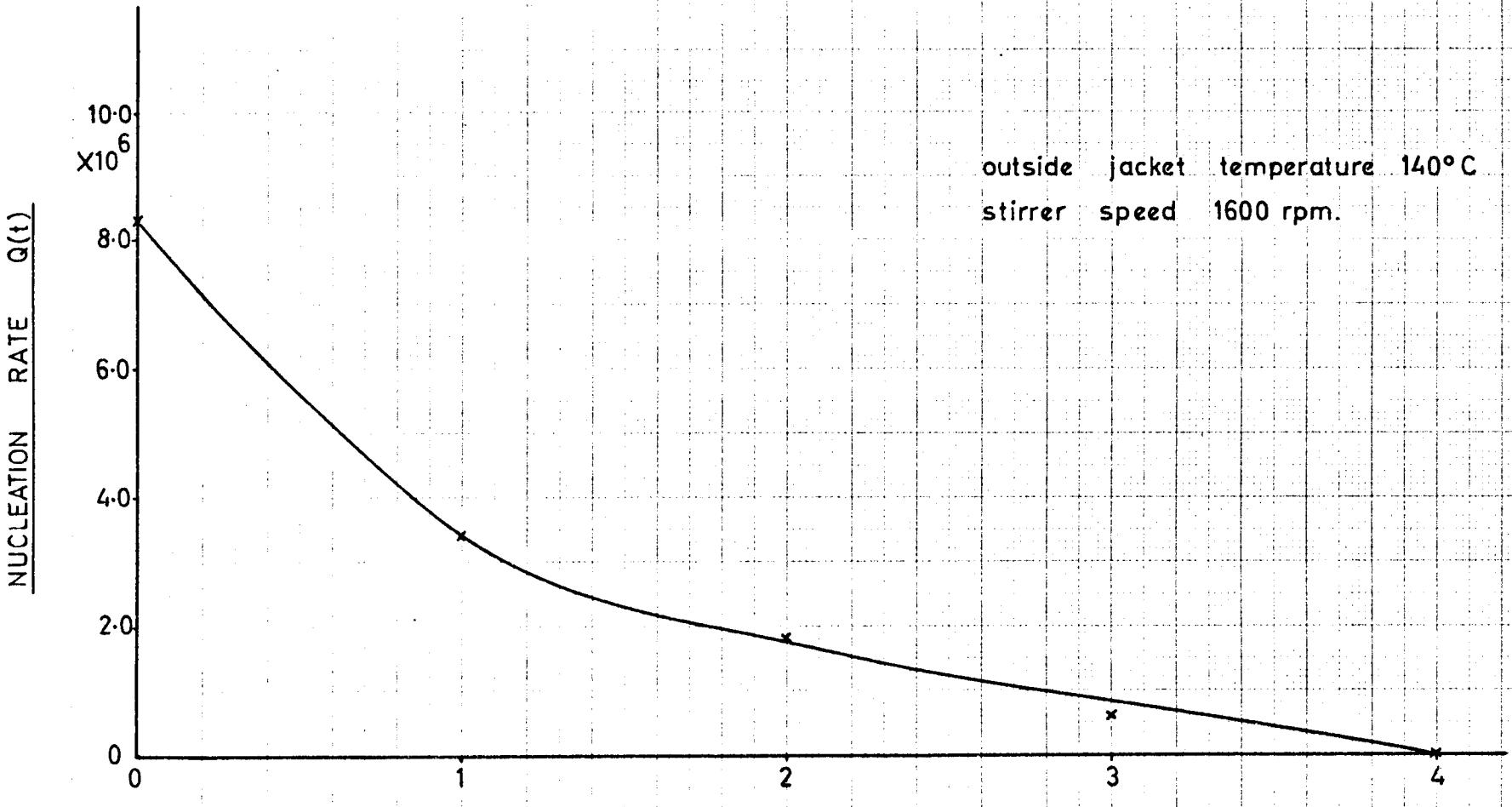

FIG. 30

of ℓ_o, the critical nuclei size, in equation (5-16) and calculating the corresponding values of Q(t). The result is shown graphically in Figure 31. It is seen that the numerical value of the nucleation rate is relatively sensitive to a change in ℓ_o but of greater importance is the fact that the shape of the curve remains basically the same.

It can be seen from Figures 28, 29 and 30 that the nucleation rate at time t = 0, when the crystals can first be seen in the crystallizer, is at its largest and thereafter decreases quite rapidly in a manner rather similar to an exponential decay. It is furthermore apparent from these graphs that the higher the stirrer speed, the more rapidly the nucleation rate decays with crystallization time. This is particularly noticeable in the case of the stirrer speed of 1600 r.p.m., where after 4 minutes no further nucleation takes place. This means that after 4 minutes the total number of crystals in the crystallizer remains constant and all the solid material coming out of solution is used for the growth of these crystals.

If we compare this to nucleation taking place in the continuous crystallizer, at the same stirrer speed of 1600 r.p.m., we see immediately that a totally different mechanism is taking place. In a continuous crystallizer operating under steady state conditions, the total number of crystals in the vessel must remain constant. Crystals are continuously being removed from the vessel in the outlet stream. This means that in order to preserve the number balance an equal number must be introduced into the

SENSITIVITY OF THE NUCLEATION RATE TO THE CRITICAL NUCLEI SIZE

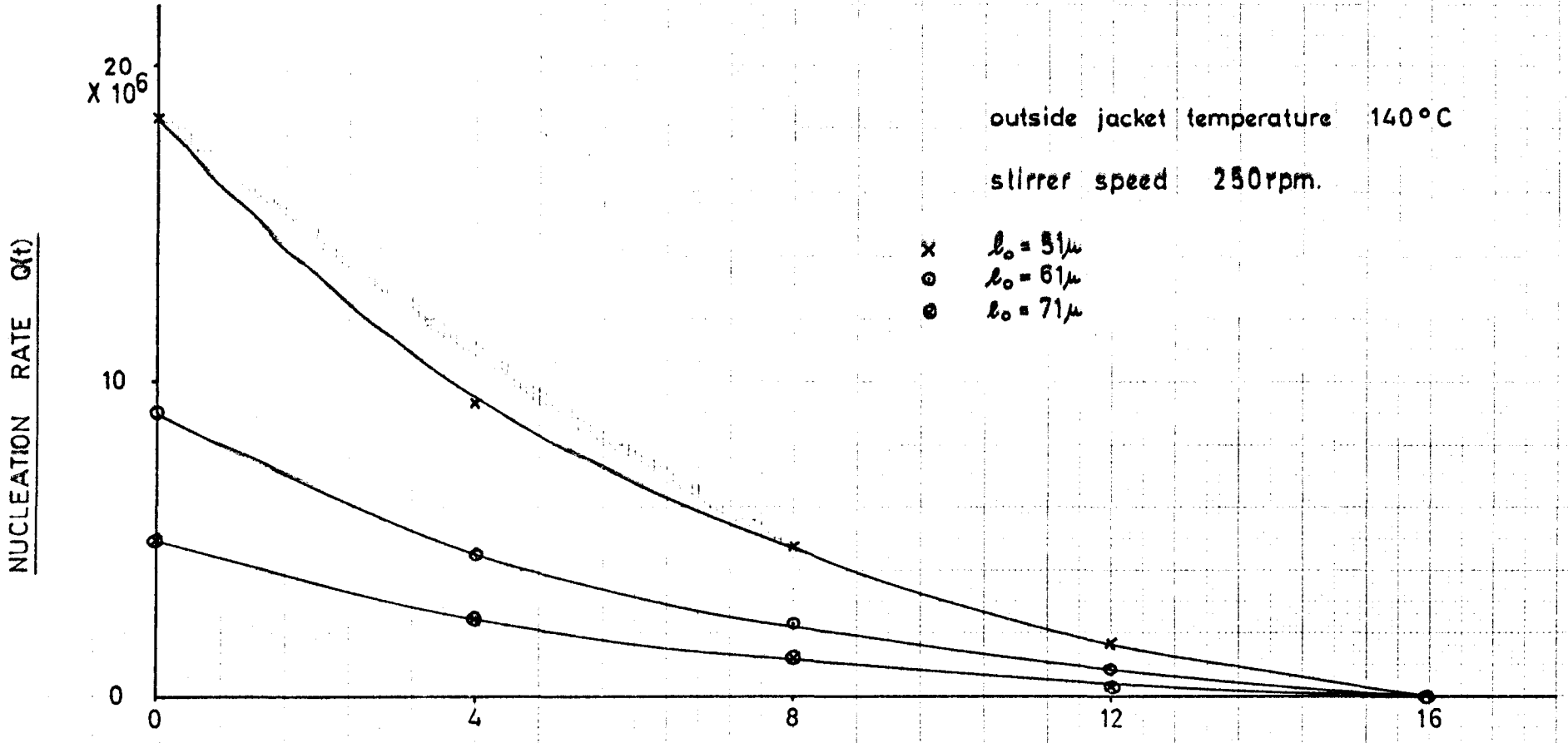

FIG. 31

vessel. Since the feed stream did not contain any seed crystals, the only way crystals can be introduced is by nucleation. Therefore the number of crystals leaving in the exit stream must equal the number produced by nucleation. Nucleation in the continuous crystallizer is thus taking place continuously at a steady rate, whereas in the batch case at the same stirrer speed of 1600 r.p.m. it is only occuring in the initial stages. It is postulated that nucleation of APT crystals takes place in the following way. Embryo order themselves at active sites on the crystal surface but do not necessarily grow there. They then chip off from the surface and form nuclei.

In the batch crystallization experiments the nucleation rate is higher initially and then decays fairly rapidly thereafter. The higher the stirrer speed the higher the rate of decay. This effect of stirrer speed on the rate of decay can be accounted for as follows.

It has been established that as the stirrer speed increases the critical nuclei size decreases (Table I). The same amount of material is being made available for nucleation at the three different stirrer speeds, as conditions in the crystallizer were identical in all three cases (Section 5.3.1), and since the nuclei are smaller at higher stirrer speeds more can be formed per unit time. Once enough of these nuclei have been formed to take up all the solid material coming out of solution, nucleation stops and only crystal growth occurs. It is therefore to be expected that the nucleation rate will decay more rapidly as the stirrer speed is increased.

In the continuous crystallizer the nucleation rate remains constant for a given set of crystallization conditions. Now since it has been postulated that embryo ordering takes place at active sites on the crystal surface, nucleation and growth are in fact in completion with each other for these sites.

It should be remembered that no matter how the crystallization conditions in the continuous crystallizer were altered, the solution concentration always remained constant at $\sim$160 gm WO_3/litre, which is higher than was obtained in any of the batch crystallization experiments. This rather strange result strongly supports the proposed theory of competition between nucleation and growth for the following reason. If competition between nucleation and growth is taking place then the rate of mass deposition of solid material on the crystal surface would be expected to decrease and hence would result in an increase in the supersaturation. This can however, not occur indefinitely. Some stage is reached when a sufficiently high supersaturation (which is the driving force for both nucleation and growth) has been attained at which both nucleation and growth can occur simultaneously on the crystal surface under steady state conditions.

The proposed mechanism of competition between nucleation and growth for active sites on the crystal surface also explains the low growth rates in the continuous crystallizer compared to the batch crystallizer. In the batch crystallizer, at a stirrer speed of 1600 r.p.m, the nucleation rate drops off to zero after a very short period and crystal growth can continue uninhibited.

In the continuous crystallizer, growth and nucleation take place simultaneously, and because of the competition the growth rate is thus inhibited and is far lower than in the batch case.

In order to test the proposed nucleation mechanism the following procedure was adopted. Since nucleation and growth are in direct competition, some of the available sites will be used exclusively for nucleation others exclusively for growth.

Defining y to be the fraction of the available sites in the continuous crystallization process which are used exclusively for growth. Then the "true growth rate" p_1 as given by the batch results as related to the growth rate p obtained from the continuous results is given by:

$$y = \frac{p}{p_1} \tag{5-79}$$

y was evaluated for the continuous experiments the results being shown in the table below.

Table VII. y Values for continuous crystallizer experiments

Expt No	p_1 (Evaluated from equation (5-78)	p (From experimental results)	$y = \frac{p}{p_1}$
1	2.300	.433	.189
2	1.775	.384	.216
3	1.000	.242	.242
4	1.425	.377	.265
5	1.275	.314	.246
6	1.775	.334	.188
7	1.975	.258	.131

The surface of the crystals used for nucleation or ordering of embryos is given by.

$$U = V(1 - y) \int_{\ell_o}^{\infty} g(\ell)\ell^2 d\ell \qquad (5\text{-}80)$$

If the proposed nucleation theory is realistic it is to be expected that the nucleation rate will be strongly dependent on U.

The nucleation rate N and surface area U were both evaluated for each experiment, N being obtained from the cumulative weight distribution curves and U from the above equation using the values of y given in Table VII.

The results are presented in the table below.

Table VIII. Nucleation rate as a function of crystal surface area being used for embryo ordering

Expt No	N $cm^{-3}\ min^{-1}$	U cm^2
1	518	166.8
2	668	265.8
3	1755	486.5
4	1072	455.2
5	2065	594.0
6	1053	248.0
7	2405	661.0

In figure 32 the above results are plotted in the form N versus U. A reasonably good straight line can be drawn through the points, which also passes through the origin indicating that the nucleation rate is proportional, and hence strongly dependent on, the surface area of the crystals on which embryo are ordered. This result tends to indicate that the proposed mechanism for nucleation is a good representation of what is actually occuring in the crystallizer.

VARIATION OF THE NUCLEATION RATE WITH CRYSTAL SURFACE AREA

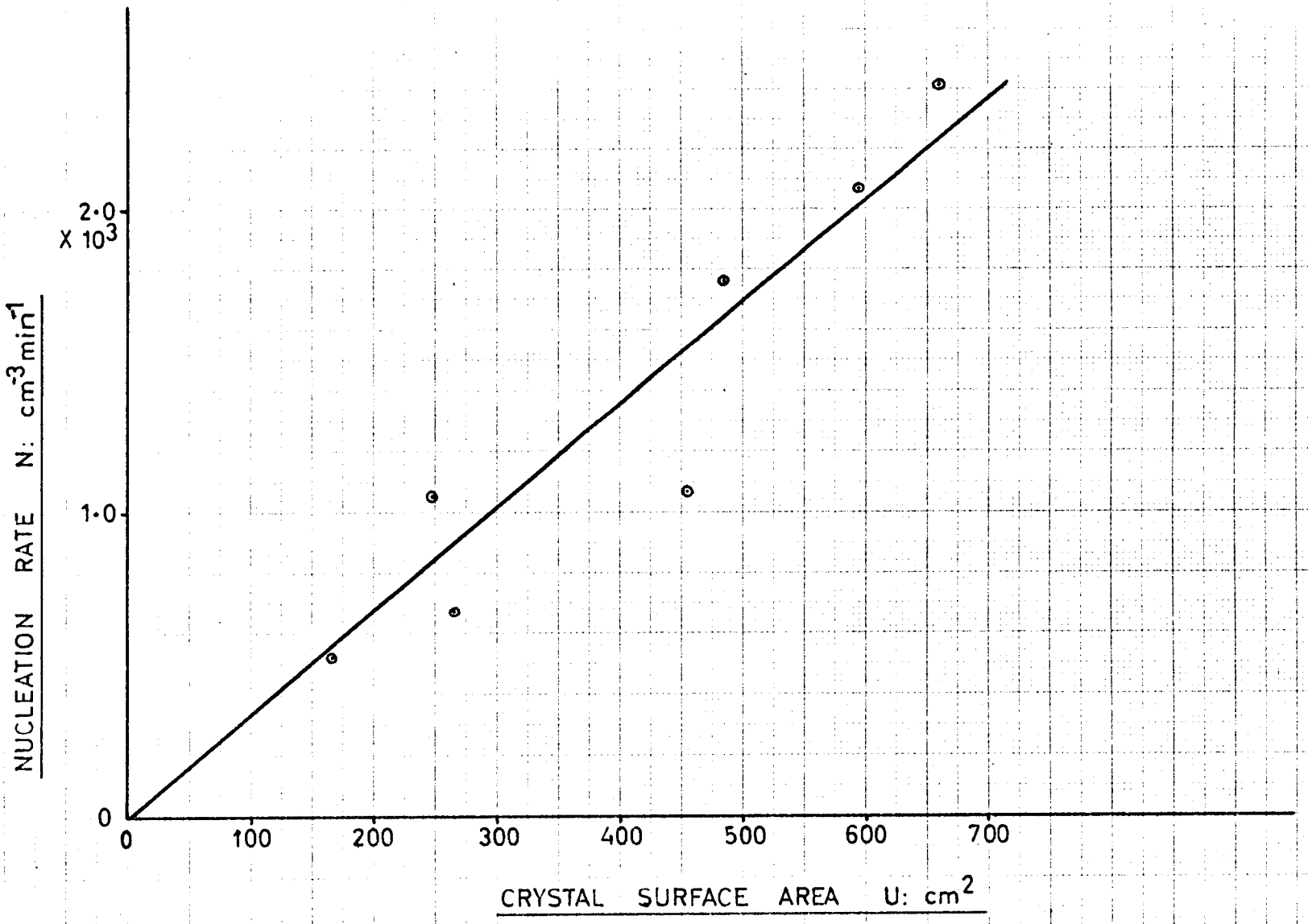

FIG. 32

CHAPTER VI

A SUMMARY OF THE MAJOR RESULTS

1. Batch crystallization experiments performed with seed crystals APT (see Chapter IV) showed that the growth rate was independent ofthe crystal size.

2. Experiments performed in the continuous, mixed product removal, crystallizer confirmed the result that the growth rate of APT crystals is independent of the crystal size

3. The critical nuclei size of APT crystals was shown to be in the range of 25-60 microns, dependent on the stirrer speed.

4. The growth rate of APT crystals was found to be independent of the stirrer speed indicating that the crystal growth was not a diffusion controlled process.

5. Both the batch and continuous crystallization results indicated that there was some termination process in the growth rate of APT crystals. Experimental evidence did not favour the mechanism of termination by the break-up of crystals due to collisions. It was postulated that the termination in the growth was caused by the presence of impurities on the crystal surface. Based on the work of Gorshtein and Baliner, on the impurities present in APT crystals after crystallization from an ammonium tungstate solution, and on theoretical considerations, a growth rate model incorporating a termination term was developed.

This model was of the form.

$$p = k_7(1 - k_{12}c_x)(c - c_s)$$

This model was shown to fit both the batch and continuous results reasonably well.

6. The growth rate of crystals evaluated from the continuous crystallization experiments were found to be considerably lower than those obtained for the batch experiments under similar conditions. It was postulated that the difference was due to different nucleation mechanisms occuring in the two cases. In the batch case the nucleation rate at time t = 0 was at its highest and thereafter decayed rapidly, whereas in the continuous case nucleation remained constant throughout the duration of the run. Furthermore experimental evidence indicated that competition between nucleation and growth was taking place. Since nucleation in the batch crystallizer only had a short duration because of the rapid decay, the growth rate was not really affected, whereas in the batch case nucleation was occuring at a constant rate and hence, due to this competition, the growth rate was subsequently lowered.

7. The nucleation rate of the crystals in the continuous crystallizer was shown to be proportional to the surface area of the crystals on which embryo "ordering" was taking place.

APPENDIX A

THE DETERMINATION OF THE CUMULATIVE WEIGHT FRACTION PARTICLE SIZE DISTRIBUTION FROM THE SEDIMENTATION BALANCE CURVE

The curve obtained from the sedimentation balance is a plot of the mass of the crystals on the scale pan versus the settling time. A typical curve is drawn below.

Figure A.1.

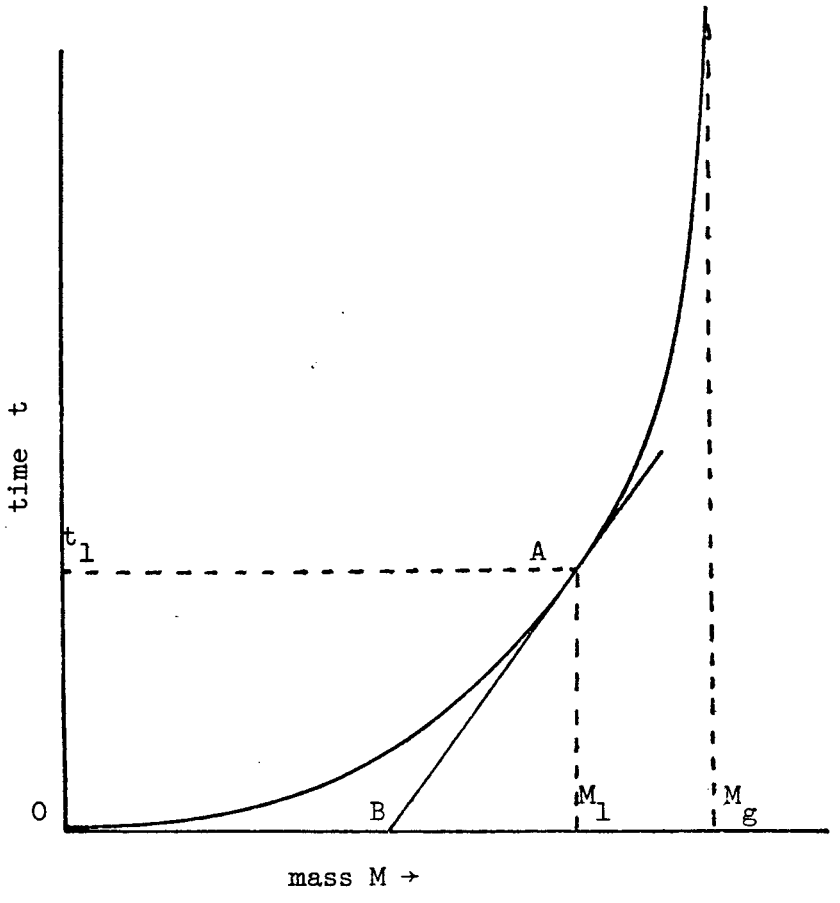

Consider a point A on this curve with co-ordinates (M_1, t_1). Let a tangent drawn to the curve at the point A, cut the M axis at point B.

From the above drawing, the slope of this tangent is:

$$\left(\frac{dt}{dM}\right)_{t=t_1} = \frac{t_1}{M_1 - OB} \qquad \text{(A-1)}$$

rearranging this equation:

$$OB = M_1 - t_1\left(\frac{dM}{dt}\right)_{t=t_1} \qquad \text{(A-2)}$$

Consider now the actual settling of the particles from a homogeneous suspension in a cylindrical vessel.

Let the original height of the suspension be h.

If particles of size ℓ_s say, have a terminal velocity of $\frac{h}{t}$, then after time t all particles of size greater than ℓ_s will have fallen to the bottom. The fractional weight of these particles is:

$$\int_{\ell_s}^{L} V(\ell).d\ell$$

where: L : is the maximum particle size present in the suspension.

$V(\ell)$: is the weight fraction of particles greater than size ℓ.

For particles of size less than ℓ_s, some but not all will have fallen to the bottom. This fraction of the particles will be:

$$\int_{o}^{\ell_s} QV(\ell).d\ell$$

where: Q is some fraction dependent on the particle size.

The total fraction that has fallen to the bottom is thus:

$$\theta = \int_{\ell_o}^{\ell_s} QV(\ell).d\ell + \int_{\ell_s}^{L} V(\ell).d\ell \qquad \text{(A-3)}$$

In order to find Q, we consider some size ℓ, less than ℓ_s, with a terminal velocity u.

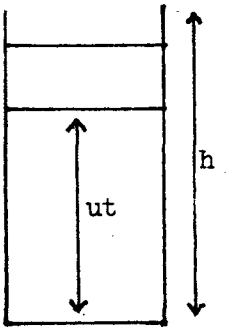

After a time t all particles in a column of height ut will have fallen out, so that

$$Q = \frac{ut}{h} \qquad \text{(A-4)}$$

Replacing for Q from (A-4) above into equation (A-3) gives:

$$\theta = \int_0^{\ell_s} \frac{ut}{h} V(\ell)\,d\ell + \int_{\ell_s}^{L} V(\ell)\,d\ell \qquad \text{(A-5)}$$

Differentiating with respect to t gives:

$$\frac{d\theta}{dt} = \int_0^{\ell_s} \frac{u}{h} V(\ell).d\ell \qquad \text{(A-6)}$$

because $\int_{\ell_s}^{L} V(\ell).d\ell$ is independent of t.

Multiplying both sides of equation (A-6) by t we get:

$$t\,\frac{d\theta}{dt} = \int_0^{\ell_s} \frac{ut}{h} V(\ell).d\ell \qquad \text{(A-7)}$$

Combining equations (A-7) and (A-5)

$$t\,\frac{d\theta}{dt} = \theta - \int_{\ell_s}^{L} V(\ell).d\ell \qquad \text{(A-8)}$$

Considering Figure A.1.

At any time t_1, the weight fraction of crystals that have fallen to the bottom is given by.

$$\theta = \frac{M_1}{M_g} \tag{A-9}$$

Dividing equation (A-2) through by M_g we get.

$$\frac{OB}{M_g} = \theta - t_1\left(\frac{d\theta}{dt}\right)_{t=t_1} \tag{A-10}$$

At any particular time t_1, equation (A-8) becomes:

$$t_1\left(\frac{d\theta}{dt}\right)_{t=t_1} = \theta - \int_{\ell_s}^{L} V(\ell).d\ell \tag{A-11}$$

From equations (A-10) and (A-11) we have:

$$\frac{OB}{M_g} = \int_{\ell_s}^{L} V(\ell).d\ell \tag{A-12}$$

now: $\int_{\ell_s}^{L} V(\ell)d\ell$ is the cumulative weight fraction of the crystals greater than size ℓ_s.

The cumulative weight fraction of the crystals up to size ℓ_s is related to this as follows:

$$W(\ell) = 1 - \int_{\ell_s}^{L} V(\ell).d\ell \tag{A-13}$$

$\therefore$ $W(\ell)$ can easily be found from the sedimentation balance curve by drawing a tangent to the curve at any point and finding the fraction $\frac{OB}{M_g}$,

where M_g is the total mass of the crystals settled.

N.B. The symbols used in this appendix have no relation to any symbols used previously in this dissertation.

APPENDIX B

EVALUATION OF α_1 AND α_2 FROM THE CUMULATIVE WEIGHT DISTRIBUTION CURVES OF THE CRYSTALS

The cumulative weight fraction of crystals up to size ℓ is defined as:

$$W(\ell,t) = \frac{\rho_s \int_0^{\ell} \ell^3 f(\ell,t)\,d\ell}{\rho_s \int_0^{\infty} \ell^3 f(\ell,t)\,d\ell} \tag{B-1}$$

From equation (5-8)

$$w(\ell,t) = \rho_s \ell^3 f(\ell,t) \tag{5-8}$$

therefore:

$$W(\ell,t) = \frac{\int_0^{\ell} w(\ell,t)\,d\ell}{\int_0^{\infty} w(\ell,t)\,d\ell} \tag{B-2}$$

Similarly the cumulative weight fraction of crystals greater than size ℓ is given by

$$V(\ell,t) = \frac{\int_{\ell}^{\infty} w(\ell,t)\,d\ell}{\int_0^{\infty} w(\ell,t)\,d\ell} \tag{B-3}$$

$$= 1 - W(\ell,t) \tag{B-4}$$

α_1 and α_2 are related to $w(\ell,t)$ as follows:

$$\alpha_1 = \frac{\int_0^\infty \ell w(\ell,t)\,d\ell}{\int_0^\infty w(\ell,t)\,d\ell} \tag{B-5}$$

$$\alpha_2 = \frac{\int_0^\infty \ell^2 w(\ell,t)\,d\ell}{\int_0^\infty w(\ell,t)\,d\ell} \tag{B-6}$$

For convenience sake a function $Z(\ell,t)$ is defined as:

$$Z(\ell,t) = \frac{w(\ell,t)}{\int_0^\infty w(\ell,t)\,d\ell} \tag{B-7}$$

giving:

$$\alpha_1 = \int_0^\infty \ell Z(\ell,t)\,d\ell \tag{B-8}$$

$$\alpha_2 = \int_0^\infty \ell^2 Z(\ell,t)\,d\ell \tag{B-9}$$

$$W(\ell,t) = \int_0^\ell Z(\ell,t)\,d\ell \tag{B-10}$$

Taking Laplace Transforms with respect to ℓ in equation (B-10) results in

$$\overline{W}(q,t) = \frac{1}{q}\,\overline{Z}(q,t) \tag{B-11}$$

From the definition of a Laplace Transform:

$$\overline{Z}(q,t) = \int_0^\infty e^{-q\ell} Z(\ell,t)\,d\ell \qquad \text{(B-12)}$$

Expanding $e^{-q\ell}$ in series form

$$\overline{Z}(q,t) = \int_0^\infty (1 - q\ell + \tfrac{1}{2} q^2\ell^2 + \ldots)Z(\ell,t)\,d\ell \qquad \text{(B-13)}$$

$$= 1 - \alpha_1 q + \tfrac{1}{2}\alpha_2 q^2 + \ldots \qquad \text{(B-14)}$$

Taking Laplace Transforms in equation (B-4)

$$\overline{V}(q,t) = \frac{1}{q} - \overline{W}(q,t) \qquad \text{(B-15)}$$

Combining equations (B-15) and (B-11)

$$\overline{V}(q,t) = \frac{1}{q} - \frac{1}{q}\overline{Z}(q,t) \qquad \text{(B-16)}$$

replacing for $\overline{Z}(q,t)$ from equation (B-14)

$$\overline{V}(q,t) = \frac{1}{q} - \frac{1}{q}(1 - \alpha_1 q + \tfrac{1}{2}\alpha_2 q^2 + \ldots)$$

$$= \alpha_1 - \tfrac{1}{2}\alpha_2 q + \ldots \qquad \text{(B-17)}$$

But $\overline{V}(q,t) = \int_0^\infty e^{-q\ell} V(\ell,t)\,d\ell$

$$= \int_0^\infty V(\ell,t)\,d\ell - q\int_0^\infty \ell V(\ell,t)\,d\ell + \tfrac{1}{2} q^2 \int_0^\infty \ell^2 V(\ell,t)\,d\ell + \ldots \qquad \text{(B-18)}$$

Equating coefficients in equations (B-19) and (B-17) gives:

$$\alpha_1 = \int_0^\infty V(\ell,t)d\ell \qquad \text{(B-20)}$$

$$\alpha_2 = 2\int_0^\infty \ell V(\ell,t)d\ell \qquad \text{(B-21)}$$

α_1 and α_2 can therefore be readily obtained from the cumulative weight distribution curve $W(\ell,t) = 1 - V(\ell,t)$.

APPENDIX C

BATCH CRYSTALLIZATION RESULTS

GROWTH RATE EXPERIMENTS WITH SEED CRYSTALS (CHAPTER IV)

GROWTH RATE: p: microns/min	AVERAGE SIZE OF CRYSTALS $\bar{\ell}$	SOLUTION CONCENTRATION gms.WO_3/litre
.302	50.70	159.82
.317	64.33	163.92
.312	84.40	159.34
.318	57.60	162.03
.321	85 00	160.67
.301	64.00	158.96
.172	35.50	149.42
.150	51.30	146.31
.179	63 80	149.50
.167	52.20	148.71
.160	59.90	148.36
.159	83.50	149.61
.088	48.6	138.23
.052	61.5	136.08
.074	83.9	140.13
.064	45.2	138.60
.078	58.5	137.31
.070	82.5	139.69

CUMULATIVE WEIGHT FRACTION W(ℓ, t) AS A FUNCTION OF CRYSTAL SIZE ℓ, FOR DIFFERENT TIMES t

Experimental Conditions Outside jacket temperature : 140°C

Stirrer speed 250 rpm

CRYSTALLIZATION TIME							
4 mins		8 mins		12 mins		16 mins	
ℓ	W(ℓ,4)	ℓ	W(ℓ,8)	ℓ	W(ℓ,12)	ℓ	W(ℓ,16)
91.0	1.00	91.0	1.00	111.0	1.00	111.0	1.00
79.5	.922	79.5	.864	91.0	.742	91.0	.454
71.0	.525	71.0	.200	86.0	.452	79.5	.160
65.0	.197	65.0	.119	79.5	.177	71.0	.076
59.5	.144	59.5	.042	71.0	.110	65.0	.020
56.5	.105			59.5	.032		
51.0	.050						

Experimental Conditions

Outside jacket temperature: 140°C

Stirrer speed: 250 rpm

Variation of α_1 with crystallization time:

α_1 microns	t mins
69.00	4
74.30	8
83.94	12
90.24	16

Variation of $\frac{p}{(c - c_s)}$ with $\frac{1}{V}$

t mins	p microns/ min.	$(c - c_s)$ gms. WO_3/ litre	$\frac{p}{c - c_s}$	$\frac{1}{V}$
4	2.880	90.5	3.18×10^{-2}	2.64×10^{-3}
8	2.350	91.2	2.58×10^{-2}	2.91×10^{-3}
12	2.085	94.5	2.20×10^{-2}	3.21×10^{-3}
16	1.900	100.1	1.90×10^{-2}	3.48×10^{-3}

CUMULATIVE WEIGHT FRACTION W(ℓ, t) AS A FUNCTION OF CRYSTAL SIZE ℓ, FOR DIFFERENT TIMES,

Experimental Conditions Outside jacket temperature: 140°C

Stirrer speed: 800 rpm

CRYSTALLIZATION TIME							
4 mins		8 mins		12 mins		16 mins	
ℓ	W(ℓ,4)	ℓ	W(ℓ,8)	ℓ	W(ℓ,12)	ℓ	W(ℓ,16)
91.0	1.00	91.0	1.00	91.0	1.00	91.0	1.00
79.5	.928	79.5	.981	86.0	.916	86.0	.893
71.0	.876	71.0	.843	79.5	.710	79.5	.613
65.0	.804	65.0	.587	71.0	.426	71.0	.410
59.5	.697	59.5	.471	65.0	.271	65.0	.283
56.5	.586	56.5	.406	59.5	.174	59.5	.206
53.5	.472	53.5	.342	56.5	.116	56.5	.160
51.0	.384	51.0	.284	51.0	.042	53.5	.123
46.5	.251	46.5	.232			51.0	.103
43.5	.163	43.5	.184			46.5	.067
40.5	.045	40.5	.136				

Experimental Conditions:

Outside jacket temperature: 140°C

Stirrer speed: 800 rpm

Variation of α_1 with crystallization time

α_1 microns	t mins.
55.90	4
57.90	8
71.36	12
71.58	16

Variation of $\frac{p}{(c - c_s)}$ with $\frac{1}{V}$

t mins	p microns/ min.	$(c - c_s)$ gms WO_3/ litre	$\frac{p}{c - c_s}$	$\frac{1}{V}$
4	2.790	90.5	3.12×10^{-2}	2.64×10^{-3}
8	2.310	91.2	2.53×10^{-2}	2.91×10^{-3}
12	1.995	94.5	2.11×10^{-2}	3.21×10^{-3}
16	1.800	100.1	1.80×10^{-2}	3.48×10^{-3}

CUMULATIVE WEIGHT FRACTION W(ℓ,t) AS A FUNCTION OF CRYSTAL SIZE ℓ, FOR DIFFERENT TIMES t

Experimental Conditions: Outside jacket temperature 140°C

Stirrer speed: 1600 rpm

CRYSTALLIZATION TIME							
4 mins		8 mins		12 mins		16 mins	
ℓ	W(ℓ,4)	ℓ	W(ℓ,8)	ℓ	W(ℓ,12)	ℓ	W(ℓ,16)
56.5	1.00	91.0	1.00	91.0	1.00	111.0	1.00
53.5	.993	79.5	.986	79.5	.937	91.0	.958
51.0	.954	71.0	.966	71.0	.857	79.5	.846
46.5	.864	65.0	.905	65.0	.773	71.0	.704
43.0	.779	56.5	.748	56.5	.605	65.0	.577
40.5	.668	51.0	.609	51.0	.477	56.5	.408
38.0	.562	43.0	.422	43.0	.356	53.3	.346
36.0	.507	40.5	.347	40.5	.277	46.5	.185
32.0	.357	36.0	.177	36.0	.175	43.0	.123
29.5	.202	32.0	.122	32.0	.093	36.0	.093
26.0	.081	26.0	.085	29.5	.045	32.0	.065
24.5	.066	24.5	.060				

Experimental Conditions

Outside jacket temperature: 140°C

Stirrer speed: 1600 rpm

Variation of α_1 with crystallization time

α_1 microns	t mins.
36.37	4
46.46	8
52.04	12
60.86	16

Variation of $\frac{p}{(c - c_s)}$ with $\frac{1}{V}$

t mins	p microns/ min.	$(c-c_s)$ gms. WO_3 litre	$\frac{p}{(c - c_s)}$	$\frac{1}{V}$
4	2.89	90.5	3.19×10^{-2}	2.64×10^{-3}
8	2.35	91.2	2.58×10^{-2}	2.91×10^{-3}
12	1.96	94.5	2.07×10^{-2}	3.21×10^{-3}
16	1.75	100.1	1.75×10^{-2}	3.48×10^{-3}

CUMULATIVE WEIGHT FRACTION W(ℓ,t) AS A FUNCTION OF CRYSTAL SIZE ℓ, FOR DIFFERENT TIMES t

Experimental Conditions: Outside jacket temperature 130°C

Stirrer speed: 1600 rpm

CRYSTALLIZATION TIME							
5 mins		10 mins		15 mins		20 mins	
ℓ	W(ℓ,5)	ℓ	W(ℓ,10)	ℓ	W(ℓ,15)	ℓ	W(ℓ,20)
46.5	1.00	91.0	1.00	79.5	1.00	91.0	1.00
43.0	.848	79.5	.960	71.0	.927	79.5	.946
40.5	.756	65.0	.889	65.0	.821	71.0	.831
38.0	.725	56.5	.741	59.5	.663	65.0	.703
36.0	.664	51.0	.581	53.5	.431	56.5	.486
32.0	.533	43.0	.385	46.5	.270	51.0	.382
29.5	.428	38.0	.241	43.0	.121	43.0	.243
26.0	.201	36.0	.170	38.0	.070	38.0	.112
24.5	.159	32.0	.104	29.5	.051	29.5	.078
23.0	.117	27.5	.082				

Experimental Conditions

Outside jacket temperature: 130°C

Stirrer speed: 1600 rpm

Variation of α_1 with crystallization time

α_1 microns	t mins.
32.2	5
47.5	10
53.5	15
54.8	20

Variation of $\frac{p}{(c - c_s)}$ with $\frac{1}{V}$

t mins	p microns/ min.	$(c - c_s)$ gms. WO_3/ litre	$\frac{p}{(c - c_s)}$	$\frac{1}{V}$
5	2.642	88.8	2.975×10^{-2}	2.63×10^{-3}
10	2.010	89.3	2.255×10^{-2}	2.89×10^{-3}
15	1.873	91.5	2.050×10^{-2}	3.16×10^{-3}
20	1.461	95.2	1.535×10^{-2}	3.46×10^{-3}

CUMULATIVE WEIGHT FRACTION $W(\ell, t)$ AS A FUNCTION OF CRYSTAL SIZE ℓ, FOR DIFFERENT TIMES t

Experimental Conditions: Outside jacket temperature 120°C

Stirrer speed 1600 rpm

CRYSTALLIZATION TIME							
6 mins		12 mins		18 mins		24 mins	
ℓ	$W(\ell,6)$	ℓ	$W(\ell,12)$	ℓ	$W(\ell,18)$	ℓ	$W(\ell,24)$
59.5	1.00	79.5	1.00	79.5	1.00	91.0	1.00
56.5	.968	71.0	.975	71.0	.935	79.5	.901
51.0	.874	59.5	.895	65.0	.768	71.0	.809
43.0	.709	53.5	.780	56.5	.565	65.0	.646
38.0	.569	46.5	.630	51.0	.410	56.5	.490
36.0	.502	40.5	.481	43.0	.275	51.0	.377
32.0	.410	36.0	.360	38.0	.131	43.0	.265
29.5	.312	32.0	.238	27.5	.094	40.5	.184
27.5	.172	26.0	.108			36.0	.112
26.0	.123					27.5	.063

Experimental conditions

Outside jacket temperature: 120°C

Stirrer speed: 1600 rpm

Variation of α_1 with crystallization time:

α_1 microns	t mins.
33.8	6
47.2	12
52.0	18
55.2	24

Variation of $\frac{p}{(c - c_s)}$ with $\frac{1}{V}$

t mins	p microns/ min.	$(c - c_s)$ gms WO_3/ litre	$\frac{p}{(c - c_s)}$	$\frac{1}{V}$
6	2.101	84.5	2.49×10^{-2}	2.75×10^{-3}
12	1.890	85.1	2.22×10^{-2}	3.02×10^{-3}
18	1.565	86.5	1.81×10^{-2}	3.33×10^{-3}
24	1.421	94.9	1.50×10^{-2}	3.65×10^{-3}

APPENDIX D

CONTINUOUS CRYSTALLIZATION RESULTS

Experiment No. 1.

Outside jacket temperature : 150°C

Stirrer speed 1600 rpm

$\frac{W_o}{W}$ 2.022

Residence time : T 41.2 mins

Growth rate P .433 microns/min

CUMULATIVE WEIGHT FRACTION VERSUS CRYSTAL SIZE

CRYSTAL SIZE : ℓ	$W(\ell)$
157.0	.935
111.0	.822
91.0	.723
79.5	.637
71.0	.582
65.0	.513
56.5	.424
51.0	.356
43.0	.267
38.0	.158
29.5	.075
26.0	~ 0

$\log_{10}[\frac{1}{\ell^3} \cdot \frac{dW(\ell)}{d\ell}]$ versus ℓ

ℓ	$\log_{10}[\frac{1}{\ell^3} \cdot \frac{dW(\ell)}{d\ell}]$
35	-6.5693
45	-6.7145
55	-7.1328
65	-7.4408
75	-7.7226
85	-7.9450
95	-8.2186
105	-8.4848
115	-8.6390
125	-8.8440
135	-9.0106
145	-9.1844

Experiment No.2

Outside jacket temperature : 150°C

Stirrer speed 1600 rpm

$\frac{W_o}{W}$ 2.210

Residence time : T 49.4 mins

Growth rate P .384 microns/min.

CUMULATIVE WEIGHT FRACTION VERSUS CRYSTAL SIZE

CRYSTAL SIZE : ℓ	$W(\ell)$
157.0	1.00
111.0	.882
91.0	.739
79.5	.646
71.0	.570
59.5	.476
53.5	.434
46.5	.375
40.5	.333
38.0	.299
32.0	.153
29.5	.125

$\log_{10}[\frac{1}{\ell^3} \cdot \frac{dW(\ell)}{d\ell}]$ versus ℓ

ℓ	$\log_{10}[\frac{1}{\ell^3} \cdot \frac{dW(\ell)}{d\ell}]$
45	-7.0061
55	-7.2882
65	-7.5544
75	-7.7042
85	-7.8563
95	-8.0482
105	-8.2321
115	-8.4828
125	-8.7986
135	-9.0899

Experiment No. 3

Outside jacket temperature : 160°C

Stirrer speed 1600 rpm

$\frac{W_o}{W}$ 2.490

Residence time : T 59.7 mins

Growth rate P .242 microns/min

CUMULATIVE WEIGHT FRACTION VERSUS CRYSTAL SIZE

CRYSTAL SIZE : ℓ	$W(\ell)$
157.0	1.00
111.0	.972
91.0	.877
79.5	.803
71.0	.725
59.5	.613
53.5	.500
46.5	.390
40.5	.314
38.0	.229
36.0	.162
29.5	.084

$\log_{10} [\frac{1}{\ell^3} \cdot \frac{dW(\ell)}{d\ell}]$ versus ℓ

ℓ	$\log_{10}[\frac{1}{\ell^3} \cdot \frac{dW(\ell)}{d\ell}]$
35	-6.4873
45	-6.7380
55	-6.9796
65	-7.3615
75	-7.6968
85	-7.9711
95	-8.1938
105	-8.4962
115	-8.8808

Experiment No. 4.

Outside jacket temperature : 150°C

Stirrer speed 1600 rpm

$\frac{w_o}{w}$ 2.335

Residence time : T 51.95 mins

Growth rate P .377 microns/min

CUMULATIVE WEIGHT FRACTION VERSUS CRYSTAL SIZE

CRYSTAL SIZE : ℓ	$W(\ell)$
157.0	1.00
111.0	.843
91.0	.725
79.5	.626
71.0	.481
59.5	.352
53.5	.264
46.5	.210
43.0	.153
40.5	.122
36.0	.107

$\log_{10}[\frac{1}{\ell^3} \cdot \frac{dW(\ell)}{dt}]$ versus ℓ

ℓ	$\log_{10}[\frac{1}{\ell^3} \cdot \frac{dW(\ell)}{dt}]$
45	-6.9605
55	-7.1124
65	-7.3233
75	-7.5129
85	-7.7911
95	-8.0894
105	-8.3157
115	-8.5006

Experiment No. 5.

Outside jacket temperature : 170°C

Stirrer speed 1600 rpm

$\frac{W_o}{W}$ 2.39

Residence time : T 46.24 mins

Growth rate P .314

CUMULATIVE WEIGHT FRACTION VERSUS CRYSTAL SIZE

CRYSTAL SIZE : ℓ	$W(\ell)$
157.0	1.00
111.0	1.00
91.0	.890
79.5	.780
71.0	.707
65.0	.637
56.5	.465
51.0	.359
46.5	.295
43.0	.231
40.5	.132
38.0	.076

$\log_{10}[\frac{1}{\ell^3} \cdot \frac{dW(\ell)}{d\ell}]$ versus ℓ

ℓ	$\log_{10}[\frac{1}{\ell^3} \cdot \frac{dW(\ell)}{d\ell}]$
45	-6.6778
55	-6.9215
65	-7.2782
75	-7.6189
85	-7.8447
95	-8.0894
105	-8.5129

Experiment No. 6.

Outside jacket temperature : 170°C

Stirrer speed 1600 rpm

$\frac{w_o}{w}$ 2.21

Residence time : T 37.9 mins

Growth rate P .334 microns/min

CUMULATIVE WEIGHT FRACTION VERSUS CRYSTAL SIZE

CRYSTAL SIZE : ℓ	W(ℓ)
157.0	1.00
111.0	.976
91.0	.688
79.5	.631
71.0	.557
65.0	.510
56.5	.423
51.0	.362
43.0	.262
40.5	.161
36.0	.121
32.0	.107

$\log_{10}[\frac{1}{\ell^3} \cdot \frac{dW(\ell)}{d\ell}]$ versus ℓ

ℓ	$\log_{10}[\frac{1}{\ell^3} \cdot \frac{dW(\ell)}{d\ell}]$
37.5	-6.5474
42.5	-6.7399
47.5	-6.8989
52.5	-7.1046
57.5	-7.2557
62.5	-7.4647
67.5	-7.5850
72.5	-7.6576
77.5	-7.8007

Experiment No. 7

Outside jacket temperature : 160°C

Stirrer speed 1600 rpm

$\frac{W_o}{W}$ 2.50

Residence time : T 48.4 mins

Growth rate P .258 microns/min.

CUMULATIVE WEIGHT FRACTION VERSUS CRYSTAL SIZE

CRYSTAL SIZE : ℓ	$W(\ell)$
157.0	.980
111.0	.797
91.0	.726
79.5	.655
71.0	.581
65.0	.517
59.5	.466
56.5	.392
53.5	.361
51.0	.314
46.5	.250
43.0	.155

$\log_{10}[\frac{1}{\ell^3} \cdot \frac{dW(\ell)}{d\ell}]$ versus ℓ

ℓ	$\log_{10}[\frac{1}{\ell^3} \cdot \frac{dW(\ell)}{d\ell}]$
42.5	-6.5243
47.5	-6.7230
52.5	-6.9571
57.5	-7.1163
62.5	-7.3478
67.5	-7.4884
72.5	-7.6474
77.5	-7.7670
82.5	-7.9310
87.5	-8.0953
92.5	-8.2000
97.5	-8.3054

APPENDIX E

LITERATURE CITED

1. BOTSARIS, G.D. & DENK, E.G.: Ind. Eng. Chem. Fundamentals. 9, No.2, (1970)

2. BRANSOM, S.H.: Brit. Chem. Eng., December 1960, 838

3. BRANSOM, S.H., DUNNING, W.J. & MILLARD,B.: Disc. Faraday Soc. 5, 83, (1949)

4. GARSIDE, J. & MULLIN, J.W.: Trans. Inst. Chem. Eng. 46, 1, (1968)

5. GORSHTEIN, G.I. & BALINER, A.K.: Zhurnal Prikladnoi Khimii, 42, 2707, (1969)

6. HEELEY,G.P.: Ph.D. Thesis, Manchester, (1968)

7. HIXON, A.W. & KNOX, K.L.: Ind. Eng. Chem. 43, 2144, (1951)

8. HULBURT, H.M. & KATZ,S.: Chem. Eng. Science 19, 555, (1964)

9. ISHII, T.: Bull. Tokyo Inst. Technol. No.67, (1965)

10. KNAPP,H.: Ph.D. Thesis, Darmstadt, (1963)

11. LARSON,M.A., TIMM, D.C. & WOLFF,P.R.: A.I.Ch.E. Journal 14, No. 3, 448, (1968)

12. McCABE, W.L. & STEVENS,R.P.: Chem. Eng. Progress 47, No.4, 168, (1951)

13. MASON,R.E.A. & STRICKLAND-CONSTABLE,R.F.: Nature, 197, 897, (1963)

14. MELIA, T.P. & MOFFITT, W.P.: I. & E.C. Fundamentals 3, No.4, 313, (1964)

MELIA, T.P. & MOFFITT, W.P.: Journal of Colloid Science 19, 433, (1964)

15. MURRAY, D.C. & LARSON, M.A.: "Laboratory Study of a Continuous Mixed Suspension Crystallizer" A report from Iowa State University of Science and Technology, Ames, Iowa (1963)

16. NABARRO, F.R.N.: "Theory of Crystal Dislocations", p. 313, Clarendon Press, Oxford (1967)

17. RANDOLPH, A.D. & RAJAGOPAL, K.: I.& E.C. Fundamentals 9, No.1, 165, (1970)

18. RUMFORD, F. & BAIN, J.: Trans. Inst. Chem. Eng. 38, 10 (1960)

19. RUSHTON, J.H.: A.I.Ch.E. Joint Meeting No. 10, June 1965.

20. TIMM, D.C. & LARSON, M.A.: A.I.Ch.E. Journal 14, No.3, 452, (1968)

21. TURNBULL, D.: Journal of Applied Physics 19, 775, (1948)

22. WATTS, P.: Ph.D. Thesis, Manchester, (1967)